27

Roll Stabilization for Fast Monohulls by Using Passive and Active Lifting Appendages

By

Talha ULUSOY

B.Sc. in Mechanical Engineering
Turkish Naval Academy, 1999

Submitted to the Department of Ocean Engineering
in Partial Fulfillment of the Requirements for the Degree of

Master of Science in Naval Architecture and Marine Engineering

at the

Massachusetts Institute of Technology

February, 2004

Author:.....
Department of Ocean Engineering
July 8, 2003

Certified by:.....
Paul D. Sclavounos
Professor of Naval Architecture
Thesis Advisor

Accepted by:.....
Michael Triantafyllou
Professor of Ocean Engineering
Chairman, Departmental Committee on Graduate Studies

To my mother...

Roll Stabilization for Fast Monohulls by Using Passive and Active Lifting Appendages

By

Talha ULUSOY

Submitted to the Department of Ocean Engineering on July 8, 2003
in partial fulfillment of the requirements for the degree of
Master of Science in Naval Architecture and Marine Engineering

Abstract

Roll stabilization for monohulls is an important issue in naval architecture. Several methods including roll stabilization tanks, active control fins, rudder roll stabilization systems, and bilge keels are commonly used for roll stabilization purposes and each one of them has its own advantages and disadvantages. In this thesis roll stabilization is studied by using passive and active roll stabilization configurations with hydrofoils.

The main objective of this research is to identify an effective roll stabilization system for use on high-speed monohull vessels. The analysis of the performance of a passive hydrofoil configuration is used as a starting point for the development of active control mechanisms. A generic fast monohull was created for study purposes and the SWAN-2 code (ShipWaveANalysis), a state-of-the-art time domain simulation program, was used for the analysis of the linear free-surface flow around the vessel. Simulations were carried out in regular waves incident at angles ranging from 90°, 105°,120°,135° and 150° degrees relative to the ship axis, 90° being beam waves and 180° degree being head waves. The ship was equipped with a hydrofoil fixed amidships, quarter to aft and aft to determine the sensitivity of roll motion on the longitudinal position of the lifting appendage. It was found that the most efficient location for the hydrofoil is amidships leading to a 20% to 60% roll motion reduction (depending on the wave angle and ship speed) of the RMS value of roll motion in an ISSC spectrum. Also studies were performed to determine the planform area of the hydrofoil for optimal roll motion reduction. In addition, four different Froude numbers are used, ranging from 0.3 to 0.9, to evaluate the effect of the speed on the effectiveness of the lifting appendage. As expected, higher speeds lead to better seakeeping performance, namely better roll reduction compared to lower speeds.

Passive hydrofoils were found to be very effective in reducing the rolling motion. Active roll control mechanisms were also investigated by seeking the optimal time-dependent variation of the modulus and phase of the hydrofoil angle of attack and found to be very effective leading to increased roll reduction. The development of such optimal control algorithms is expected to lead to an enhanced roll seakeeping performance over a broader range of sea state conditions and ship speeds.

Thesis Supervisor: Paul D. Sclavounos
Title: Professor of Naval Architecture

Acknowledgements

The following thesis was written during spring 2003 at "Laboratory for Ship and Platform Flow" in Massachusetts Institute of Technology.

I owe lots of thanks to Professor Paul D. Sclavounos. I took several subjects under his teaching that contributes much to my study here at MIT. Thanks to Dr. Sungeun Kim for his advices and explanations on subject, sometimes on the phone and sometimes with e-mail as well as face to face meetings. Thanks to Yile Li, Kwang Hyun Lee, Shiran Purvin and Iason Chatzakis. They were my officemates during my study. Whenever I had a question they were ready to answer. I really appreciate their help.

Thanks to my parents, Fatma Ulusoy and Mehmet Ulusoy, and my brothers Eyüp Ulusoy, Yasin Ulusoy, Yusuf Ulusoy with whom my life is more meaningful and enjoyable.

And special thanks to my wife, Berna Ulusoy, who was suffering while I was working hard. It would be much harder without her support.

Talha ULUSOY
Cambridge, Massachusetts, 2003

Table of Contents

List of Figures

1. Introduction

1.1. Background

Roll motion has always been one of the most important concerns for conventional and high speed monohull vessels because of the weak damping and the potentially large response amplitude at resonance, affecting people, cargo, structure and even military systems including fire control and aviation.

Several methods have been used to solve or minimize the effects of this potential problem. The most common methods are the use of active and passive fins, bilge keels, active and passive tanks and rudders. Each method has its own advantages and disadvantages in different sea states.

In the area of Naval Architecture and Marine Engineering, we have seen a great increase in the development and use of three-dimensional panel methods that are capable of simulating the steady and unsteady free surface potential flows past ships. These methods are quite robust and reliable in simulating free surface potential flow past high speed vessels that conventional strip theory applications are not valid for.

A state-of-the-art method, SWAN-2, introduced above implicitly will be used to investigate a possible passive and active roll reduction mechanism with hydrofoils using linear theory in potential flow.

1.2. Overview

In this thesis, the influence of passive and active hydrofoil roll control systems on the roll motion responses of a high speed semi-displacement monohull will be investigated. A generic monohull created for study purposes will be worked on.

The time domain 3-D Rankine Panel Method SWAN-2 will be utilized to get the roll motion parameters, e.g. response amplitude operators (RAO), of the studied monohull.

In chapter 2, the theoretical background of the physical problem studied in this thesis will be explored. The boundary value problem, the equation of roll motion, equivalent linearization approach for nonlinear roll damping and restoring terms and brief information on panel methods are included.

In chapter 3, the formulation and the numerical solution behind SWAN-2 will be explained, including the linearization of the boundary value problem, seakeeping with forward speed, discretization, and applications of SWAN-2.

In chapter 4, the roll problem is defined. The methodology carried out in this thesis will be explained. The influence of hydrofoil position, hydrofoil planform area, and ship forward speed on the effectiveness of the roll reduction system will be investigated in separate sections.

In chapter 5, the idea behind the active control mechanism will be introduced. Several examples of active roll control system explicitly showing the remarkable effects are included.

Chapter 6 includes the results, the discussions about the results and some remarks to conclude the subject.

Chapter 7 includes the references and bibliography.

Chapter 8 contains the nomenclature.

Appendixes A through D contain all the results of runs, for various speeds, hydrofoil locations and planform areas cases.

2. Theoretical Background

In this thesis, the effects of passive and active lifting appendages, namely hydrofoils, on the roll motion of fast monohulls were examined. The results of passive lifting appendages system were used as a starting point for the active roll control systems with hydrofoils.

A generic monohull was created for study purposes. All the numerical solutions were achieved by using 3-D Rankine Panel Method SWAN-2. The following chapter outlines the theoretical background of the physical problem.

2.1. Boundary Value Problem

The physical problem can be approximated under the assumption of an inviscid and incompressible fluid and an irrotational flow. Since we are concerned with ship motions in waves, we can obtain useful results by neglecting nonlinear and viscous effects. Since the nonlinear and viscous effects are not assumed to significantly affect the parameters investigated in this thesis, a potential flow model can thus be utilized for solving the required boundary value problems. The potential function describing the resulting velocity field is a harmonic function in the fluid domain satisfying the following equation

$$\nabla^2\Phi = \Phi_{xx} + \Phi_{yy} + \Phi_{zz} = 0 \tag{1}$$

where $\Phi(\vec{x},t)$ is the total fluid velocity potential. The fluid velocity vector is then defined as

$$\overline{V}(\vec{x},t) = \nabla\Phi \tag{2}$$

where $\vec{x} = x\vec{i} + y\vec{j} + z\vec{k}$ is the displacement vector with respect to the (x, y, z) coordinate system moving with the vessel's mean position as shown in Figure 1.

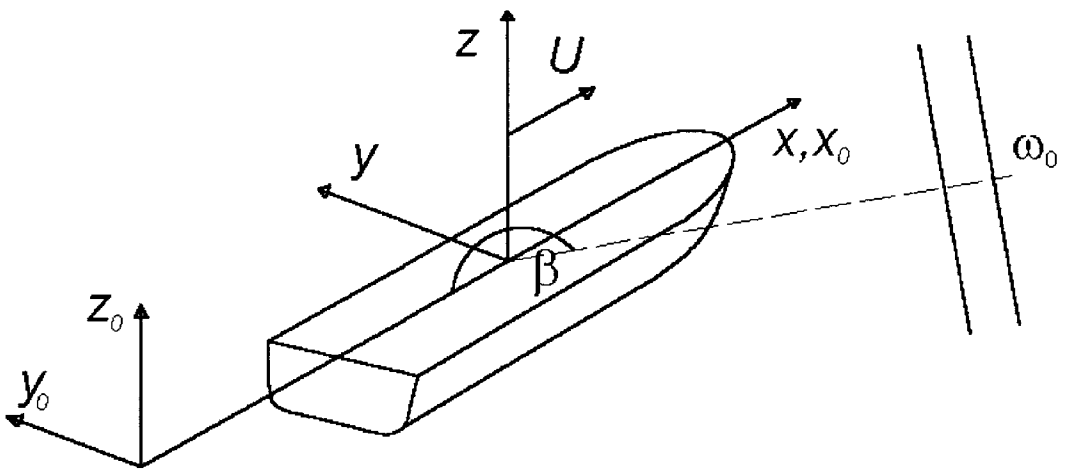

Figure 1: Vessel advancing with forward speed U in ambient waves

A ship advancing at constant forward speed U along the positive x-axis is illustrated in Figure 1, where the (x, y, z) reference coordinate system translates with the vessel's mean position. The calm water surface corresponds to $z = 0$. Plane progressive waves with heading β relative to the x-axis and absolute frequency ω_0 relative to the inertial coordinate system (x_0, y_0, z_0) are incident upon the ship. In potential flow, the velocity potential of a plane progressive wave is given as

$$\phi_I(\vec{x},t) = \mathrm{Re}\left\{\frac{igA}{\omega_0}\frac{\cosh[k(z+H)]}{\cosh[kH]}e^{-ikx\cos\beta - iky\sin\beta + i\omega t + i\varepsilon}\right\} \tag{3}$$

where g is the acceleration due to gravity, A is the incident wave amplitude, H is the water depth, ε is a random phase angle, Re is the real part operator, ω_0 is the absolute frequency of the incident waves and ω is the frequency of encounter given as

$$\omega = |\omega_0 - Uk\cos\beta| \tag{4}$$

The wave-number k is related to ω_0 through the dispersion relation as

$$\omega_0^2 = kg\tanh(kH) \tag{5}$$

A linear superposition of regular plane progressive waves with velocity potentials of the form of (3) can be utilized to simulate an irregular sea state.

By integrating the equations of momentum conservation, Bernoulli's Equation relates the pressure field to the kinematic properties of the flow

$$p - p_a = -\rho(\frac{\partial \Phi}{\partial t} + \frac{1}{2}\nabla\Phi \cdot \nabla\Phi - \frac{1}{2}U^2 + gz) \tag{6}$$

The fluid domain is bounded by the free surface which is defined by its elevation $z = \eta(x, y, t)$. The free surface must obey the kinematic free surface condition, which states that a fluid particle on the free surface at $t=0$ will stay there all time. Mathematically this means that the substantial derivative of the difference between the z–coordinate and $\eta(x, y, t)$ vanishes on the free surface. With forward speed, the kinematic free surface condition with respect to the coordinate system (x, y, z) translating with the vessel is

$$\left(\frac{\partial}{\partial t} + \nabla\Phi \cdot \nabla\right)\left(z - \eta(x, y, t)\right) = 0 \quad \text{on } z = \eta(x, y, t) \tag{7}$$

After some manipulation, keeping linear first order terms, (7) can be written as

$$\frac{\partial \eta}{\partial t} = \frac{\partial \Phi}{\partial z} \quad \text{on } z = 0 \tag{8}$$

By requiring the pressure to be atmospheric p_a on the free surface, and by substituting $\eta(x, y, t)$ for z, the dynamic free surface boundary condition with respect to the coordinate system (x, y, z) translating with the vessel is obtained from Bernoulli's equation (6) as

$$\eta(x, y, t) = -\frac{1}{g}\left(\frac{\partial \Phi}{\partial t} + \frac{1}{2}\nabla\Phi \cdot \nabla\Phi - \frac{1}{2}U^2\right)_{z=\eta(x,y,t)} \tag{9}$$

Keeping linear first order terms, (9) can be written as

$$\eta = -\frac{1}{g} \cdot \frac{\partial \Phi}{\partial t} \quad \text{on } z = 0 \tag{10}$$

Both the linear kinematic and dynamic free surface boundary conditions can be combined in one single condition as follows

$$\frac{\partial^2 \Phi}{\partial t^2} + g\frac{\partial \Phi}{\partial z} = 0 \quad \text{on } z = 0 \tag{11}$$

On the submerged part of the vessel surface S_B, a no-flux condition must be imposed. This is the body boundary condition, which states that the component of the fluid velocity in the direction of the normal vector $\vec{n}$ must equal the vessel's velocity $\vec{V}_B$ at the same point on the submerged part of S_B

$$\frac{\partial \Phi}{\partial n} = \vec{V}_B \cdot \vec{n} \quad \text{for } \vec{x} \in S_B \tag{12}$$

The normal vector $\vec{n} = (n_1, n_2, n_3)$ by definition, points out of the fluid domain and into the vessel.

The seafloor is subject to a no-flux condition for all t

$$\frac{\partial \Phi}{\partial z} = 0 \quad \text{for } z = -H \tag{13}$$

The Boundary Value Problem (BVP) is then finally closed by requiring the gradient of the velocity potential to decay to zero as $\vec{x}$ approaches infinity for all finite t

$$|\nabla \Phi| \to 0, \quad |\vec{x}| \to \infty \tag{14}$$

2.2. Plane Progressive Waves

The free surface elevation defined by a plane progressive wave formulation is simple but at the same time a significantly practical means of representation of a sea state. The propagating wave has amplitude that is sinusoidal in time with a radian frequency and it moves in phase velocity. The wave elevation can be described in the following form

$$\eta(x, y, t) = A\cos\left[k(x\cos\beta + y\sin\beta) - \omega_0 t + \varepsilon\right] \tag{15}$$

By using linear theory, a long-crested irregular sea can be written as a superposition of wave elevations

$$\eta(x,y,t)=\sum_{j=1}^{N}A_j\cos\left[k_j(x\cos\beta+y\sin\beta)-\omega_{0j}t+\varepsilon_j\right] \tag{16}$$

where A is the wave amplitude, ω_0 is the absolute wave frequency, β is the wave direction relative to the x-axis, ε is a random phase angle and k is the wavenumber defined as the number of waves per unit distance. The dispersion relation relates the wavenumber with the wave frequency. For deep water (5) turns into

$$\omega_0^2=kg \tag{17}$$

The following figure, borrowed from [12], describes clearly several characteristics of the propagating wave.

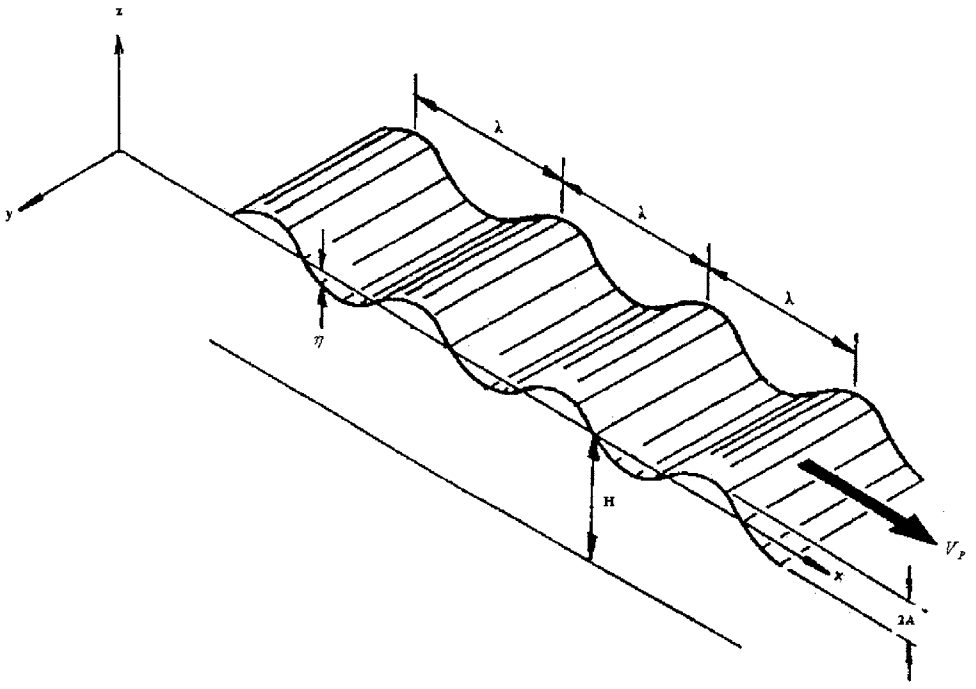

Figure 2: The three dimensional propagating wave

2.3. The Seakeeping Problem

In brief, the seakeeping problem consists of determining the response of a body subject to any given irregular sea state. The response can be any wave-induced motion or load on the vessel, but only the vessel roll motion will be discussed here. In this thesis, a statistical representation

of the sea state will be utilized, and the irregular sea state can thus be described by a representative wave spectrum $S_\zeta(\omega_0)$, which contains statistical information about the wave energy in the vessel operation area. By assuming small vessel displacements $\xi_j(t)$, $j=1,...,6$, and small wave slopes, the seakeeping problem can be modelled as a linear system. The power of linearity is that it allows the vessel's total response to be found as the sum of the responses due to each plane progressive wave present in an irregular sea state.

The input to the linear system will be a long-crested, unidirectional, irregular sea spectrum $S_\eta(\omega_0)$. This is modelled by giving a sum of plane progressive waves, (18) , representing the spectrum with total wave elevation as input to the system.

$$\eta(t) = \sum_{i=1}^{N} \eta_i(t) = \sum_{i=1}^{N} \mathrm{Re}\left\{ A_i e^{i\varepsilon_i + i\omega_0 t} \right\} \tag{18}$$

The velocity potential of these plane progressive waves is given by expression (3). A_i is related to the wave spectrum in the following manner:

$$A_i = \sqrt{2 S_\eta(\omega_0)_i \Delta\omega_0} \tag{19}$$

$S_\eta(\omega_0)_i$ is the value of the spectrum at frequency ω_{0_i}, and $\Delta\omega_0$ is the constant difference between successive frequencies. By virtue of linearity, the response due to each component of the wave spectrum can be analysed separately, and the total response will simply be a linear superposition of the individual responses.

By assuming the vessel's response to be sinusoidal in time, its total response to the excitation in its six degrees of freedom is given as

$$\xi_j(t) = \mathrm{Re}\left\{ \Xi_j e^{i\omega t} \right\} \quad j = 1,...,6 \tag{20}$$

where Ξ_j is the complex number

$$\Xi_j = \left|\Xi_j\right| e^{i\chi_j} \quad j = 1,...,6 \tag{21}$$

is the amplitude and χ_j is the phase of the j^{th} response mode. These are the principal unknowns in the seakeeping problem in the frequency domain. For the sake of simplicity, the frequency-domain version of the seakeeping problem will be discussed here.

The ratio of the response amplitude $|\Xi_j|$ to the wave amplitude A is known as the Response Amplitude Operator (RAO). The square of the RAO multiplied with the wave-spectrum $S_\eta(\omega)$ equals the response spectrum, which integrated over all frequencies produces the variance of the motion responses σ_j^2, which is defined as

$$\sigma_j^2 = \int_0^\infty \left\{ \left| \frac{\Xi_j}{A_i} \right|^2 S_\eta(\omega) \right\} d\omega \quad j = 1,...,6 \tag{22}$$

The standard deviation of the response σ_j, the physical quantity of real interest, is now found easily by taking the square root of (22). Since the wave elevation by virtue of the central limit theorem may be assumed to be a stationary Gaussian process, the response may be taken as Gaussian as well, and the statistical properties of the response are known if equation (22) can be solved.

2.4. Roll Motion in Irregular Waves

Transverse Motions: The transverse motions, roll, sway and yaw, are uncoupled from the longitudinal modes of motions if only the linearized equations of motion of a ship symmetric port/starboard are considered. This argument is not valid for extreme seaways, where the treatment of all six degrees of freedom may be required simultaneously. In this thesis only the situation where the transverse motions (roll, sway, and yaw) are decoupled from the longitudinal motions (surge, heave, and pitch) will be investigated. The transverse motions are strongly coupled to one another, but the character of each motion is different. Sway and yaw motions have no hydrostatic restoring forces and do not display any resonant behavior. Roll, on the other hand, has restoring forces and typically displays very marked resonant motions.

Roll is certainly the most severe angular motion experienced by a ship, often exceeding the "small angle" range of ten or fifteen degrees. These large roll angles can make working on the ship difficult and can lead to motion sickness. Further, the transverse motions are responsible for significant athwartship accelerations. The forces resulting from these accelerations must be resisted by machinery foundations and cargo lashings. These same accelerations also make

it difficult for the ship's personnel to operate the ship. In fact, roll motions are a major limiting factor in the operability of offshore platforms.

The hydrodynamics involved in the computation of the transverse motions is more complicated than that of the longitudinal motions, since viscous effects play an important role. For instance, if a ship is underway, a sway velocity or a yaw angle relative to the path of the ship (or both) can place the ship hull at an apparent angle of attack to the flow. Significant transverse lift forces and moments are created on the ship hull and appendages as a result of the generation of vorticity. For accurate predictions, terms representing these effects may have to be added to the roll equations.

Roll Motion: Roll is by far the most difficult motion of a ship to predict and it is strongly coupled with sway and yaw. It is an accepted fact of ship hydrodynamics that the damping arising from the creation of waves (the principal source of damping for heave, pitch, sway and yaw) is almost small for the rolling of typical ship forms. Other mechanisms for damping, such as viscous effects, occur naturally. However, these mechanisms lead to roll damping which is no larger than the wave damping, and thus the total damping from all sources is still small. It is typical for roll motions to have an effective nondimensional damping ratio of considerably less than 5 percent for a barehulled ship. Waves that have an encounter frequency near roll resonance can, and do, cause typical ships to roll severely. These large roll angles can give rise to strong nonlinearities in the hydrodynamic damping and sometimes in the static roll restoring moment. These conditions further complicate any analysis of roll motions.

In order to discuss roll motions, we will assume that the ship is exposed to a single, unidirectional wave train and the transverse motions in response to this wave are sinusoidal. The linearized equations of motion are given for this situation based on slender-body theory. Inclusion of the nonlinearities mentioned above is not generally possible in such a set of equations, since they lead to responses that include frequencies other than the exciting frequency. Exact treatment of these nonlinearities requires a solution in the time domain, with the hydrodynamic effects represented as convolution integrals that contain memory effects.

However, it is common to include roll nonlinearities in an approximate way, using the concept of equivalent linear coefficients. These linear coefficients are selected so that they have the same integrated effect over one cycle of sinusoidal motion as the sum of the linear and nonlinear terms has over the same cycle. The assumption is that motion, including the nonlinearities, is still approximately sinusoidal, and that the principal effect of the nonlinearities is to change the amplitude of the response.

In order to characterize the roll behavior of a ship, the damped oscillatory motion in calm water that results from the application of a time-harmonic pure roll moment will be examined. Ignoring the coupling damping terms, the roll equation becomes that of a simple harmonic oscillator with damping and restoring and can be rewritten in the form of linear equivalent damping and restoring terms B^*_{44} and C^*_{44} as

$$\left[-\omega^2(I_{44}+A_{44})+i\omega B^*_{44}+C^*_{44}\right]\Xi_4 = X_4 \tag{23}$$

Even though the equations here is for the uncoupled roll motion (to make the representation easy), all solutions were achieved using fully coupled system in SWAN.

This is the equation usually adopted for the analysis of roll motions. It should be emphasized that use of an uncoupled roll equation implies that the center of the coordinate system is at the roll center, that the above-mentioned two coupling terms are ignored, and that a different roll center may be required for each frequency.

The damping parameter is the most crucial one for the ship response. The ratio of the roll amplitude to the effective wave slope amplitude is called the roll response amplitude operator (RAO). A typical ship without roll suppression devices such as bilge keels will have a value of nondimensional damping ratio less than 5 percent. This means that at resonance, the ship will roll at more than 10 times the effective wave slope (RAO > 10). Thus, it is not uncommon to observe significant rolling in what appears to be an almost calm sea.

It has been found through careful experimentation that the part of the roll damping that is not predicted by potential theory is not only a nonlinear function of roll angle, but is also a nonlinear function of roll frequency and forward speed of the ship. It has also been found that there are many components to the roll damping, each of which arises through a separate physical process.

Though there are some caveats that will be discussed later, the linear-random theory provides considerable insight into the rolling behavior of ships. The asymptotic behavior of the RAO for rolling in beam seas is the same as that for pitch in head seas; it tends toward zero at high wave frequency, and to wave slope at low frequencies.

The main difference between the pitch and the roll RAO is that the rolling RAO almost always has a much more pronounced resonant peak, both higher and narrower than is the case for pitch. Because of the low damping, resonant ship rolling amplitudes in response to regular waves vary typically between twice and ten times wave slope amplitude and this has an important effect upon the character of the rolling spectrum.

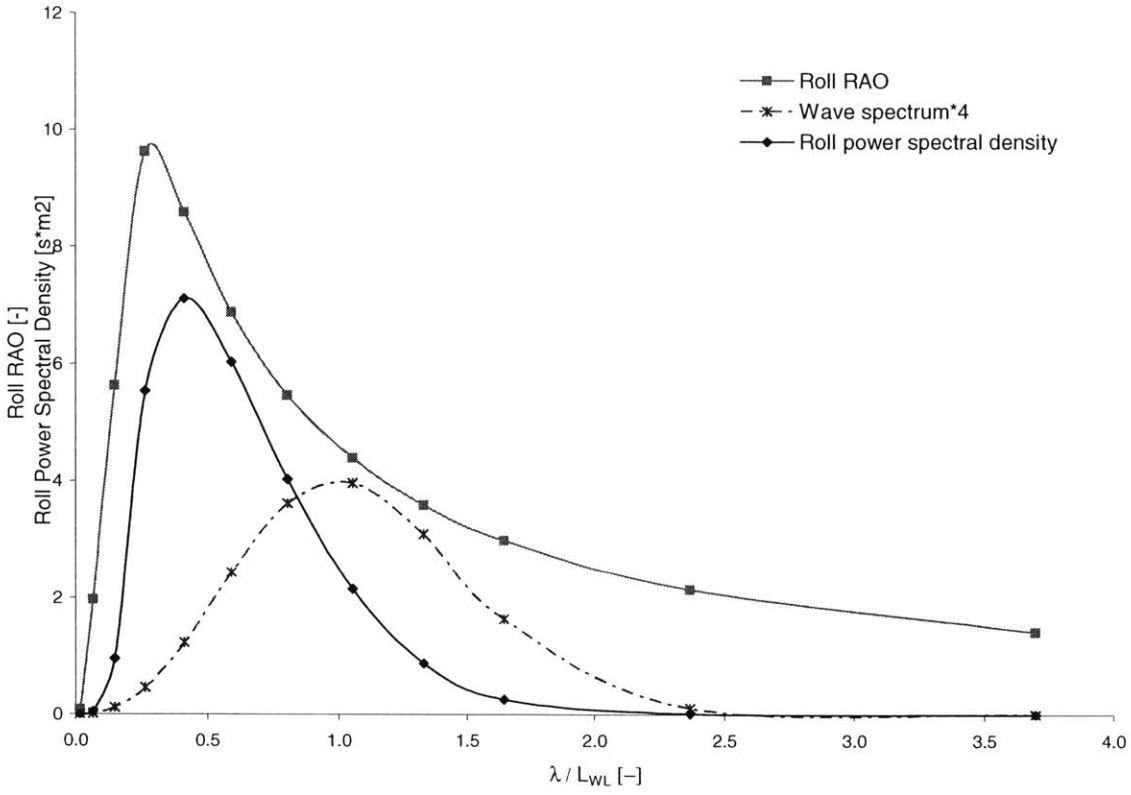

Figure 3: Illustration of the Relation of Roll Response with Roll RAO and Sea Spectra

Figure 3 illustrates a typical situation of rolling in irregular long-crested waves where the wave direction is somewhere near the beam sea case, and there is significant energy in the wave spectrum at a wave frequency corresponding to the resonant encounter frequency. In the graph a typical wave elevation spectrum is shown together with the roll RAO and the calculated roll response spectrum. What happens is that once squared, the narrow peak of the RAO is the only part that is significant, the roll response spectrum shape is controlled by the RAO, and the magnitude of roll depends almost entirely upon the magnitude of wave spectral density near resonance.

Because ship rolling is ordinarily much more sharply "tuned" to a particular encounter frequency band, ships often appear to roll mainly in their own natural rolling period rather than in the dominant period of encounter determined by vessel speed, wave direction, and the ambient wave spectrum. If there is some energy in the encountered wave spectrum in a frequency band that corresponds to roll resonance, the sharply peaked RAO of a lightly

damped vessel can amplify the response to this portion of the wave spectrum to the point that the overall roll response is dominated by roll response components in the resonant period. This is why the relatively simple passive roll damping devices such as tanks, which are effective mainly at resonance, are as successful as they are when applied to an initially lightly damped ship.

In a very rough wind-driven beam or quartering sea almost any conventional ship will roll heavily because the range of practically attainable natural rolling periods is usually within the range of wave frequencies present. In more moderate wind-driven seas the rolling may be less severe, not only because the waves are less steep, but because lower frequency components which might cause resonant rolling may not be present. If the latter is the case, the ship is then in a supercritical condition with respect to rolling. It can also be concluded that a long rolling period can be advantageous, since in general it shifts the supercritical range to rougher seas.
The case of ship rolling when at speed at oblique headings to short-crested waves is much more complicated than in long-crested oblique waves. Relatively large changes in speed or heading may be required to reduce heavy resonant rolling because when the ship is moved out of resonance with one band of wave components the many wave directions present makes it more likely to approach synchronism with another band.

The caveats previously alluded to about the application of the linear-random theory to rolling are centered upon whether or not the basic assumption, linearity of response, is satisfied. The mechanism producing the damping of pitch and heave is largely the radiation of ship generated waves, a mechanism that is linear to reasonable accuracy. But, as explained earlier, in the case of rolling, theory usually predicts wave radiation damping that is relatively much smaller than model experiments suggest, unless the ship geometry is such that rolling will produce radiated waves of significant magnitude (extremely shallow draft barges or some work boats). For more normal large ship forms it is necessary to augment the wave radiation damping suggested by the basic theory by semi-empirical corrections for bilge keels, various viscous effects and the oscillatory dynamic lift forces upon appendages. Although the majority of these augmentations are nonlinear, it is found that for high-speed ships including the important factor of dynamic lift on appendages, which is roughly linear, gave good

agreement between linear calculations and model and full-scale tests in the vicinity of resonance.

Thus, the degree to which linear-random theory will yield reasonable predictions for roll depends to an extent upon the vessel and operating conditions. Early experiments suggested that the rolling motion of a ship fitted with bilge keels and moving through the water is not too far from linear if the deck edges are not immersed, and that consequently the linear-random approach may be used in many cases. Since then, conclusions from experimental and theoretical research are less sanguine. Depending upon speed, some fraction of roll damping appears to be nonlinear. In addition, model tests of beam-sea rolling often show evidence of a weak nonlinearity in restoring moment. Unfortunately, it is not now possible to give simple rules about the conditions and ship geometry where the nonlinear effects are important enough to invalidate the linear-random approach, except perhaps to suggest that the lower the speed and the lighter the apparent damping the more important the nonlinearities may become.

Mechanisms involved in roll damping: A much more fundamental approach to the problem of roll damping involves the examination of the individual mechanisms that lead to roll damping. This method has been favored by Japanese researchers and most of the work on this approach has been done in Japan. A considerable insight into the most important parameters governing roll damping has been achieved by carefully examining each ingredient. These components are:

- The moment resulting from the drag (skin friction) of the hull in contact with seawater, a viscous fluid.
- The moment on the bare hull arising as a result of pressures caused by viscous separation of the flow and formation of eddies, principally near sharp bilges.
- The moment arising from hull side forces (lift forces), which are due to the apparent angle of attack of the hull when the ship is rolling underway.
- The moment resulting from the creation of waves when the ship rolls. This is the moment normally computed by linear potential theory.
- The moment resulting from normal (pressure) forces on just the bilge keels.

- The moment resulting from the modification of the flow around the hull caused by the existence of bilge keels.
- The moment arising from wave making of the bilge keels (normally a small quantity for normal-sized bilge keels).

Because these nonlinearities are weak in the mathematical sense for moderate roll angles, and because roll is usually sharply tuned, there are practical ways of overcoming the difficulties in using linear spectral prediction methods. Several approaches have been suggested and most involve an equivalent statistical linearization scheme where the nonlinear system is replaced by a conditionally linear one in which the RAO is a function of average or rms roll angle. This leads to an iterative solution where the roll magnitude predicted is compared with updated estimates until reasonable convergence is obtained. Additional information can be found in [11].

2.5. Equivalent Linearization of Damping and Restoring Forces in Roll

It has been found through careful experimentation that the part of the roll damping that is not predicted by potential theory is not only a nonlinear function of roll angle, but is also a nonlinear function of roll frequency and forward speed of the ship. It has also been found that there are many components to the roll damping, each of which arises through a separate physical process.

Since the roll damping and the restoring force are highly nonlinear, we find it useful to give some compact information of how to approximate these forces in linear terms. These nonlinearities come from the viscous separation of the flow around the ship and the changes of center of roll during roll motion.

It is common practice to find an approximate solution for a nonlinear dynamics problem by identifying and solving a substitute "equivalent" linear system. In such a technique it is

necessary to make some assumption about the probability distribution of the dynamic response of the system.

Let us denote the response of the ship by $x(t)$, then $g(x,\dot{x},\ddot{x})$ represents the associated nonlinear inertia/hydrodynamic/restoring forces and $F(t)$ is the external excitation force, assumed to be a stationary non-Gaussian stochastic process. The response of the ship is governed by the equation

$$g(\vec{x}) = F(t) \tag{24}$$

where $\vec{x} = (x_1, x_2, x_3) = (x, \dot{x}, \ddot{x})$. The function $g(\vec{x})$ in principle depends on the entire history of the response. We assume here that $g(\vec{x})$ depends polynomially on $\vec{x}$. For a ship affected by linear inertia terms, a Morrison-type viscous damping and a restoring force exist and given as

$$g(\vec{x}) = (M + A)\ddot{x} + B|\dot{x}|\dot{x} + Cx + Dx^n \tag{25}$$

where M is the body mass, A is the hydrodynamic added mass, B is viscous damping coefficient, and C, D are the linear and nonlinear restoring coefficients respectively. In practice it is often sufficient to derive an equivalent linear system the statistical properties of which are in some sense a best approximation of the corresponding properties of (24)-(25). This system can be assumed to be of the form

$$m\ddot{x} + b\dot{x} + cx = F(t) \tag{26}$$

where the constants m, b, c are yet undetermined. An error function can be defined as

$$\varepsilon = g(\vec{x}) - m\ddot{x} - b\dot{x} - cx \tag{27}$$

which must be minimized in some way. The most common method is to minimize the mean square of ε with respect to the constants m, b, c, or

$$\frac{\partial}{\partial m} E[\varepsilon^2] = \frac{\partial}{\partial b} E[\varepsilon^2] = \frac{\partial}{\partial c} E[\varepsilon^2] = 0 \tag{28}$$

where $E[.]$ denotes the mean value of the quantity involved. The conditions (28) generate three nonlinear equations for m, b, c, the solutions of which in principle determine the desired constants.

The derivation and solution of these equations will be made clearer by using the notation

$$a_1 = m \quad a_2 = b \quad a_3 = c \tag{29}$$

$$x_1 = \ddot{x} \quad \mathrm{x}_2 = \dot{x} \quad \mathrm{x}_3 = x \tag{30}$$

Let

$$f(x_1, x_2, x_3) = m\ddot{x} + b\dot{x} + cx = a_1 x_1 + a_2 x_2 + a_3 x_3 \tag{31}$$

then ε^2 can be written as

$$\varepsilon^2 = (g - f)^2 = g^2 - 2gf - f^2 \tag{32}$$

where $g = F(t)$ by virtue of (24). Therefore, equations (28) reduce to the form

$$\frac{\partial}{\partial a_i} E[f^2] = 2\frac{\partial}{\partial a_i} E[fg] \tag{33}$$

where $a_i, i = 1,2,3$ are our unknowns.

It follows from (31) that

$$f^2 = a_1^2 x_1^2 + a_2^2 x_2^2 + a_3^2 x_3^2 + 2a_1 a_2 x_1 x_2 + 2a_1 a_3 x_1 x_3 + 2a_2 a_3 x_2 x_3 \tag{34}$$

Let us denote the symmetric covariance matrix of the random variable x_i, by C_{ji} as

$$[C] = C_{ij} = E[x_i x_j] = C_{ji} \tag{35}$$

It follows that

$$E[f^2] = a_1^2 C_{11} + a_2^2 C_{22} + a_3^2 C_{33} + 2a_1 a_2 C_{12} + 2a_1 a_3 C_{13} + 2a_2 a_3 C_{23} \tag{36}$$

A more compact notation can be obtained by introducing the vector

$$\vec{a} = \begin{pmatrix} a_1 \\ a_2 \\ a_3 \end{pmatrix} \tag{37}$$

We can now rewrite (36) as follows

$$E[f^2] = \vec{a}^T [C] \vec{a} \tag{38}$$

which is a quadratic form. It is now easy to verify

$$\begin{pmatrix} \frac{\partial E[f^2]}{\partial a_1} \\ \frac{\partial E[f^2]}{\partial a_2} \\ \frac{\partial E[f^2]}{\partial a_3} \end{pmatrix} = 2C\vec{a} = 2 \begin{pmatrix} E[x_1 g] \\ E[x_2 g] \\ E[x_3 g] \end{pmatrix} \tag{39}$$

where the relation

$$\frac{\partial}{\partial a_i} E[fg] = E[x_i g] \tag{40}$$

was used, making use of the property that $g = F$ is independent of a_i.

In equation (40), our unknowns are $\vec{a}$, $\vec{x}$ and the matrix C which is a function of $\vec{x}$. Therefore, a further reduction will be necessary. The quantity g is a known nonlinear function of $\vec{x}$, or

$$g = g(x_1, x_2, x_3) \tag{41}$$

as defined by (25). Let us consider the one-dimensional case $g = g(x)$ for the sake of simplicity and study the mean value

$$E[xg(x)] = \int_{-\infty}^{+\infty} xg(x)p(x)dx \tag{42}$$

where $p(x)$ is the probability density function of x, a priori unknown.

If we assume that x is a Gaussian process with zero mean and probability density function

$$p(x) = \frac{1}{\sqrt{2\pi}\sigma} e^{\frac{-x^2}{2\sigma^2}} \tag{43}$$

Taking the derivative $p'(x)$ we obtain the relation

$$xp(x) = -\sigma^2 p' \tag{44}$$

which upon substation in (42) leads to

$$E[xg(x)] = \sigma^2 \int_{-\infty}^{+\infty} g(x)p'(x)dx \tag{45}$$

An integration by parts leads to the desired result in the one-dimensional case

$$E[xg(x)] = \sigma^2 \int_{-\infty}^{+\infty} g'(x)p(x)dx = C_{11}E[g'(x)] \tag{46}$$

The extension of this result to the three-dimensional case follows along similar lines. Here it is important to recall that the random variables (x_1, x_2, x_3) are jointly Gaussian with probability density function.

The final expression generalizing (46) is

$$E[x_1 g(x_1, x_2, x_3)] = \sum_i C_{1i} E\left[\frac{\partial g}{\partial x_i}\right] \tag{47}$$

It follows that the right-hand side of (39)generalizes to $2[C]E[\nabla g]$ and the solution of (39) for the unknown vector $\vec{a}$ becomes explicit, or

$$\vec{a} = E[\nabla g(x_1, x_2, x_3)] \tag{48}$$

This is the principal result of the equivalent linearization-normalization technique. Therefore, under the condition that the processes x_1, x_2, x_3 are Gaussian, the vector $\vec{a}$ containing the equivalent linear mass a_1, damping a_2, and restoring coefficient a_3 are given by (48), assuming that the mean values in the right-hand side can be evaluated. At this point it is important to make use of the equation (31). The combination of (48) and (31) and the assumption that $F(t)$ is Gaussian leads to a nonlinear system of equations for (a_1, a_2, a_3) the solution of which is often possible in closed form.

2.6. The Equations of Roll Motion

When a vessel is advancing with forward speed in ambient waves, it will be subject to a time varying pressure distribution exerted on its hull. The pressure gives rise to time-dependent forces resulting in vessel time dependent oscillations in all or a subset of its six rigid body modes of motion $\xi_j(t)$, $j=1,...,6$. The application of Newton's 2nd law results in the following set of equations for dynamic equilibrium

$$\sum_j \left[M_{ij}\ddot{\xi}_j(t) + C_{ij}\xi_j(t) \right] = F_i(\ddot{\xi}_j, \dot{\xi}_j, \xi_j, t) \qquad i = j = 1,...,6 \tag{49}$$

M_{ij} is the vessel's inertial matrix, and C_{ij} is the matrix of the vessel's hydrostatic coefficients. The hydrodynamic forces F_i, depend on the history of the vessel's accelerations, velocities and displacements. They are in general non-linear quantities, but an assumption of small vessel motions and wave slopes justifies a linearization of the equations of motion.

As mentioned in the previous section, the frequency-domain version of the equations of motion will be stated here. These are related to their time-domain equivalents by a Fourier transform.

With the assumption of the vessel responses $\xi_j(t)$ being of the form of (20), the hydrodynamic forces F_i in (49) can be broken down to the following expression

$$F_i(t) = \mathrm{Re}\left\{ \left[X_i(\omega_0) + \left(\omega^2 A_{ij}(\omega) - i\omega B_{ij}(\omega) \right) \Xi_j \right] e^{i\omega t} \right\} \quad i = j = 1,...,6 \tag{50}$$

Substitution of (50) into equation (49) and dropping the real part operator results in the frequency-domain equations of motion

$$\sum_j \left[-\omega^2 \left(M_{ij} + A_{ij}(\omega) \right) + i\omega B_{ij}(\omega) + C_{ij} \right] \Xi_j = X_i(\omega) \quad i = j = 1,...,6 \tag{51}$$

For pure roll motion, decoupled from sway and yaw, the equation of motion is simply

$$\left[-\omega^2 \left(I_{44} + A_{44}(\omega) \right) + i\omega B_{44}(\omega) + C_{44} \right] \Xi_4 = X_4(\omega) \tag{52}$$

A_{ij} is the added mass coefficient matrix and B_{ij} is the damping coefficient matrix of the vessel. Note their dependence on the frequency of encounter, ω. $X_i(\omega) = A \cdot F_{ex_i}(\omega)$ is the complex

exiting force vector containing all Froude-Krylov and diffraction forces due to the incident wave with amplitude A. The amplitude of the exciting force is mostly a function of the absolute frequency of the ambient wave, ω_0. For high-speed vessels, forward speed effects will however be present. The three quantities discussed above are the only unknowns that have to be determined to solve for the principal unknowns Ξ_j, and they are found by solving the boundary value problem described in 2.1.

The RAO of an uncoupled roll motion can now be found from (51) after some manipulation as

$$\left|\frac{\Xi_4}{A \cdot k}\right| = \frac{\left|F_{ex_4}(\omega)\right|}{\left\{\left[C_{44} - \omega^2\left(I_{44} + A_{44}(\omega)\right)\right]^2 + \omega^2 B_{44}^2(\omega)\right\}^{1/2}} \tag{53}$$

where wavenumber k is introduced to make the roll RAO term a dimensionless value.

The roll RAO will, for any sea-state, give you the standard deviation of the roll response by making use of expression (22).

2.7. The Effect of Lifting Appendages on High-Speed Vessels' Roll Motion

Prandtl's lifting line theory was utilized as a mathematical model to approximate the lifting force on a finite aspect ratio lifting surface. Simply, the lifting forces from hydrofoils attached to the hull change the response of the ship creating anti-rolling moments about the ship centreline.

2.7.1. Prandtl's Lifting Line Theory

Here, only the very basic steps and results of Prandtl's lifting line theory will be given.

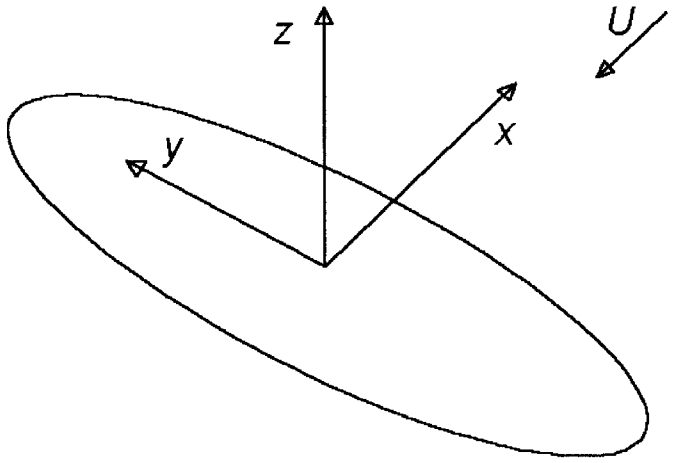

Figure 4: 3D Lifting Surface advancing at forward speed U

Prandtl's lifting line theory states that the three-dimensional lift force for a foil with span s and chord distribution $c(y)$ along the span advancing at forward speed U as shown in Figure 4 is given as

$$L = \frac{1}{2}\rho C_L S U^2 \tag{54}$$

where ρ is the fluid density, S is the planform area of the hydrofoil, U is the forward speed, and C_L is the three-dimensional lifting force coefficient. When the lifting surface advances with forward speed at some angle of attack, a wake sheet of free vortices inducing a downwash, or vertical fluid velocity, trails the foil. This downwash is the source of one of the most important three-dimensional effects of lifting surfaces, namely the induced drag D_i given as

$$D_i = \frac{1}{2}\rho C_D S U^2 \tag{55}$$

where C_D is the three-dimensional drag coefficient.

The lift and drag coefficients given by equations (54) and (55) respectively can be evaluated to simple expressions if an elliptic circulation distribution along the span s of a symmetric foil is assumed. This can be obtained by giving the lifting surface an elliptic geometrical shape, and the lift and drag coefficients can be given as

$$C_L = 2\pi \frac{AR}{AR+2}\alpha \tag{56}$$

$$C_D = 4\pi \frac{AR}{(AR+2)^2}\alpha^2 = \frac{C_L^2}{\pi AR} \tag{57}$$

The aspect ratio AR is for a three-dimensional lifting surface given as the ratio of the span s to the mean chord c_0. In general, aspect ratio is defined as

$$AR = \frac{s^2}{S} \tag{58}$$

In this case, with the lifting surface having an elliptical geometry, the aspect ratio becomes $AR = \frac{4s}{\pi c_0}$.

Prandtl's lifting line theory is strictly speaking only valid for large aspect ratios. It has however proven to give remarkably good results even for relatively small aspect ratios, with small relative errors. It is also important to emphasize that the lifting line theory is only valid for "thin" lifting surfaces at relatively small angles of attack. If the angle of attack exceeds approximately 12-13 degrees (depending on geometry and thickness of the foil), the physical phenomenon of stall will occur. Stall is a condition where the flow separates at the leading edge of the foil, and lift is lost.

2.7.2. The Influence of Lifting Appendages on the Roll Equations of Motion

The introduction of lifting appendages on the vessel alters the damping and restoring coefficients and the exciting force of the vessel. For a given vessel speed, hydrofoil size and hydrofoil shape, the lift force given by equation (54) will according to Prandtl's lifting line theory only depend on the time-dependent hydrofoil angle of attack $\alpha(t)$.

When advancing with forward speed U in ambient waves, the vessel, and thus the hydrofoil, will undergo oscillatory displacements altering the foil's effective angle of attack. The effective angle of attack will be further altered by fluid velocity components due to the

downwash of the foil and the wave velocity components. The result is a time-dependent angle of attack $\alpha(t)$, which at any time t is given as

$$\alpha(t) = \alpha_0 - \xi_5(t) + \frac{\frac{\partial \phi_I}{\partial z} - \dot{\xi}_3(t) - y_{foil}\dot{\xi}_4(t) + x_{foil}\dot{\xi}_5(t)}{U + \dot{\xi}_1(t) - \frac{\partial \phi_I}{\partial x}} \tag{59}$$

where ξ_5 is the pitch angle, $\dot{\xi}_1$ is the surge velocity, $\dot{\xi}_3$ is the heave velocity, $\dot{\xi}_4$ is the roll velocity, $\dot{\xi}_5$ is the pitch velocity, ϕ_I is the incident wave potential and x_{foil} and y_{foil} is the longitudinal and transverse position of the hydrofoil with respect to the origin of the coordinate system (x, y, z) located at midship.

A safe assumption for high-speed vessels is that the forward speed U is much greater than the surge velocity and wave velocity in the x-direction. α_0 is assumed to be zero during this study. These assumptions justify a linearization of (59), resulting in the following expression for $\alpha(t)$

$$\alpha(t) = -\xi_5(t) + \frac{\frac{\partial \phi_I}{\partial z} - \dot{\xi}_3(t) - y_{foil}\dot{\xi}_4(t) + x_{foil}\dot{\xi}_5(t)}{U} \tag{60}$$

Then, the time-dependent lift force for a hydrofoil attached to a vessel advancing with forward speed U in ambient waves can be written in the form

$$L(t) = \mathrm{Re}\left\{L_{3D}e^{i\omega t}\right\} \tag{61}$$

By combining (61) with (60) and the expression for the vessel responses (20), L_{3D} is found as

$$L_{3D} = F\left[-\Xi_5 - \frac{1}{U}i\omega\Xi_3 + \frac{x_{foil}}{U}i\omega\Xi_5 - \frac{y_{foil}}{U}i\omega\Xi_4 + \frac{1}{U}\frac{\partial \phi_I}{\partial z}\right] \tag{62}$$

with F defined as

$$F = \pi\rho SU^2\frac{AR}{2+AR} \tag{63}$$

The validity of the expressions (59)-(63) is based on the assumption of quasi-steady flow around the lifting appendage. This assumption is valid for small reduced frequencies, Ω, where

$$\Omega = \frac{\omega c}{U} \tag{64}$$

For all practical seakeeping problems where lifting appendages are involved, the vessel velocity U is reasonably high. The product of the chord, c, and the frequency of encounter, ω, will be a small quantity compared to U, and an assumption of small reduced frequency may thus be justified.

The vertical force given by (62) may now be included in the decoupled roll equation of motion (52), resulting in the following equation

$$\begin{aligned} &-\omega^2(I + A_{44})\Xi_4 + i\omega B_{44}\Xi_4 + C_{44}\Xi_4 = \ldots \\ &X_4 + \sum_{i=1}^{2}\left[y_i \times F(-\Xi_5 - \frac{1}{U} i\omega\Xi_3 + \frac{x_i}{U} i\omega\Xi_5 - \frac{y_i}{U} i\omega\Xi_4 + \frac{1}{U}\frac{\partial}{\partial z}\phi_I(x_i, y_i)\right] \end{aligned} \tag{65}$$

In the statement of (62), surge motions are neglected.

Collecting terms proportional to the complex amplitudes Ξ_3, Ξ_4 and Ξ_5 and the exciting forces from equation (65), the damping and restoring coefficients and exciting forces with lifting appendages present become

$$B_{44}^{\ with\_foil} = B_{44} + \sum_{i=1}^{2} y_i^{\,2} \cdot \frac{F}{U} \tag{66}$$

$$B_{43}^{\ with\_foil} = \sum_{i=1}^{2} y_i \cdot \frac{F}{U} \tag{67}$$

$$B_{45}^{\ with\_foil} = -\sum_{i=1}^{2} y_i \cdot x_i \cdot \frac{F}{U} \tag{68}$$

$$C_{44}^{\ with\_foil} = C_{44} \tag{69}$$

$$C_{45}^{\ with\_foil} = \sum_{i=1}^{2} y_i \cdot F \tag{70}$$

$$X_4^{with\_foil} = X_4 + \sum_{i=1}^{2} \frac{i\omega}{U} \cdot y_i \cdot F \cdot e^{-k \cdot T - ik(x_i \cdot \cos\beta + y_i \cdot \sin\beta)} \tag{71}$$

In (66)-(71), F is given by equation (63), T is the foil draft, U is the vessel speed, β is the wave heading, and k is the wave number of the ambient waves. If the lateral distances from centerline (y_i) are equal for port and starboard hydrofoils, normally they are, the equations (67), (68) and (70) become zero. Thus, in general, only $B_{44}^{with\_foil}$ and $X_4^{with\_foil}$ terms affect the equation of roll motion for passive hydrofoil roll control case. The detailed analysis on these new terms will be performed in the following chapter.

2.8. Panel Methods

Panel methods are developed to solve complex, open form, three-dimensional fluid dynamic problems where greater accuracy is required. Panel methods are based on potential flow theory where oscillating amplitudes of the fluid and the body are small relative to the dimensions of the body cross-section.

Panel method relies on the assumption that any irrotational, incompressible flow can be represented by a proper distribution of sources, sinks or doublets over its bounding surfaces. A source is defined as a point from which a fluid is imagined to flow out uniformly in all directions. A sink is a 'negative' source, where fluid is 'sucked' in uniformly. A doublet is a combination of source and sink. G represents the potential of a source at an arbitrary point inside a control volume such that

$$G = -\mu \frac{1}{4\pi} \cdot \frac{1}{r} \tag{72}$$

where r is the distance from the source to the arbitrary point where the potential is to be evaluated and μ is the 'strength' of the source, defined as the total flux outwards (or inwards) across a small closed surface surrounding the arbitrary point.

The governing mathematical identity utilized to solve fluid hydrodynamic problems is called Green's second Identity, which is derived from the divergence theorem.

$$\int_{CV} \left(\phi \nabla^2 G - G \nabla^2 \phi\right) dV = \int_{CS} \left(\phi \frac{\partial G}{\partial n} - G \frac{\partial \phi}{\partial n}\right) dS \tag{73}$$

This identity basically relates the governing equation of the physical problem to the velocity potential on the bounding surfaces of the boundary value problem. On the left hand side of the identity the second term turns into zero due to Laplace Equation. This fact indicates that an infinite control volume problem in space is reduced to a finite closed form problem over the bounding surfaces of the body.

Rankine Source potential with unit strength takes the explicit form of

$$G(x,y,z,\xi,\eta,\zeta) = -\frac{1}{4\pi}\frac{1}{r} = -\frac{1}{4\pi}\frac{1}{\left[(x-\xi)^2+(y-\eta)^2+(z-\zeta)^2\right]^{1/2}} \tag{74}$$

(x, y, z) is the vector pointing to an arbitrary point in space and (ξ,η,ζ) is the vector pointing to the source point.

Using the Rankine Source as the Green Function in equation (73), and substitution of required boundary conditions reduces (73) into two integro-differential equations which is solved by SWAN-2 and described on the next chapter.

3. SWAN-2 Implementation

SWAN-2 is a state of the art general purpose Rankine Panel Method for the solution of the time-domain free surface flows and responses of ships, high-speed vessels and stationary structures from zero to high speeds. In this chapter, a brief introduction on SWAN-2 will be given. For further detailed information, one can be referred to [3], [4] and [23].

3.1. Formulation

The ship illustrated in Figure 5 advances with a constant forward speed U in the direction of the positive x-axis. The (x, y, z) reference coordinate system is fixed on the mean position of the vessel with $z = 0$ corresponding to the calm position of the free surface.

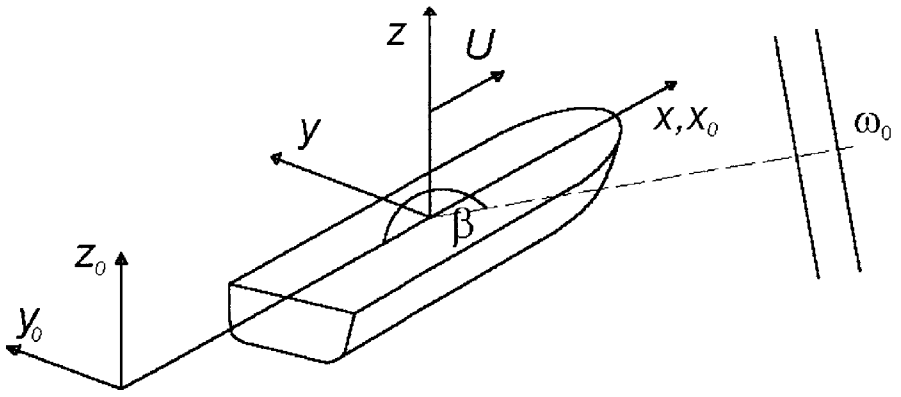

Figure 5: Illustration of SWAN-2 Coordinate System

The boundary value problem is solved relative to the (x, y, z) translating coordinate system. The water depth H may be finite and uniform. Regular plane progressive waves are incident on the ship, with absolute frequency ω_0 relative to the earth fixed coordinate system (x_0, y_0, z_0) and heading β relative to the positive x-axis; $\beta = 180°$ corresponds to head waves and $\beta = 0°$ to following waves.

In SWAN-2, by using perturbation theory and linearity, the total velocity potential $\Phi(\vec{x},t)$ can be decomposed into three components.

$$\Phi(\vec{x},t) = \phi_0(\vec{x}) + \phi_I(\vec{x},t) + \phi(\vec{x},t) \tag{75}$$

$\phi_0(\vec{x})$ is the double body basis flow. A double body flow is the flow past the vessel and her positive image above the free surface, resulting in the free surface acting as a rigid lid. The basis flow is subject to the Laplace equation in the fluid domain and zero normal flux on $z=0$. The selection of the double body as the basis flow is one important difference between SWAN-2 and previous attempts to solve the hydrodynamic problems of seakeeping and wave resistance. Discussions of this issue can be found in [7], [17] and [23]. $\phi_I(\vec{x},t)$ is the incident wave potential of a plane progressive wave as given by equation (3). Finally, $\phi(\vec{x},t)$ is the time-dependent wave disturbance potential due to the vessel displacement around its mean position. This potential arises from steady dynamic sinkage and trim, wave radiation due to rigid ship motions in waves, and diffraction of the incident potential $\phi_I(\vec{x},t)$.

The two primary assumptions behind the linearization of the free surface conditions and the body boundary conditions satisfied by the time-dependent disturbance potential $\phi(\vec{x},t)$ are $|\nabla\phi| << |\nabla\phi_0|$ and $|\eta(\vec{x},t)| << |\eta_0(\vec{x})|$, where $\eta(\vec{x},t)$ denotes the free surface elevation due to each disturbance. The assumptions above indicate that the velocity potential and wave disturbance due to the basis flow is assumed to be much larger than the corresponding quantities for the disturbance flow.

3.2. Linearization of Boundary Value Problem

With the double body flow as the basis flow, the basis wave elevation follows from equation (9)

$$\eta_0 = \frac{U}{g}\frac{\partial\phi_0}{\partial x} - \frac{1}{2g}\nabla\phi_0 \cdot \nabla\phi_0 \tag{76}$$

By virtue of assumptions explained in 3.1. , the free surface conditions (7) and (9) can be linearized about the $z=0$ plane. This leads to the following conditions for the disturbance potential $\phi(\vec{x},t)$ and wave elevation $\eta(\vec{x},t)$

$$\left[\frac{\partial}{\partial t}-(\vec{U}-\nabla\phi_0)\cdot\nabla\right]\eta=\frac{\partial^2\phi_0}{\partial z^2}\eta+\frac{\partial\phi}{\partial z}\quad \text{on } z=0 \tag{77}$$

$$\left[\frac{\partial}{\partial t}-(\vec{U}-\nabla\phi_0)\cdot\nabla\right]\phi=-g\eta+\left[\vec{U}\cdot\nabla\phi_0-\frac{1}{2}\nabla\phi_0\cdot\nabla\phi_0\right]\quad \text{on } z=0 \tag{78}$$

In the derivation of (77) and(78) , it is assumed that η_0 is a sufficiently small quantity for the statements (77) and (78) to be transferred to the *z=0* plane with small error.

By assuming small oscillatory displacements of the vessel, linearization of the exact body boundary condition can be performed by evaluating these at its mean translating position. By virtue of the decomposition of the velocity potential into basis, incident, and disturbance components, the body boundary conditions can now be evaluated for each component separately. The basis flow $\phi_0(\vec{x})$ is subject to the following boundary condition on the mean vessel position $\overline{S}_B$

$$\frac{\partial\phi_0}{\partial n}=\vec{U}\cdot\vec{n}\ \text{ on }\ \overline{S}_B \tag{79}$$

The vessel's oscillatory displacements and rotations due to ambient waves may be written $\xi_j(t)$, $j=1,..,6$. The time-dependent disturbance velocity potential $\phi(\vec{x},t)$ may then be decomposed as follows

$$\phi=\sum_{j=1}^{6}\phi_j+\phi_7 \tag{80}$$

ϕ_j are the radiation potentials corresponding to each displacement mode *j*, and ϕ_7 is the diffraction potential . By virtue of linearity, all velocity potentials in (80) satisfy the free surface conditions (77) and (78), and they are subject to the following body boundary conditions

$$\frac{\partial \phi_7}{\partial n} = -\frac{\partial \phi_I}{\partial n} \text{ on } \bar{S}_B \tag{81}$$

$$\frac{\partial \phi_j}{\partial n} = \sum_{j=1}^{6}\left(\frac{\partial \xi_j}{\partial t} n_j + \xi_j m_j\right) \text{ on } \bar{S}_B \tag{82}$$

ϕ_I is the ambient wave potential, and the n_j and m_j terms are given as

$$(n_1, n_2, n_3) = \vec{n} \tag{83}$$

$$(n_4, n_5, n_6) = \vec{x} \times \vec{n} \tag{84}$$

$$(m_1, m_2, m_3) = (\vec{n} \cdot \nabla)(\vec{U} - \nabla \phi_0) \tag{85}$$

$$(m_4, m_5, m_6) = (\vec{n} \cdot \nabla)\left[\vec{x} \times (\vec{U} - \nabla \phi_0)\right] \tag{86}$$

Together with conditions (13) and (14), the linearized equations in this section complete the statement of the linearized BVP solved numerically by SWAN-2. Special cases of this BVP utilized in solving the problems of interest in this thesis are outlined in the following sections. For a complete overview of SWAN-2 applications, refer to [3] and [4].

3.3. Ship Seakeeping with Forward Speed

This is the most general case, and involves solving the complete set of boundary value problems for all unknown velocity potentials ϕ_i, i=0,...,7. The basis flow ϕ_0 is subject to conditions (79) and zero normal flux on $z = 0$, while the disturbance potential $\phi(\vec{x},t)$ is subject to conditions (77), (78), (81) and (82). The output from SWAN-2 will be various seakeeping quantities of interest. A complete list of possible output parameters can be found in the [4].

3.3.1. Transom Sterns

Another interesting application covered by SWAN-2 is the possibility of modelling thin lifting wake sheets in the fluid domain. This makes the solution of steady and unsteady flow past transom stern vessels possible.

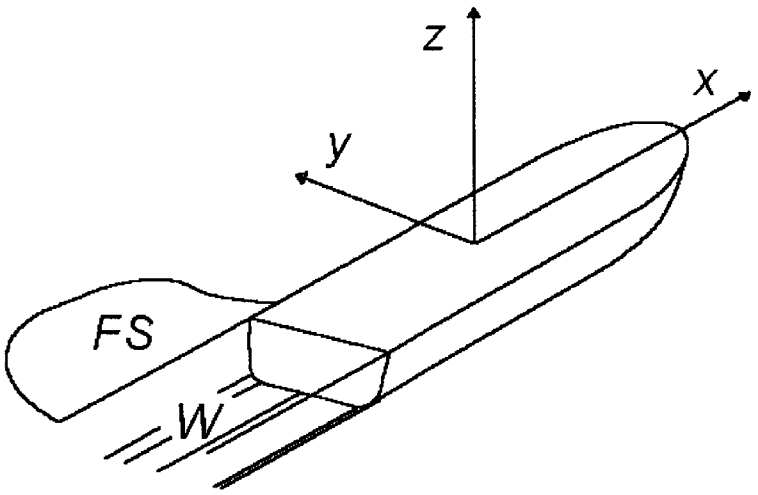

Figure 6: Transom Stern Vessel with Free Surface Wake W.

Lifting surface theory provides the tools necessary for solving this problem by forcing the velocity potential to satisfy the so-called Kutta condition at the vessel's transom. The Kutta condition requires smooth detachment of the flow at the transom, resulting in finite fluid velocity at the transom's trailing edge, which leaves the rest of the transom dry. The dry transom is the source of the induced resistance. The total velocity potential $\Phi(\vec{x},t)$ must also be continuous over the free surface wake *W*.

The linearized free surface conditions (77) and (78) are enforced on the free surface wake *W* downstream of the transom as well as on the rest of the free surface *FS*. At the transom, the dynamic Kutta condition imposes a dynamic pressure on the free surface that balances the hydrostatic pressure due to the given transom draft. Along with the kinematic Kutta condition, this ensures continuity in pressure along the detaching streamlines of the transom. For details about the derivation and mathematical statements of the Kutta conditions, see [7].

3.3.2. Motion Control Lifting Appendages

It is common in high-speed vessel design to include motion control lifting appendages for the purpose of altering ship motions in waves and its steady dynamic sinkage / trim in calm water.

It is possible, in SWAN-2, to add these appendages to the hull. In the present version, only passive lifting appendages can be modeled.

The motion control lifting appendages are modeled as point forces at user-specified positions on the hull. The mathematical model utilized is Prandtl's lifting line theory, as outlined in section 2.7.1. Hydrodynamic interaction between the appendages and hull are not accounted for. SWAN-2 does, however, account for effects due to the vessel's forward speed U, the incident wave velocity vector, rigid body linear and angular displacement vector, and rigid body linear velocity and angular velocity vector. Induced drag from lifting appendages is not accounted for, and the user must evaluate the added resistance due to the presence of a lifting appendage separately.

The lift force L for a lifting appendage attached to a vessel with constant forward speed in calm water is found from equation (54). For a vessel advancing in ambient waves, the effective angle of attack will be a function of time due to the vessel's displacements $\xi_j(t)$ and the wave velocity vector. The time-dependent contribution to the angle of attack utilized by SWAN-2 is given by expression (60), and the corresponding time dependent lift force $L(t)$ is given by equation (62).

The total lift force is assumed to act vertical at the center point of the lifting appendage. Its contribution to the total force and moment acting on the vessel is then included in the equations of motions in the manner outlined in section 2.7.2.

3.4. Numerical Solution

The boundary value problems governed by equations(13), (14), (77), (78), (79), (81), (82) for the basis and disturbance flow are solved in SWAN-2 by making use of Green's 2nd identity (73) for the velocity potential and its normal derivative over the fluid domain boundaries. The Rankine point source given by equation (74) is used as the unit strength Green function. The ship's mean wetted surface is denoted by $\overline{S}_B$, the free surface by FS, and the free surface

wake sheets behind the transom by W. The application of Green's 2nd identity then leads to the following integral equation for the velocity potentials of the BVP of section 3.2 and their normal derivatives over the fluid domain boundaries

$$-\frac{1}{2}\phi(\vec{\xi},t)+\iint_{\bar{S}_B+FS+W^{\perp}}\phi(\vec{x},t)\frac{\partial G(\vec{x};\vec{\xi})}{\partial n_x}dS_x-\iint_{\bar{S}_B+FS}\frac{\partial\phi(\vec{x},t)}{\partial n_x}G(\vec{x};\vec{\xi})dS_x=0 \qquad (87)$$

where $\vec{x}=(x,y,z)$ and $\vec{\xi}=(\xi,\eta,\zeta)$.

The contribution from a closed surface at infinity vanishes due to the decay of $\phi(\vec{x},t)$ and $G(\vec{x};\vec{\xi})$ as $|\vec{x}|\to\infty$ for fixed values of $\vec{\xi}$ and t. In equation (87), $\phi(\vec{x},t)$ can represent either the basis or any of the disturbance potentials, and equation (87) can thus be utilized to solve all the linearized boundary value problems defined in section 3.2.

The normal gradient ϕ_n is known on the body surface $\bar{S}_B$. On the free surface, ϕ_n equals to ϕ_z since the unit normal vector points out of the fluid domain. The free surface conditions (77) and (78) are then invoked to relate the normal gradients of ϕ to the tangential gradients of ϕ and ζ. The result is an integro-differential equation solved by the Rankine Panel Method implemented in SWAN-2. Over the wake panels W in the fluid domain, the jump in the potential $\phi^+-\phi^-\equiv\Delta\phi$ is equal to the corresponding value at the upstream transom trailing edge via the enforcement of the Kutta condition.

3.4.1. Spatial Discretization

The vessel surface $\bar{S}_B$ and the free surface FS are subdivided into a large number of quadrilateral panels as shown in Figure 7.

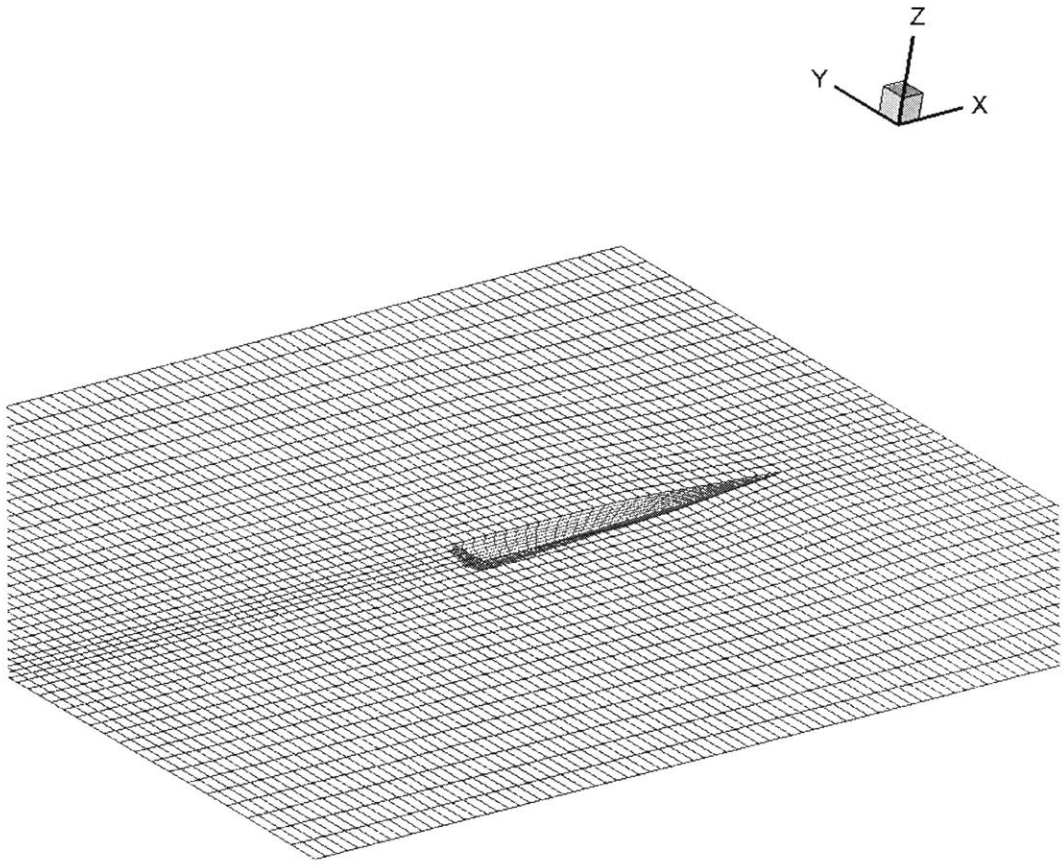

Figure 7: Spatial Discretization of Vessel and Free Surface

Over the surfaces $\overline{S}_B$ and FS, the velocity potential ϕ and wave elevation η are approximated by the following bi-quadratic spline variation

$$\phi(\vec{x},t) \cong \sum_j \phi_j(t) B_j(\vec{x}) \tag{88}$$

$$\eta(\vec{x},t) \cong \sum_j \eta_j(t) B_j(\vec{x}) \tag{89}$$

The basis functions $B_j(\vec{x})$ are bi-quadratic in the local variables, ensuring the value and the first derivative of ϕ and η to be continuous across the panels. The coefficients ϕ_j and η_j are

not identical to the values of the velocity potential and wave elevation at the center of the panels but linearly related to them through the spline coefficients of the respective panels.

3.4.2. Temporal Discretization

In time domain flows, a time-marching scheme for the approximation of the time derivatives of the state variables $\Phi(\vec{x},t)$ and $\eta(\vec{x},t)$ must be selected. In SWAN-2, the kinematic free surface condition (77) is satisfied through an implicit Euler discretization for the past solution at time $t=t_n$. The dynamic free surface condition (78) is satisfied through an explicit Euler discretization at the present time $t=t_{n+1}$. The resulting method is a mixture of both implicit and explicit discretization methods and referred to as an emplicit Euler scheme. For details about the emplicit Euler scheme, see [7].

3.4.3. Stability of Temporal Discretization

The free surface discretization is characterized by two parameters. These are the panel aspect ratio α, and the grid Froude number F_h as given below

$$\alpha = \frac{h_x}{h_y} \tag{90}$$

$$F_h = \frac{U}{\sqrt{g h_x}} \tag{91}$$

h_x and h_y are the panel dimensions in the streamwise and transverse directions respectively. The result of stability analyses of time-domain time marching schemes are a criterion restricting the non-dimensional time step β

$$\beta = \frac{\sqrt{h_x / g}}{\Delta t} \tag{92}$$

[18] and [26] analyzed in detail the stability properties of the emplicit Euler scheme utilized by SWAN-2. Their result is given in Figure 8, borrowed from [23], illustrating the critical value of β as a function of F_h and α.

Note that high ship speeds require smaller time steps, and thus longer execution time with the emplicit Euler scheme.

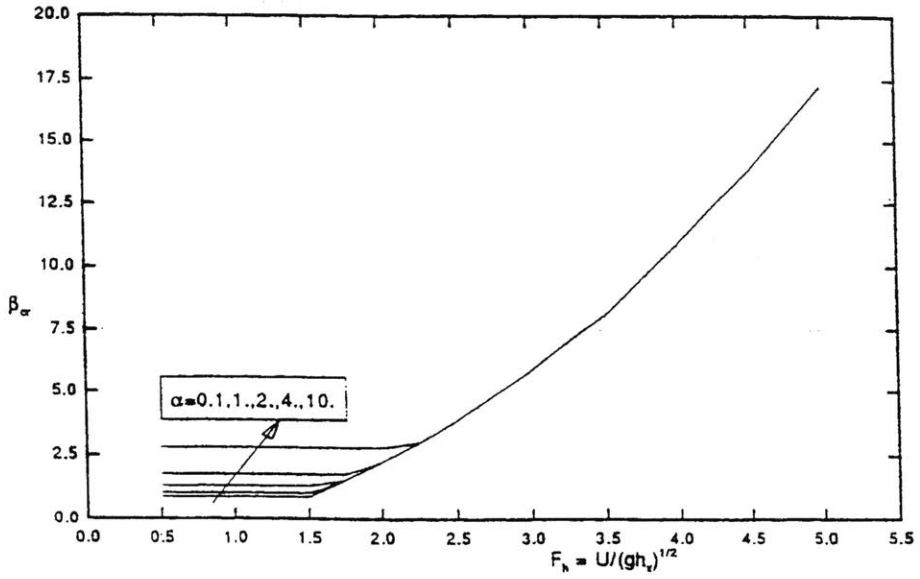

Figure 8: Stability Diagram for Emplicit Euler Time Marching Scheme

3.4.4. Radiation Condition

In the RPM method implemented in SWAN-2, the radiation condition is enforced by the design of a dissipative absorbing beach surrounding the free surface mesh as shown in Figure 9 borrowed from [7].

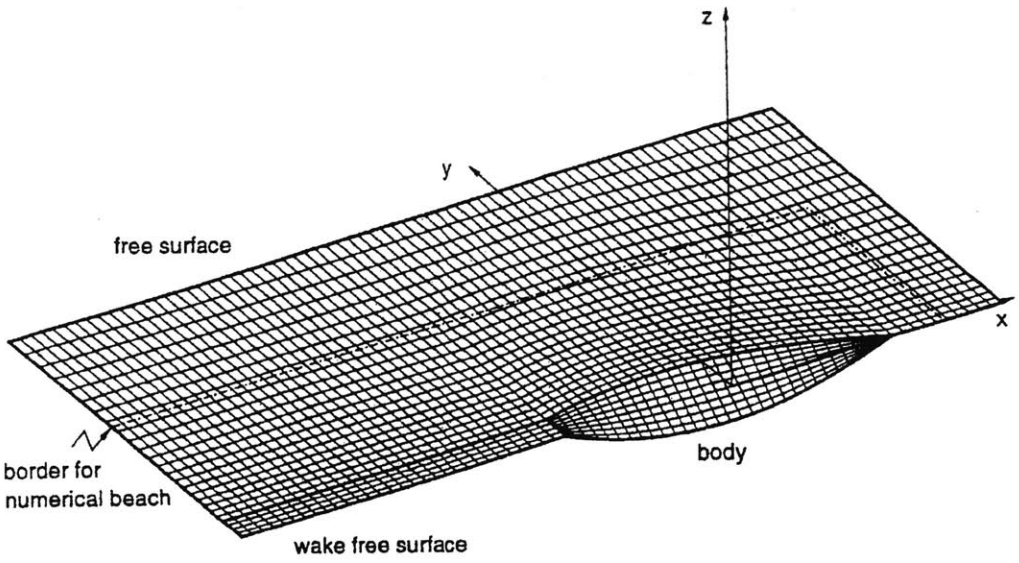

Figure 9: Dissipative Absorbing Beach surrounding the Free Surface Mesh

On the dissipative beach, the following two free surface conditions are enforced on the disturbance potential $\phi(\vec{x},t)$

$$(\frac{\partial}{\partial t}-U\frac{\partial}{\partial x})\eta=\frac{\partial\phi}{\partial z}-2\nu\eta+\frac{\nu^2}{g}\phi \tag{93}$$

$$(\frac{\partial}{\partial t}-U\frac{\partial}{\partial x})\phi=-g\eta \tag{94}$$

In the zero speed case, the conditions (93) and (94) lead to the dispersion relation

$$\omega=i\nu\pm\sqrt{gk} \tag{95}$$

The strength of the damping parameter ν is a function of the transverse spatial coordinate, and it increases towards the outer edge of the beach. At the inner edge, $\nu=0$, which ensures continuity in the transition between the beach and the free surface mesh. A more detailed description of construction and performance of the numerical beach can be found in [19].

3.4.5. Meshing

The domain boundaries in SWAN-2 are discretized by panel sheets of rectangular topology. SWAN-2 supports a total of 7 different types of panel sheets. These are listed below with a brief description of their main features. A more thorough documentation can be found in [3].

1. The free surface sheet. The free surface conditions (77) and (78) are applied for the velocity potential and the wave elevation in combination with Green's identity (73). At the boundary of the sheet, the condition of zero second derivative for ϕ and η are applied.

2. The free surface sheet that meets the hull upstream at the transom stern. Conditions are as for sheet 1 except at the transom stern, where the Kutta-type conditions described earlier are invoked to ensure continuity of ϕ and η.

3. This sheet is similar to sheet 1, but with an oval instead of rectangular panel shape. This must be used with caution if wave resistance is studied.

4. Sheet 4 is used to discretize the submerged part of the vessel. The body boundary conditions (79), (81) and (82) are enforced on the sheet, specifying a known normal velocity.

5. Sheet 5 is identical to sheet number 4, except for the Kutta condition invoked at the trailing edge of the vessel. This sheet could for instance be used to discretize the struts of a SWATH vessel.

6. This sheet is a fluid domain lifting wake sheet for the discretization of vertical or horizontal thin struts. A Kutta-type condition is invoked at the trailing edge, ensuring the velocity potential jump to be continuous from the solid boundary into the fluid domain, and thus a finite fluid velocity at the trailing edge.

7. The free surface sheet 7 corresponds to the dissipative beach, ensuring the enforcement of the radiation conditions (93) and (94). This sheet absorbs the energy of the wave disturbance radiated and diffracted by the vessel hull.

The discretization and enforcement of the proper conditions are done automatically by SWAN-2 based on the input information provided by the user.

3.4.6. Flow Solver

The enforcement of the free surface conditions (77), (78), and the body boundary conditions (79), (81), and (82) into Green's identity (73), leads to an integral equation in space and a system of ordinary differential equations in time for the problem unknowns over the panels of the domain mesh. These unknowns are

- The basis flow spline coefficients $(\phi_0)_i(t)$ $i=0,\ldots\ldots,N$
- The wave disturbance flow spline coefficients $\phi_i(t)$ $i=0,\ldots\ldots,N$
- The free surface elevation spline coefficients $\zeta_j(t)$ $j=0,\ldots\ldots,N_F$

N is the total number of discretized panels over the domain boundary, while N_F is the number of panels over the free surface-type sheets. For port/starboard symmetric vessels, only half of the domain needs to be discretized, and SWAN-2 automatically generates the image sheets.

The velocity potential ϕ and wave elevation η are then solved for each time step in the emplicit Euler scheme described in section 3.4.1 according to equations (88) and (89) respectively.

3.4.7. Hydrodynamic Pressure

The velocity potential ϕ and wave elevation η are evaluated for each time step by equations (88), (89), and their respective tangential gradients are evaluated on the midpoint of the mapped domain panels. The hydrodynamic pressure follows from application of Bernoulli's equation (6) on the total velocity potential given by equation (3).

To properly account for the memory effects present in the seakeeping problem, SWAN-2 further decomposes the wave disturbance potential into two new components

$$\phi(\vec{x},t)=\psi(\vec{x})+\varphi(\vec{x},t) \tag{96}$$

The velocity potential $\psi(\vec{x})$ is known as the impulsive velocity potential, and it enjoys the following properties

$$\psi(\vec{x})=0 \quad \text{on } FS \tag{97}$$

$$\frac{\partial\psi}{\partial n}=\vec{V}_B\cdot\vec{n} \quad \text{on } \overline{S}_B \tag{98}$$

Equation (97) states that the impulse velocity potential vanishes at the free surface, while equation (98) states that the normal derivative of the impulse velocity potential, by virtue of linearity, equals the right hand side of equations (81) and (82). Because $\psi(\vec{x})$ vanishes at the free surface, all wave effects are included in $\varphi(\vec{x},t)$. This potential satisfies a free surface condition obtained by substitution of (96) into (77) and (78).

$$\frac{\partial\varphi}{\partial n}=0 \quad \text{on } \overline{S}_B \tag{99}$$

The decomposition of the wave disturbance potential $\phi(\vec{x},t)$ into the impulse component $\psi(\vec{x})$ and the residual component $\varphi(\vec{x},t)$ is essential in order to ensure stability of the time marching algorithm for the treatment of the vessel's equation of motions.

For a fixed point in the fluid domain the hydrodynamic pressure is given by Bernoulli's equation as

$$p(\vec{x},t)=-\rho\left[\left(\frac{\partial}{\partial t}-(\vec{U}-\nabla\phi_0)\cdot\nabla\right)\Phi+\frac{1}{2}\nabla\Phi\cdot\nabla\Phi+gz\right] \tag{100}$$

In (100), all time derivatives are with respect to the coordinate system that translates with the vessel's mean position with velocity $\vec{U}$.

By virtue of the decomposition of the velocity potential by equations (75) and (96), the hydrodynamic pressure at a fixed point in the fluid domain can be obtained in terms of the

component potentials. It is interesting to note that the basis potential $\phi_0(\vec{x})$ and the impulse potential $\psi(\vec{x})$ are only functions of space, and thus time independent.

The definition of the hydrodynamic pressure over the vessel surface is a more challenging matter due to the fact that the vessel position is constantly changing with time relative to the translating coordinate system (*x,y,z*). Denote by $\vec{\delta}(t)$ the displacements of a panel center positioned somewhere on the submerged vessel's surface. Also denote the vessel's linear displacements $\vec{\xi}(t)$ and angular rotations $\vec{\alpha}(t)$ about the (*x,y,z*) axes as

$$\vec{\xi}(t) = (\xi_1, \xi_2, \xi_3) \tag{101}$$

$$\vec{\alpha}(t) = (\xi_4, \xi_5, \xi_6) \tag{102}$$

It then follows that the panel center displacement $\vec{\delta}(t)$ is given as

$$\vec{\delta}(t) = \vec{\xi} + \vec{\alpha} \times \vec{x} \tag{103}$$

For small values of $\vec{\delta}(t)$, a Taylor series expansion of the pressure on the time-dependent position of the ship hull about the mean hull position $\overline{S}_B$ will lead to the following expression for the pressure at the center of each panel

$$p(\vec{x},t)_{S_B(t)} = p(\vec{x},t)_{\overline{S}_B} + \vec{\delta} \cdot \nabla p_{\overline{S}_B} + O(\delta^2) \tag{104}$$

The spatial gradients of the hydrodynamic pressure given by Bernoulli's equation (6), involves first and second order derivatives of the velocity potential components $\phi_0(\vec{x})$, $\phi(\vec{x},t)$, $\psi(\vec{x})$ and $\varphi(\vec{x},t)$. These are all evaluated by direct differentiation of expression (88). Equation (100) is the fundamental form of Bernoulli's equation utilized by SWAN-2 for calculation of steady and time dependent forces acting on the vessel hull.

3.4.8. Hydrodynamic Forces

The hydrodynamic forces exerted by the fluid on the vessel hull are essential for the derivation of the vessel's equations of motion through application of Newton's 2nd law. The same hydrodynamic forces are also necessary for the evaluation of structural loads.

The hydrodynamic pressure at the center of each panel at the instantaneous position of the vessel is given by equation (104) with errors quadratic in the vessel displacements.

$\vec{n} = (n_1, n_2, n_3)$ is the unit normal vector pointing out of the fluid and into the vessel. Its value on the instantaneous position of the ship hull is defined as

$$\vec{n}(t) = \vec{\alpha} \times \vec{n} + O(\delta^2) \tag{105}$$

The force exerted by the fluid on the moving vessel is then given as

$$\vec{F}_h(t) = \iint_{S_B(t)} p(\vec{x}, t)\vec{n}(t)dS \tag{106}$$

$S_B(t)$ is the instantaneous wetted surface of the vessel hull, $p(\vec{x}, t)$ is given by equation (104), and $\vec{n}(t)$ is given by equation (105).

The corresponding moment about the reference axes (x, y, z) moving with the ship mean position is given by the following expression

$$\vec{M}_h(t) = \iint_{S_B(t)} p(\vec{x}, t)\vec{x}(t) \times \vec{n}(t)dS \tag{107}$$

$$\vec{x}(t) = \vec{x} + \vec{\delta} \tag{108}$$

where $\vec{x} = x\vec{i} + y\vec{j} + z\vec{k}$ and $\vec{\delta}(t)$ are defined by expression (103).

The definition of the hydrodynamic forces and moments over the ship surface S_B represented by equations (105)-(108) now makes it possible to derive the equations of motion applying Newton's second law. They also represent the basis for the evaluation of structural wave induced loads and the vessel's wave resistance and induced resistance in calm water.

The linearization of expressions (106) and (107) about the mean vessel position $\overline{S}_B$ is necessary for two reasons

1. All quantities evaluated by SWAN-2 are known over panels located at $\overline{S}_B$.
2. The linearization will reveal the steady, linear and quadratic components of the forces and moments as individual effects.

The time-dependent wetted surface of the vessel, $S_B(t)$, can be expanded about its mean position in a similar way as for the hydrodynamic pressure (104) and the normal vector (105), yielding

$$S_B(t) = \overline{S}_B + dS(t) + O(\delta^2) \tag{109}$$

where dS is the part of the wetted surface near the waterline. If dl is the differential length of a segment along the waterline of a vessel, and $\eta(t)$ is the wave elevation along the same waterline, dS may be defined as follows

$$dS(t) = dl\left(\eta - \vec{\delta}\cdot\vec{k}\right)_{WL} \tag{110}$$

In (110), dS is defined for a wall-sided vessel, but SWAN-2 can also treat vessels with significant flare in the fore and aft ship. $\vec{\delta}(t)$ is given by equation (103), and $\vec{k}$ is the unit normal in the z-direction.

The wave elevation $\eta(t)$ accounts for all time dependent wave effects including the incident waves while the displacement vector $\vec{\delta}(t)$ accounts for the vessels motions in waves and steady dynamic sinkage and trim.

The linearized hydrodynamic force exerted from the fluid on the body now takes the form

$$\vec{F}_h(t) = \iint_{\overline{S}_B} p(\vec{x},t)\vec{n}(t)dS + \oint_{WL} p(\vec{x},t)\vec{n}(t)\left(\eta - \vec{\delta}\cdot\vec{k}\right)dl \tag{111}$$

The linearized moment is obtained using the same procedure

$$\vec{M}_h(t) = \iint_{\overline{S}_B} p(\vec{x},t)\left(\vec{x}+\vec{\delta}\right)\times\vec{n}(t)dS + \oint_{WL} p(\vec{x},t)\left(\vec{x}+\vec{\delta}\right)\times\vec{n}(t)\left(\eta - \vec{\delta}\cdot\vec{k}\right)dl \tag{112}$$

With $p(\vec{x},t)$ and $\vec{n}(t)$ given by the Taylor series expanded expressions (104) and (105) respectively, the force and moment given by expressions (111) and (112) are the basis for evaluating all hydrodynamic forces and moments over the time dependent wetted surface of the vessel $S_B(t)$ in SWAN-2. This includes the forces leading to the vessels small

displacements in waves, structural loads, sinkage and trim, and the horizontal forces, namely the vessels ideal fluid resistance.

3.4.9. Vessel Equations of Motion

When investigating the seakeeping problem in the time-domain, it is important to appreciate the importance of memory effects introduced by the free surface on the vessel's response. The solution of the boundary value problem defined in sections 2.1 and 3.2 is at time t strongly affected by its history. By assuming the linear system to be time-invariant, the hydrodynamic force in Newton's law (49) can be decomposed into local and memory components. The memory forces results from the history of the wave propagation. The local force, being impulsive by nature, is due to the instantaneous motion. This decomposition leads to the following equations of motion in the time-domain

$$\sum_j \left[(M_{ij} + a_{ij})\ddot{\xi}_j(t) + b_{ij}\dot{\xi}_j(t) + (C_{ij} + c_{ij})\xi_j(t) \right] = F_{m_i}(\dot{\xi}_j, \xi_j, t) \quad j = 1,...,6 \tag{113}$$

The matrix coefficients a_{ij}, b_{ij} and c_{ij} represent the impulsive local forces. Note that the memory force F_{m_i} is independent of the instantaneous acceleration. (113) is related to its frequency-domain counterpart (51) through a Fourier transform.

According to [7], the memory force is given by the following expression

$$F_{m_i}(\dot{\xi}_j, \xi_j, t) = X_i(t) - \int_{-\infty}^{t} d\tau K(t-\tau)\dot{\xi}_j(\tau) \quad j = 1,...,6 \tag{114}$$

where $X_i(t)$ is the hydrodynamic exciting force and $K(t)$ is the velocity impulse response function.

To solve equations (113) for the vessel's six rigid body modes $\xi_j(t)$, $j=1,...,6$, it is necessary to determine the coefficients a_{ij}, b_{ij} and c_{ij} and the memory force F_{m_i}. This is obtained by solving the boundary value problem defined in section 3.2 at the instantaneous time.

The vessel equations of motion as given by equation (113) are in time-domain simulations like SWAN-2 solved for each time step, yielding the vessel kinematics and resulting forces in the course of the time-marching. The time-domain integration of (113) could thus seem straightforward. Numerical instabilities will however arise if the separation of the relevant components of the forcing into the left hand side of (113) is not treated with caution. These components include the hydrostatic restoring forces and the effective added mass, damping and restoring forces induced by the impulsive velocity potential $\psi(\vec{x})$ defined in equations (96)-(98).

The time marching of the equations of motion (113) can be studied in detail in [7]. The solution of the boundary value problem and evaluation of the hydrodynamic forces and responses happen simultaneously for each time step. The result is a time record for the vessel responses $\xi_j(t)$ and corresponding forces and structural loads.

4. Roll Motion and its Control with Hydrofoils

This chapter investigates the seakeeping performance of the vessel in roll in unidirectional sea states, with and without the influence of lifting appendages. Several parameters, including the longitudinal location, planform area, speed and heading, are varied in a systematic way, revealing trends in the hydrodynamic behavior of the vessel in waves.
Two hydrofoils are located under the keel, equally off-centered on port and starboard side of the ship. The draft of the hydrofoils are constant at T=4m. The following figure illustrates the location of the hydrofoils.

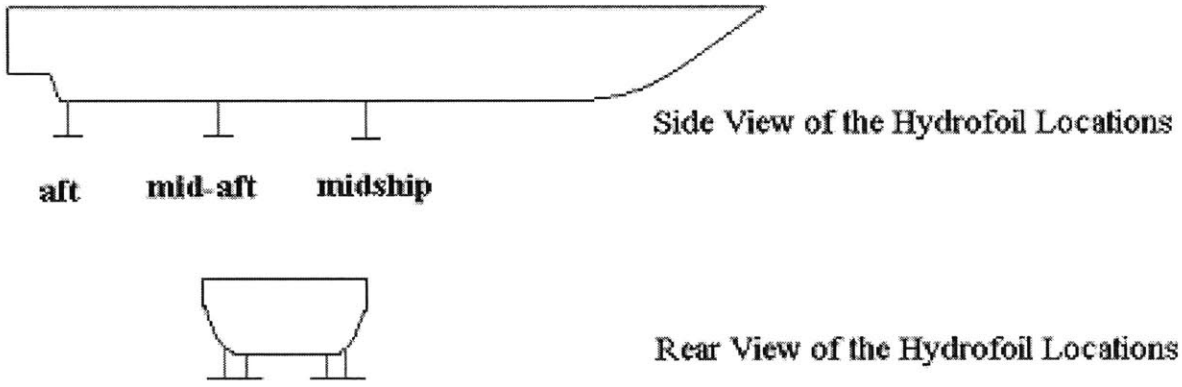

Figure 10: The locations of hydrofoils

The foil's planform area S (foil size), its longitudinal position χ_{foil}, the wave heading β, and the vessel's forward speed U are parameters that are varied systematically to determine their influence on the vessel's roll response. In the SWAN-2 simulations executed to extract the vessel's roll RAOs, Prandtl's lifting line theory as outlined in section 2.7.1 is assumed valid.

The following sections explain what the roll problem is about and a potential solution mechanism using hydrofoils.

4.1. Roll Problem Definition and Hydrofoil Usage as a Solution Mechanism

Roll motion is one of the three angular displacement modes of the ship. Roll is definitely the most important one due to the weak damping and potentially large response amplitude at resonance. This is of great concern in the design of high-speed monohull vessels, e.g. passenger ferries, commercial ships, and naval ships. Large roll motion affects the people on board, may lead damage to cargo or ship structure and can make military systems (fire control, aviation facilities) vulnerable.

Since this is a big problem for almost all monohull vessels, several solution methods have been carried out in practice. The reduction of the vessel responses at resonance may be achieved in three ways:

- Increasing the damping using bilge keels or anti-rolling fins.
- Using an anti-rolling tank, dynamically de-tuning the vessel roll response.
- De-tuning the mode of interest by shifting the value of the resonant encounter frequency away from the value where the wave excitation forces attain their maximum values. This can be done by either changing the heading or increasing/decreasing the speed.

In general, one can itemize the solution mechanisms for roll as following:

- Fins (active / passive)
- Bilge keels
- Tanks (active / passive)
- Rudders

At this point, motion control lifting appendages, namely hydrofoils, is introduced as a new roll stabilizing system, with passive and active implementation as explained later.

Hydrofoils, when attached to the fast vessels, perform two functions in general:

- They provide hydrodynamic lift to reduce hull wave making and frictional resistance, which means higher speed with same power or less power for same speed.
- They reduce vessel motions.

The first function is not significant unless the hydrodynamic lift created by the hydrofoil(s) is large enough to push the vessel up decreasing the wetted surface area. As far as this thesis concerned, the lift force created by the hydrofoils is not large enough to significantly change the vessels vertical position or wetted surface area, but large enough to create anti-rolling moment to reduce the vessel's roll motion as will be explained in the following sections.

The way how the hydrofoils affect the ship motions, particularly roll, was explained in section 2.7.2. In short; the components of the anti-rolling moment created by the lift force change the components of the roll equation motion in a way that the ship has more damping and restoring leading a remarkable reduction in roll motion. The above mentioned lift force and corresponding anti-rolling moment is primarily functions of forward speed, foil planform area, foil effective angle of attack, and the location of the foil about the vessel.

Optimization of foils for roll reduction purposes was carried out by investigating different scenarios as explained in the following sections.

4.2. Generic Monohull Information, Methodology, and SWAN-2 Simulation Execution

A generic monohull, representing a fast 100m long boat, was created for study purposes. The main data about this generic ship are as following:

- LOL : 100m
- LWL : 93m
- B : 8.9m
- D : 4.7m
- L/B : 10.4
- L/D : 19.8

- Disp. : 970,000 kg
- AWP : 670 m2
- LCB : -12.8m
- LCF : -10.9m
- VCB : -0.8m

The speed and the corresponding Froude Number information are as follows:

	Fn	*m/s*	*kts*
•	0.3	9.06	17.59
•	0.5	15.1	29.33
•	0.7	21.14	41.06
•	0.9	27.18	52.79

Simulations were carried out as in the following methodology:

- 4 different speed steps were used as Fn: 0.3, 0.5, 0.7, and 0.9. These steps will show the forward speed effect on hydrofoil effectiveness on roll reduction.
- 5 different wave heading were simulated in order to see the oblique wave effect on roll better, as β = 90, 105, 120, 135, and 150 deg.
- 3 different longitudinal hydrofoil positions were tested in order to differentiate the longitudinal position effect on roll, as χ_{foil} = midship, aft, and mid-aft (between midship and aft, like quarter). No position ahead of midship was tried because of feasibility reasons.
- 4 different hydrofoil planform area S's were used in simulations in order to show the planform area effect on roll moment and roll RAO as well as to find an optimized S_{FOIL}/A_{WP} ratio.
- An ISSC spectrum was employed in order to get the roll response and to find the standard deviation values for various conditions.

The vessel hull spatial discretization in the seakeeping simulations is shown in figure 11 together with the free surface discretization, and consists of 24 panels along the ship length and 6 panels across the half beam.

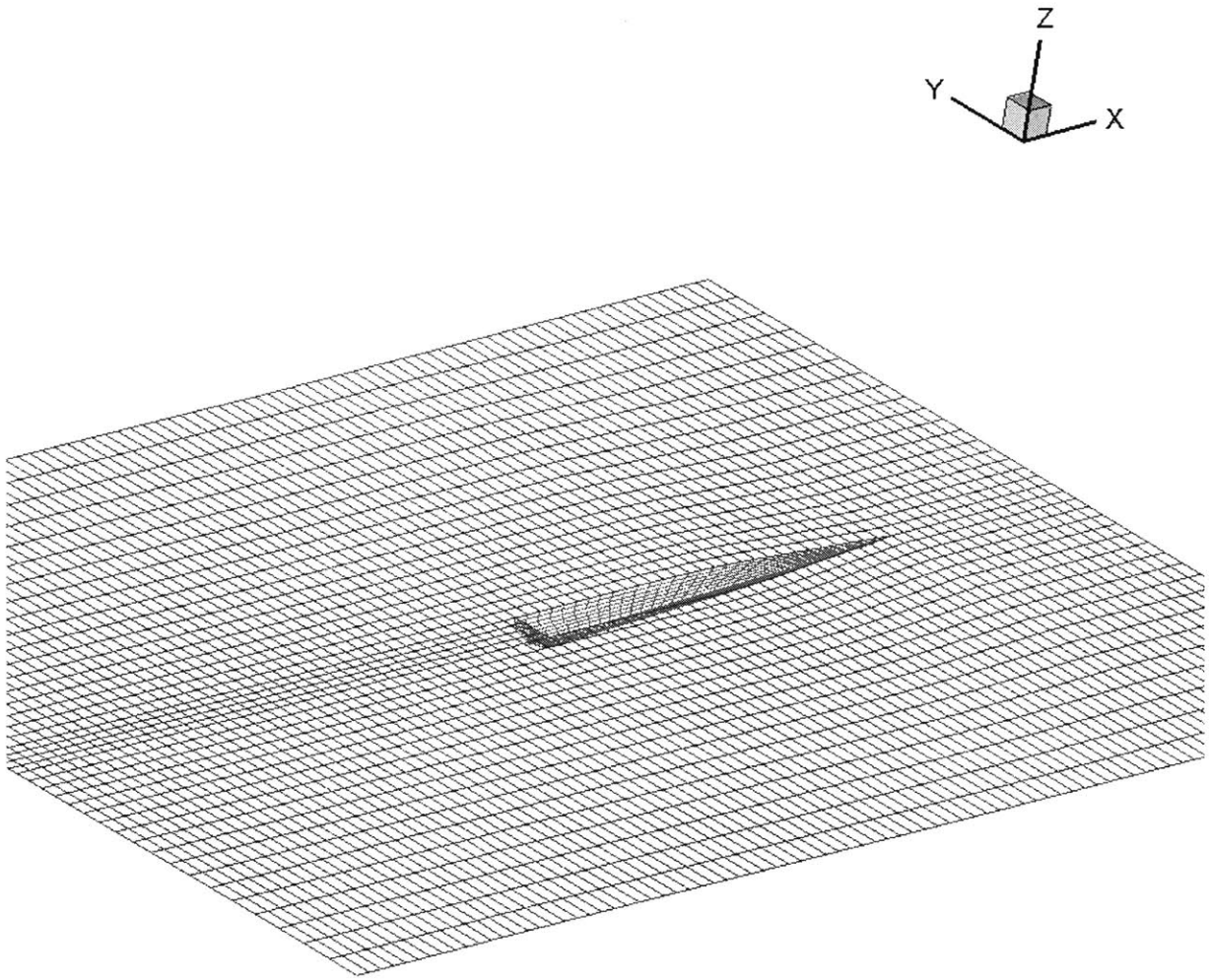

Figure 11: Spatial Discretization of Vessel Hull and Free Surface in Seakeeping Runs

The domain truncation in the seakeeping simulations is chosen to be the same as for the steady simulations in order no wave reflection from the numerical beach is incident on the vessel. The truncation is thus $0.5L_{PP}$ from bow to the upstream free surface boundary, $1.0L_{PP}$ from the centerline to the transverse free surface boundary, and $1.5L_{PP}$ from the stern to the downstream free surface boundary. This spatial discretization of the free surface is kept

constant for all seakeeping simulations, and it is shown in Figure 11 together with the spatial discretization of the hull. The total number of panels used in the seakeeping runs is 2280.

The selection of the time step is based on the default value for Δt calculated by SWAN-2 based on the vessel speed is chosen for all simulations. This value corresponds to a β-value of twice the critical value β_{cr}, ensuring temporal convergence with a safety margin of two in β.

The influence of steady dynamic sinkage ($\overline{\xi}_3$) and trim ($\overline{\xi}_5$) is in the seakeeping problem not expected to be of significant importance unless special events, for example the occurrence of slamming and green water on deck, are investigated. In the motion analyses carried out in this thesis, the effect of these parameters is therefore neglected, since their main effect would only be changing the mean value of the response from zero to the value of the steady dynamic sinkage or trim.

The unidirectional sea states in this thesis are given according to the *ISSC* wave-spectrum for a fully developed sea as given in chapter two of [5]. The wave energy is thus of the form

$$S_\zeta(\omega_0) = \frac{0.11}{2\pi}\left(\frac{\omega_0 T_1}{2\pi}\right)^{-5} \exp\left[-0.44\left(\frac{\omega_0 T_1}{2\pi}\right)^{-4}\right] T_1 H_{1/3}^2 \tag{115}$$

where ω_0 is the absolute circular frequency of the ambient waves (and not the frequency of encounter ω). $H_{1/3}$ is the significant wave height and T_1 is the mean wave period given by

$$H_{1/3} = 4\sqrt{m_0} \tag{116}$$

$$T_1 = 2\pi \frac{m_0}{m_1} \tag{117}$$

In (116) and (117), the k'th moment of the wave spectrum, m_k, is given as

$$m_k = \int_0^\infty \omega_0^k S_\zeta(\omega_0) d\omega_0 \tag{118}$$

In the seakeeping simulations, where the main objective is to determine the roll RAOs, the spectrum due to a significant wave height of $3m$ and a mean wave period of $8\ s$ is input to

SWAN-2. The spectrum is divided into 12 components, frequencies between 0.42 rad/s and 6.28 rad/s, corresponding to wave-periods of 1-15 seconds are covered in the simulations. The most interesting range of wave-periods where the seakeeping problem is relevant is thus represented. Unless otherwise stated, this is the sea state that all results are based upon.

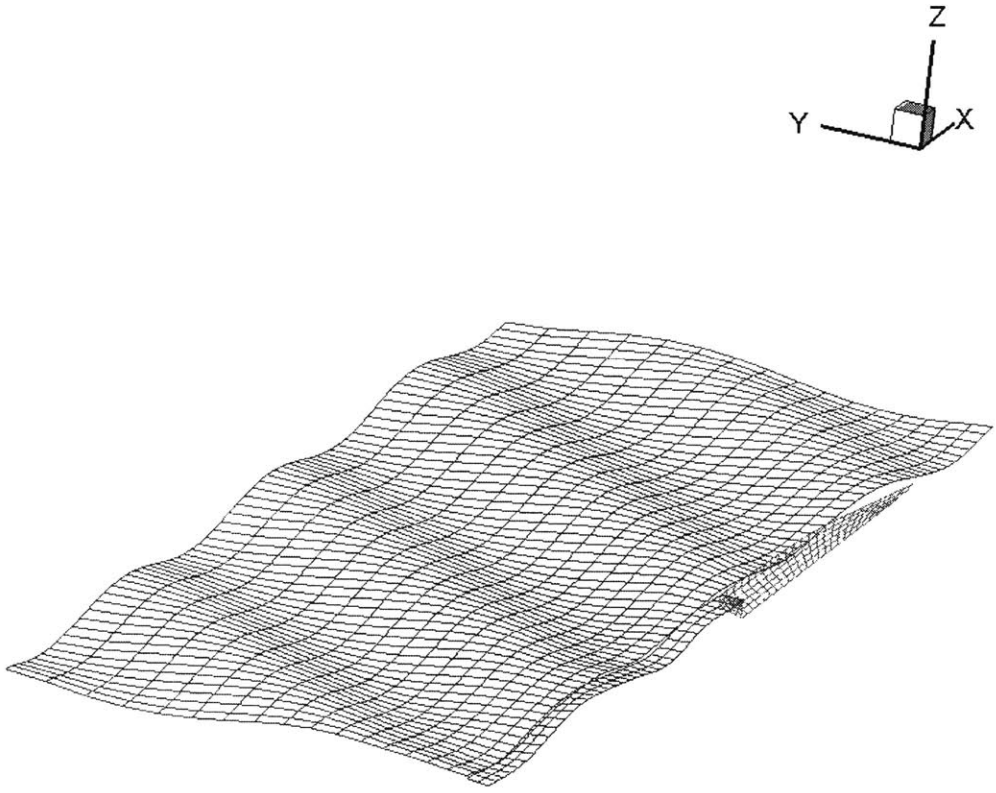

Figure 12: Vessel advancing at 52 knots (Fn: 0.9) in sea state with $H_{1/3}$=3m, T_1=6 s.

A snapshot of a SWAN-2 simulation of the vessel advancing with a forward speed of 52 knots in the sea state defined in the previous paragraph is shown in Figure 12. The free surface elevation (and thus the wave height) is magnified with a factor of two for illustration purposes.

4.3. The Influence of Foil Position along the Longitudinal Axis on Roll RAOs

To determine the longitudinal position where the foils are most effective as of roll reduction is quite important. Since it is not feasible to extend the foils beyond the beam of the ship, the effect of lateral location will not be investigated. But one can easily say that the foils should be located off center on both sides as much as the beam of the ship permits to increase the moment arm.

The following figure shows the longitudinal, lateral and vertical locations of the hydrofoils simulated for runs. 'Dots' represents the longitudinal locations. As seen in rear view, always two equally off-centered hydrofoils are located under the ship, $T \cdot 0.6$ meter deep.

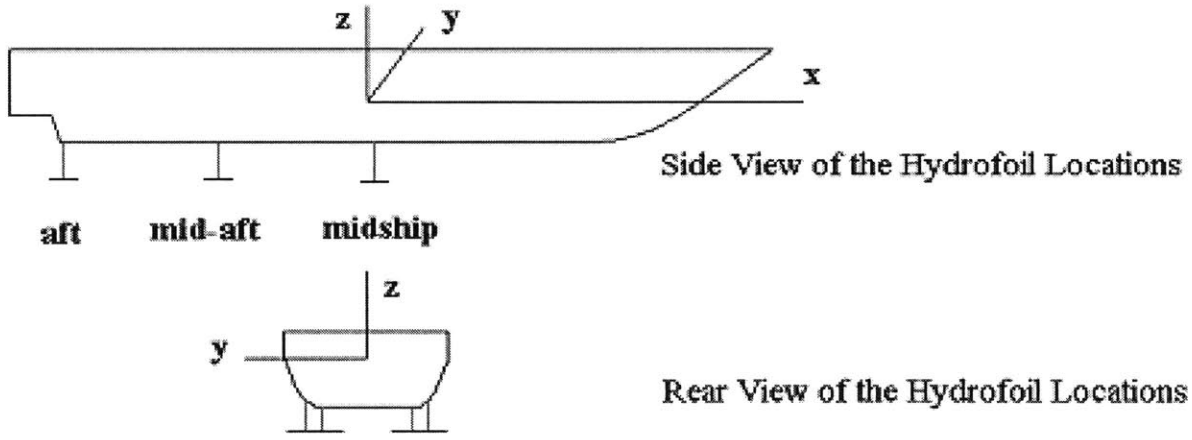

Figure 13: The (x, y, z) Locations of the Hydrofoils

Since we're not dealing with viscous flow, the boundary layer under the ship does not affect our results. In reality, special attention should be given in both locating the hydrofoils vertically and taking its effect into account while solving the flow.

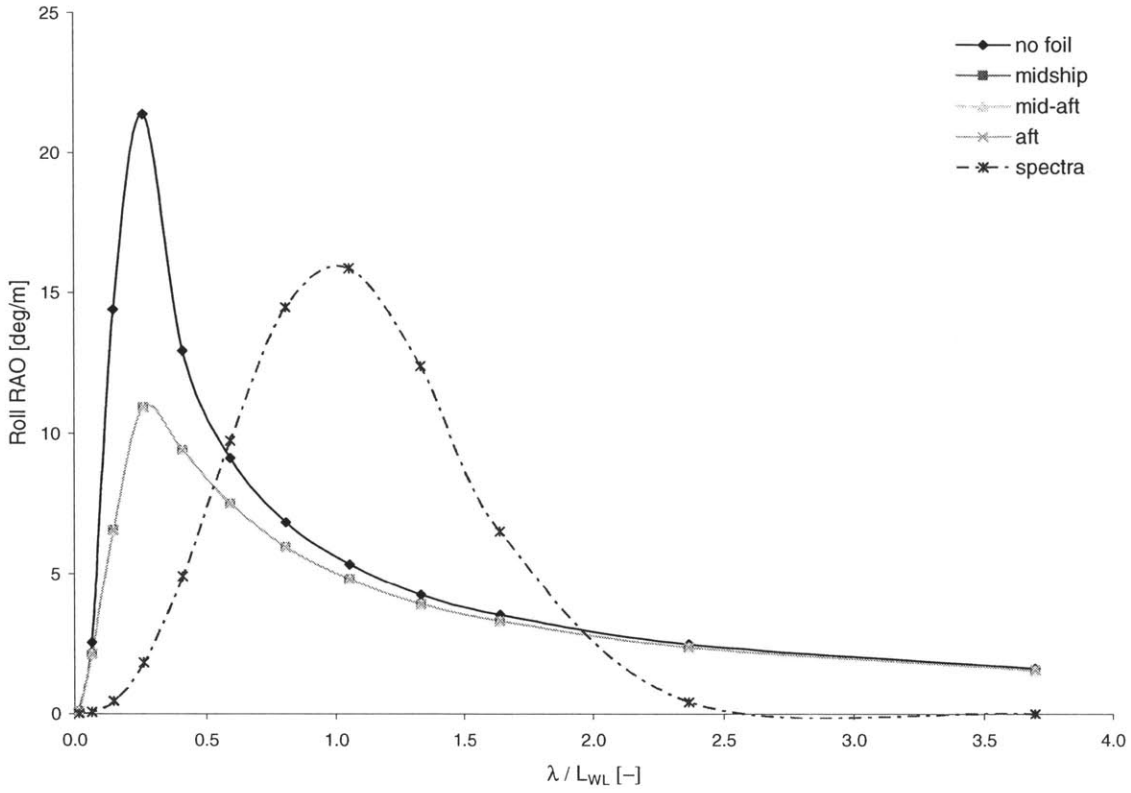

Figure 14: Roll RAO, Variation of Longitudinal Location, β =090°, S = 8 m², Fn = 0.7

When the waves coming from exactly sides (beam waves, 90°), a special situation occurs. As seen at Figure 14, the change in longitudinal positions of hydrofoils does not cause any relative reduction compared to other locations. All three locations give the same amount of reduction at this heading. Other than that, the reduction for all locations are remarkable, almost 50% less RAO value at resonant frequency for this speed.

From this result, we can at least say that in 90° beam waves, the use of hydrofoils for roll reduction purposes is quite significant, no matter where you place them longitudinally.

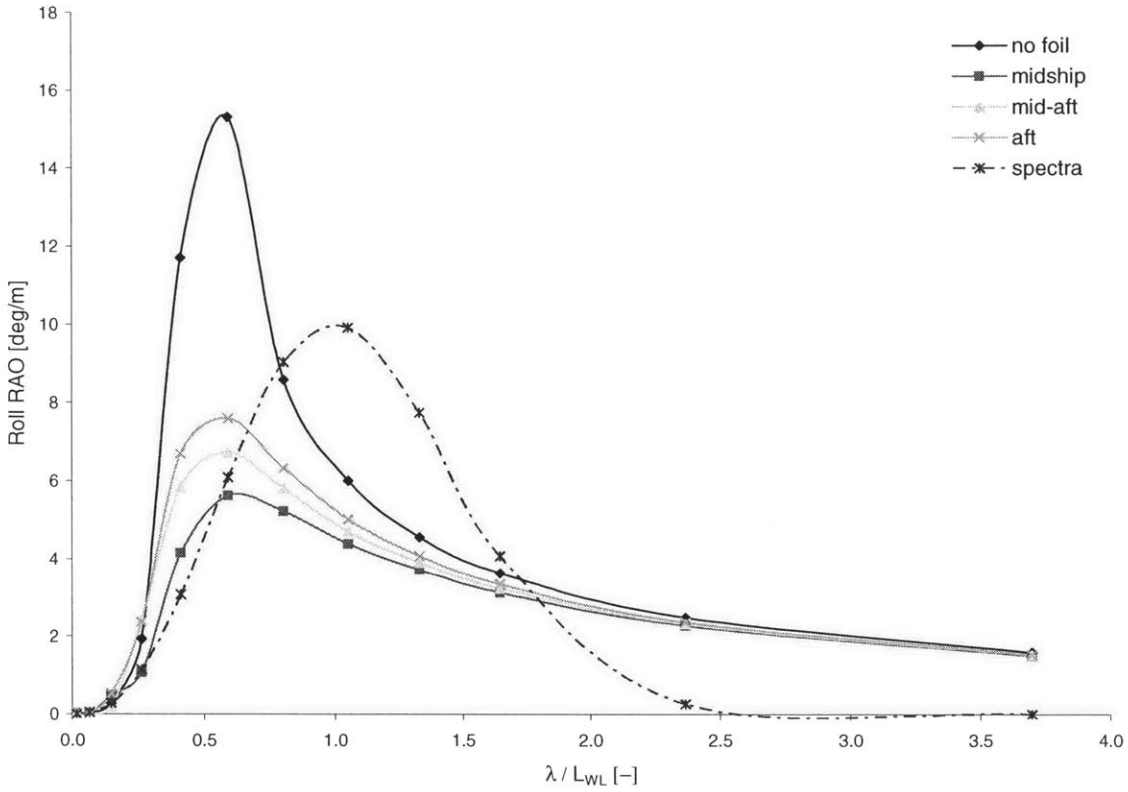

Figure 15: Roll RAO, Variation of Longitudinal Location, β =105°, S = 8 m^2, Fn = 0.7

Figure 15 gives the roll RAOs for the same ship for $\beta = 105°$. This time, the effects of the hydrofoils are not identical. The reason behind this difference was explained in section 2.7.2. Obviously the hydrofoil located at midship has a better performance compared to the others. At resonant frequency, the RAO value with the midship hydrofoil is almost 35% of the RAO value without any hydrofoil. The latter ratio is 44% for the foil at the mid-aft location, and 49% for the foil at aft of ship. These ratios depend on the wave heading, ship forward speed and foil planform areas. But the order remains the same for all wave heading, forward speed and foil planform area combinations, as the best place is midship.

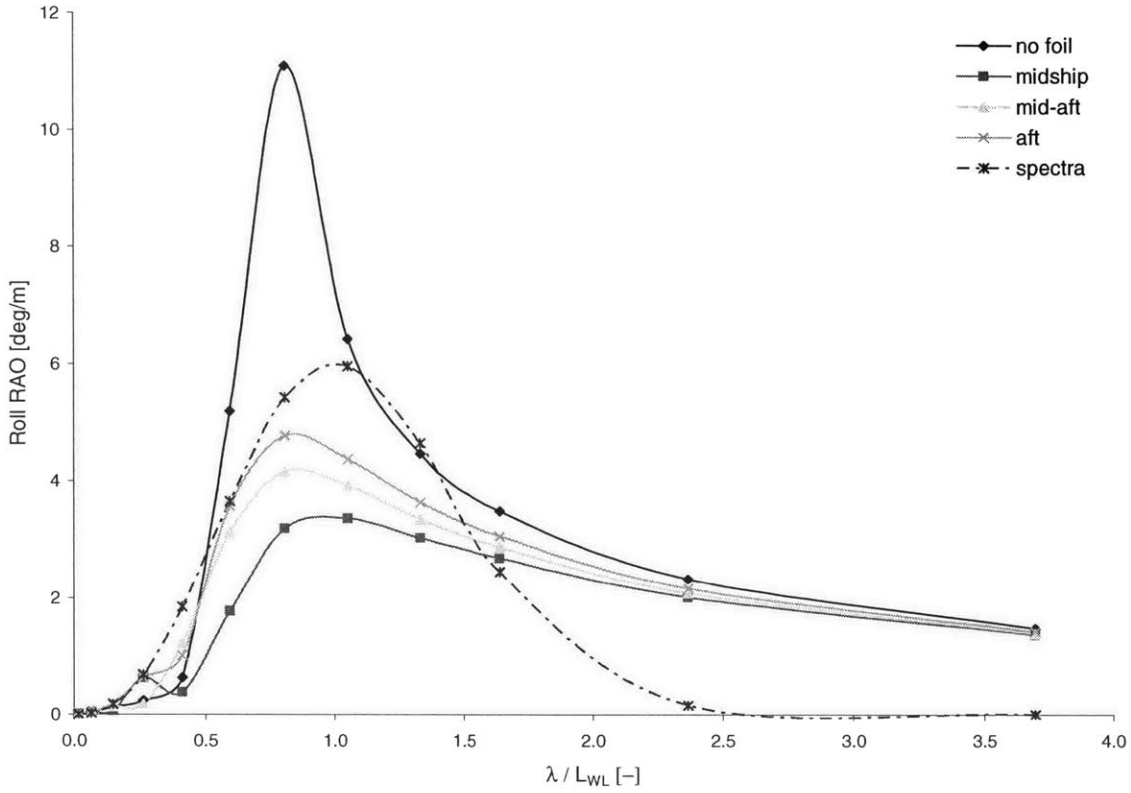

Figure 16: Roll RAO, Variation of Longitudinal Location, β =120°, S = 8 m^2, Fn = 0.7

For $\beta = 120°$ case, the ratio of the hydrofoil affected RAO to the RAO without any hydrofoil at resonant frequency is 28% for the midship hydrofoil, whereas this ratio is 37% for the mid-aft hydrofoil, and 43% for the aft hydrofoil. The reduction ratio is quite remarkable for all frequencies except very high and very low frequencies. These frequencies are not subject to our study since the roll response magnitude at these frequencies is almost zero. Thus, they do not have any practical importance in this study.

What we are trying to do employing the hydrofoils is to get less roll response values for the same sea state. Therefore it's better to take a look at Figure 17, the roll response graph for $\beta = 120°$, at Fn=0.7, with hydrofoil planform areas S=8 m^2.

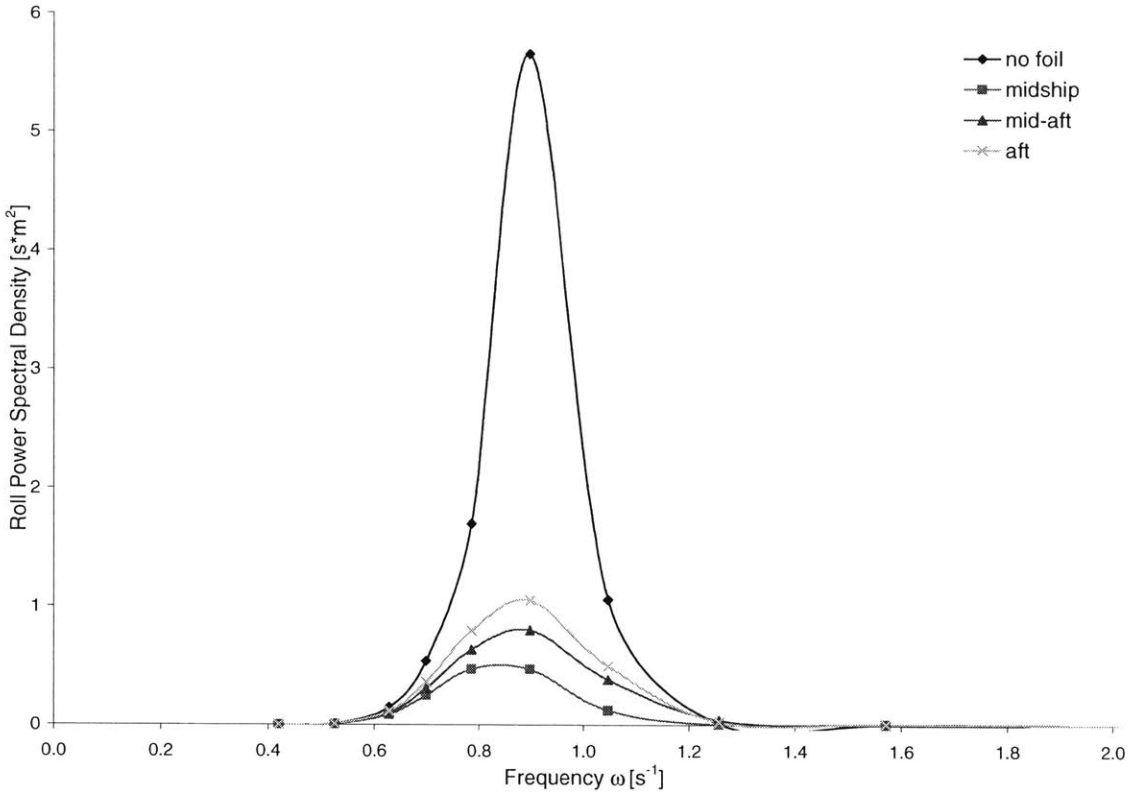

Figure 17: Roll Response, Variation of Longitudinal Location, β =120°, S = 8 m², Fn = 0.7

Since response is the most important parameter for determining the ship's behavior is sea conditions, Figure 17 gives us valuable insight on how effective the hydrofoils are. The response of the ship without hydrofoils is very high compared to any one of the conditions with hydrofoil. And the hydrofoil at midship gives us the minimum response as it does the minimum RAO values.

The standard deviation of roll response is another good indicator of how the response is distributed, correlating the ship response motions. Figure 18 is the standard deviation graph for Fn=0.7, S=8 m^2 , with varying wave heading β and varying hydrofoil longitudinal location. This graph is a sort of summary of the hydrofoil longitudinal position effect on roll motions.

Two basic conclusions from Figure 18 are:

First, the use of hydrofoil with any longitudinal location has a remarkable influence on roll RAO and response.

Second, the best longitudinal location for hydrofoils is the midship, giving the least RAO and response values for all headings.

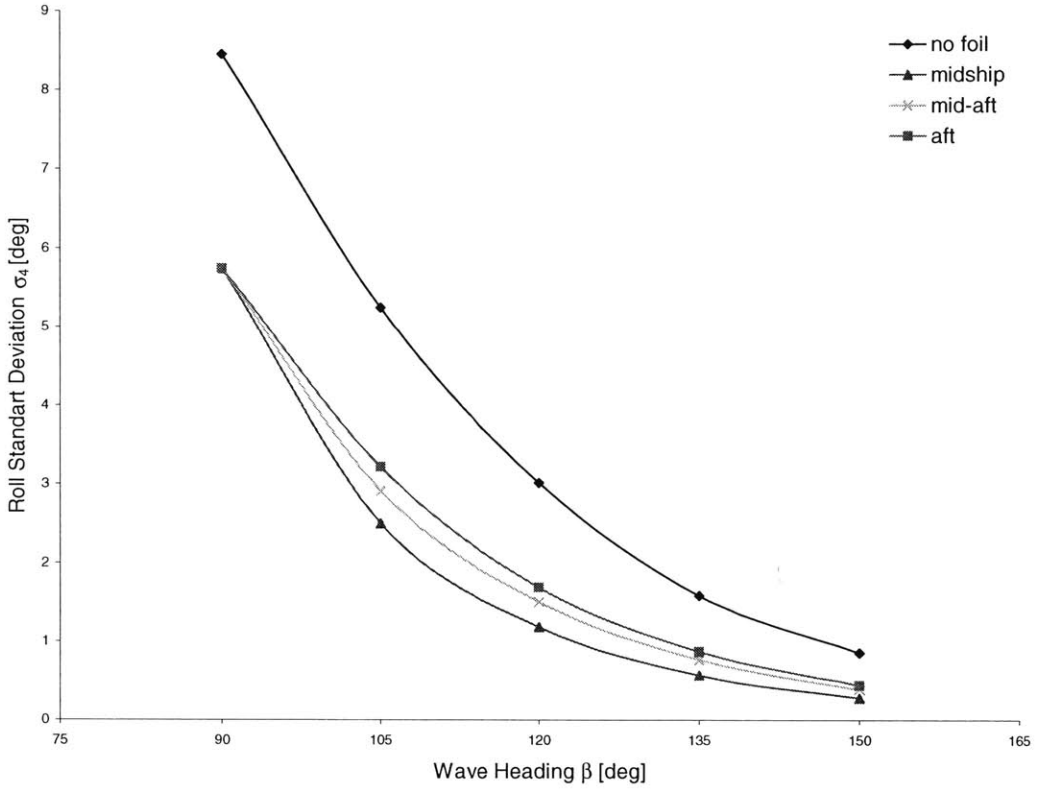

Figure 18: Roll Standard Deviation, S = 8 m^2, Fn = 0.7, with varying β and χ Location

Figure 18 summarizes the influence of change in longitudinal position of the hydrofoils on roll RAOs and responses. As explained earlier, 090° wave heading is a special situation where variation in longitudinal axis of hydrofoils does not change the influence. For all other wave headings, the hydrofoil pair located at midship give the best reduction regardless of the ship forward speed and hydrofoil planform area variations.

The relative reduction ratio in roll standard deviation is increased as the wave heading β goes up from 090° to 150°.

For all three cases, the primary reductions in roll RAO, response and standard deviation are noteworthy.

4.4. The Influence of Foil Planform Area on Roll RAOs

Since the introduced roll reduction system is mainly based on the lift force created by the pair of hydrofoils attached to ship hull, it is reasonable to try to find the effect of variation in foil planform area on roll motion reduction. One can determine the optimal planform area by looking at the relative reduction for different foil planform areas. A suitable ratio we can look for can be the A_{FOIL}/A_{WP}, planform area of the foil / Waterplane area of the ship at design draft.

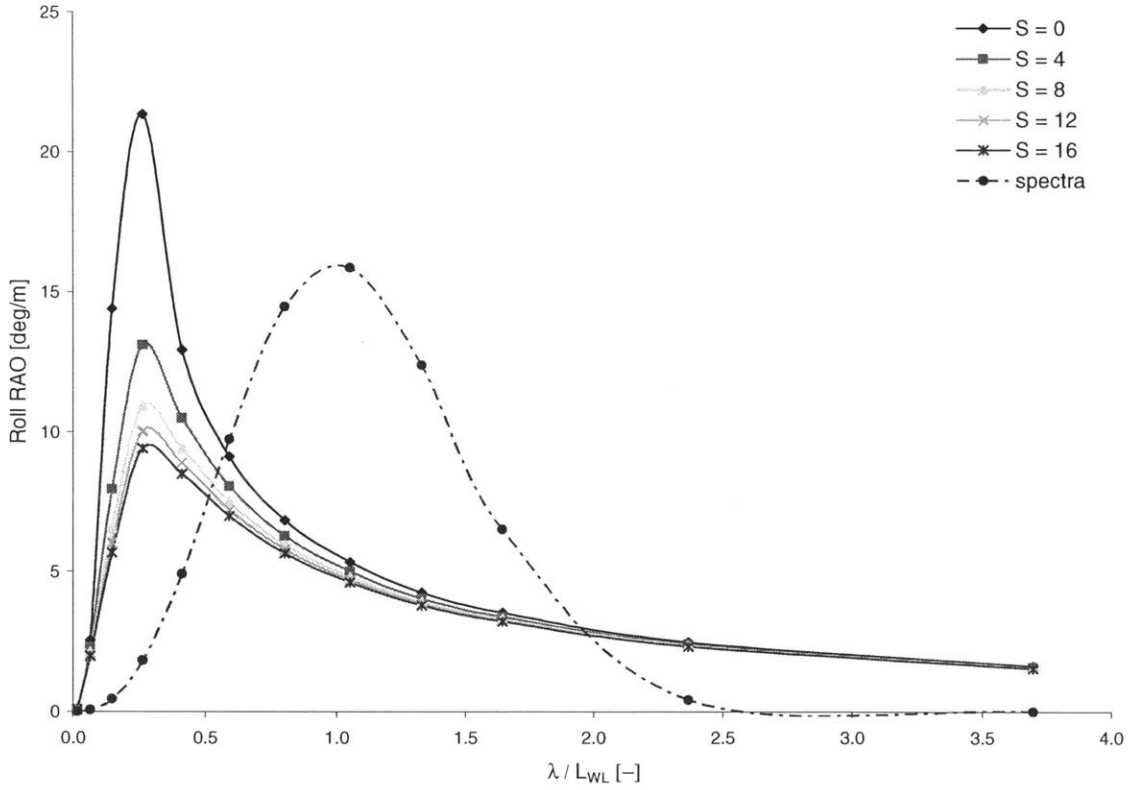

Figure 19: Roll RAOs, Fn = 0.7, β=090° and χ_{FOIL}=midship, varying S

The first thing to note on Figure 19 is the continuing decrease in roll RAO especially around resonant frequency range. The primary reduction ratio in roll RAO with a pair of hydrofoil with S=4m^2 is 38% at resonant frequency. To investigate the planform area effect, the planform areas of the hydrofoils are increased in a linear way. The biggest pair of hydrofoils with S=16m^2 give a relative reduction of 28% compared to the pair of hydrofoils with S=4 m^2. And the total reduction in roll RAO in this case is 56% compared to the case without any hydrofoil.

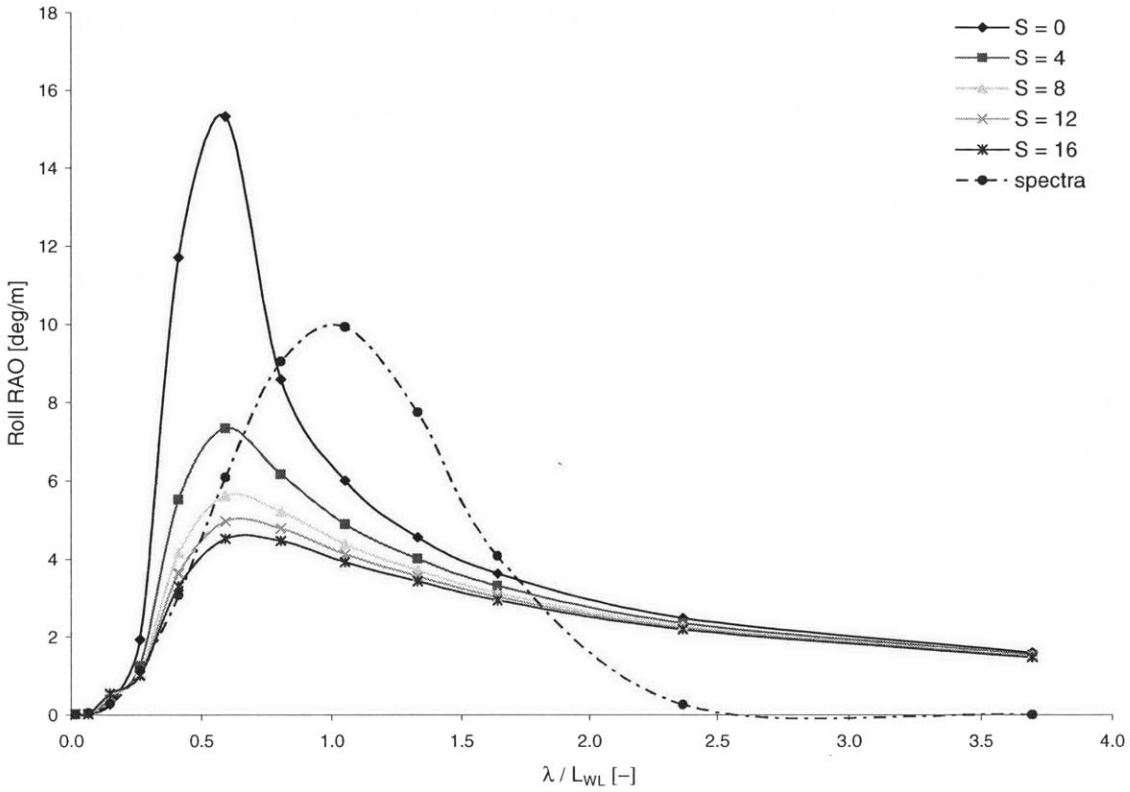

Figure 20: Roll RAOs, Fn = 0.7, β=105° and χ_{FOIL}=midship, varying S

It is necessary to give a dimensionless value of how big the hydrofoils are attached to the hull. Since the generic ship studied here has a waterplane area of 670m^2 , the corresponding dimensionless values for planform areas become:

S (m^2)	Dimensionless Value	
4	0.012	or (1.2%)
8	0.024	or (2.4%)
12	0.036	or (3.6%)
24	0.048	or (4.8%)

The second thing one can note, looking at Figure 20 and Figure 21 as well as the rest of the figures showing the RAO values for varying planform areas, is the relative reduction decreases as the hydrofoil planform area S increases. Even though the S increases linearly, the roll RAO does not decrease linearly.

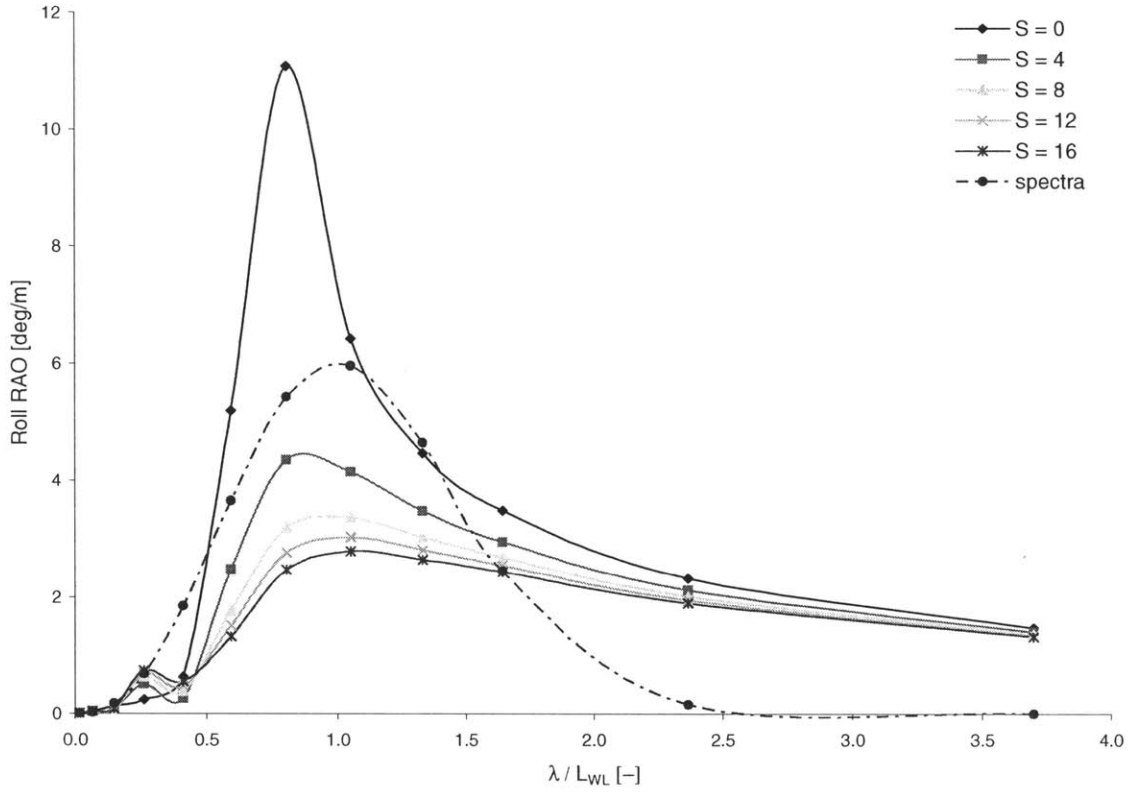

Figure 21: Roll RAOs, Fn = 0.7, β=120° and χ_{FOIL}=midship, varying S

For β=120° case, the relative reduction in roll RAO with a pair foil with S=8m^2 is 26% compared to the pair with S=4m^2. The relative reduction with a pair foil with S=12m^2 is 14% compared to the pair with S=8m^2. And the relative reduction with a pair foil with S=16m^2 is 10% compared to the pair with S=12m^2. It is apparent that there is no point of continuing to increase hydrofoil planform area in order to get less RAO values. One can also take the increased drag force into account.

The similar reduction ratios with same pattern are valid for different wave heading and forward speed situations.

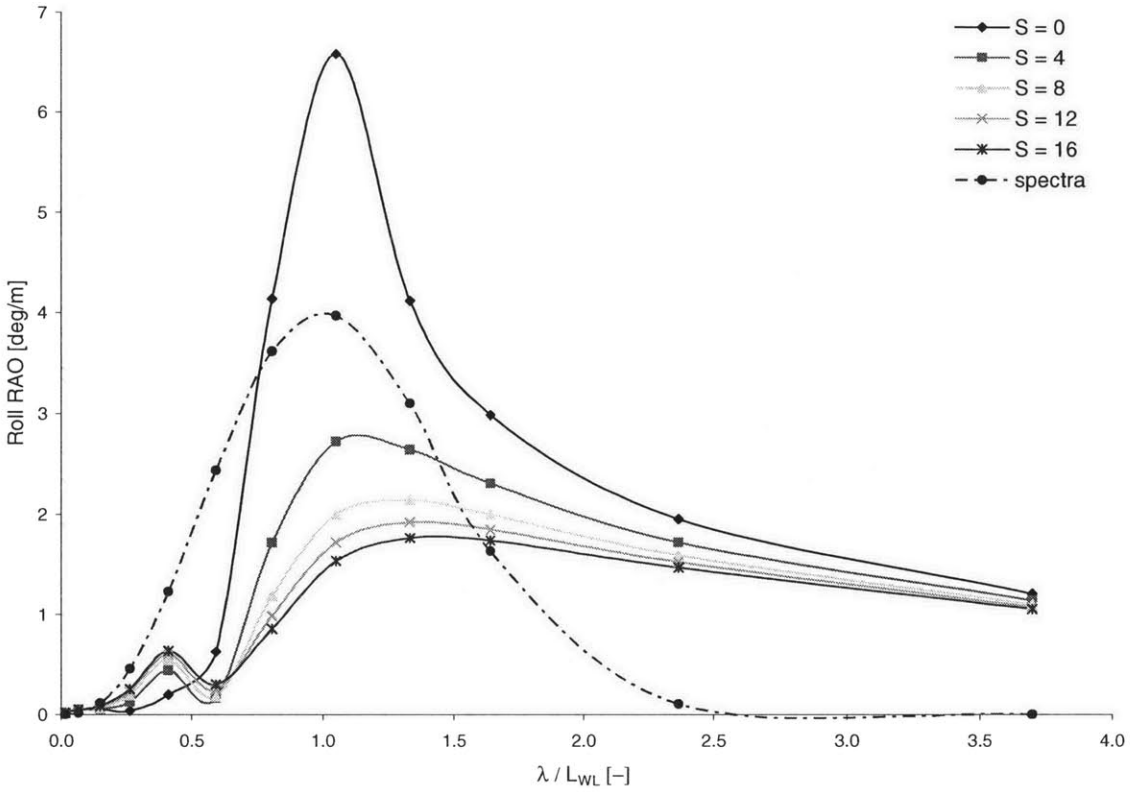

Figure 22: Roll RAOs, Fn = 0.7, β=135° and χ_{FOIL}=midship, varying S

A careful review of Figure 22 and Figure 23 as well as the figures for other wave heading situations indicates that S=8m^2 is the optimum planform area for this monohull ship since the relative reduction ratio decreases sharply beyond this planform area. S=8m^2 corresponds a dimensionless value of 0.024, meaning that the total planform area of a pair of hydrofoils is equal to 2.4% of the waterplane area of the ship at design draft.

The optimization of foil planform area is not an easy subject. This thesis is not intended to give detailed optimization of hydrofoils in roll reduction system. But some discussion on this subject can be found in chapter 6.

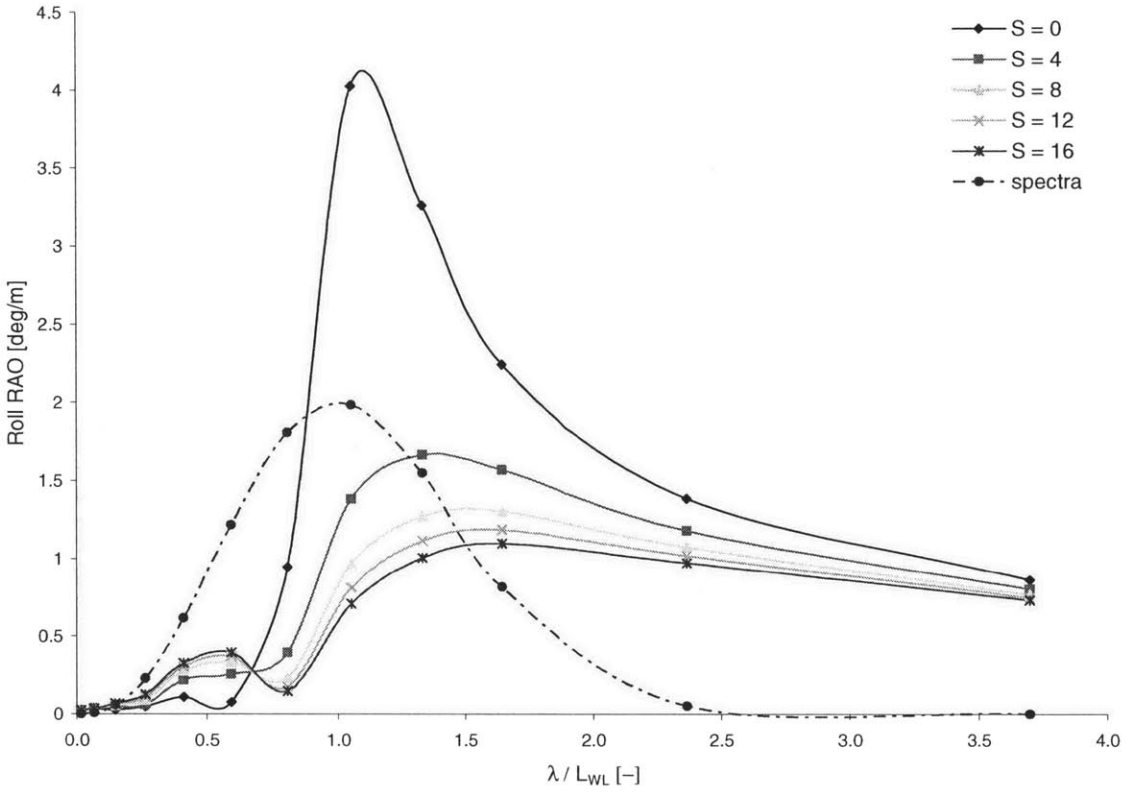

Figure 23: Roll RAOs, Fn = 0.7, β=150° and χ_{FOIL}=midship, varying S

At this point, a more detailed explanation is required about the varying S and its effects. Figure 24 shows the difference between having a constant or varying aspect ratio AR as S increases. Due to physical restrictions, such as the width of beam, we can not keep AR constant while we increase the planform area S. If not, the edges of the hydrofoils will extend beyond the beam which is not a desirable situation. Thus, the AR decreases as the planform area of the hydrofoils increases, resulting less lift force and anti-rolling moment. We can see this from the lifting line relation of C_L.

Since $C_L \propto \frac{AR}{AR+2}$, the decrease in AR gives less C_L. Thus less lifting force and less anti-rolling moment are generated. This explains the sharp decrease in relative reduction of roll RAOs. An experiment was carried out keeping AR term constant while increasing the planform area S, even though it is not feasible. Figure 24 explicitly shows that the relative reduction ratio stay almost constant even beyond S=8 m^2, giving us an almost linear decrease in roll standard deviation.

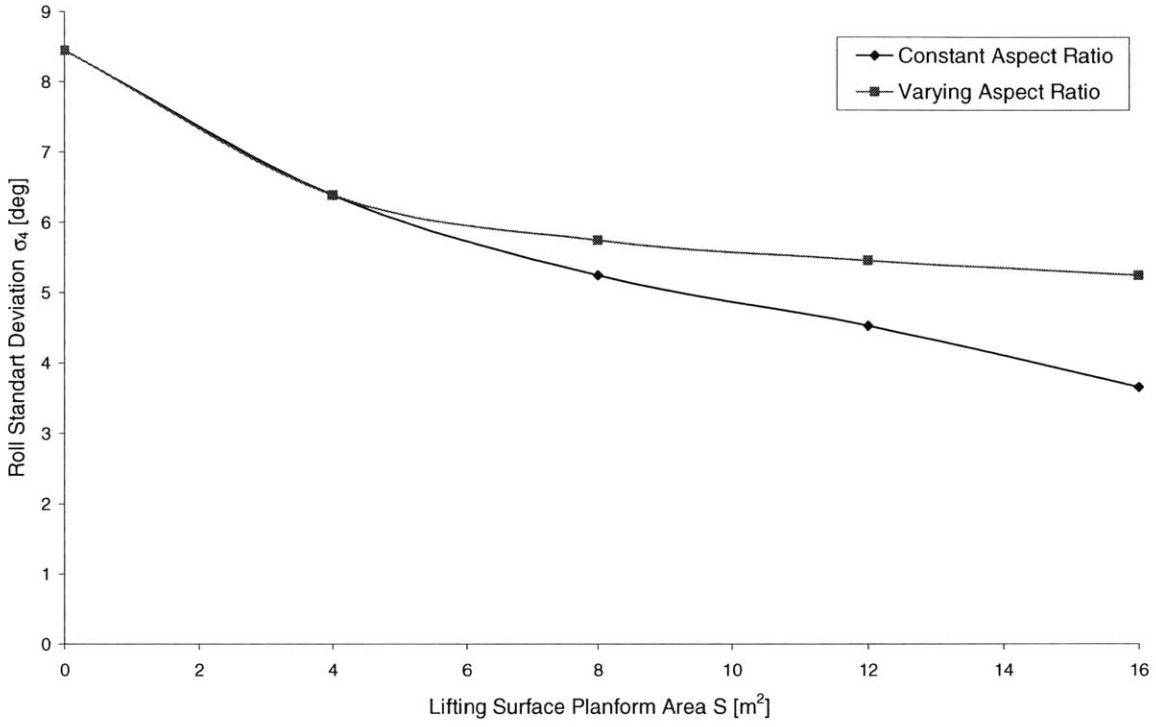

Figure 24: Variation in Roll Standard Deviation due to change in Planform Area S.

4.5. The Influence of Forward Speed on Roll RAOs

Looking at the hydrodynamic lift force equations, (62) and (63), one can easily see that the lift force, thus the anti-rolling moment created by hydrofoils, is proportional to the square of the forward speed. As we will see soon, forward speed has a dramatic influence in this roll reduction system as it does in active and passive fin roll control systems. It is the easiest way of increasing the lift force. Of course, increased speed also means that the induced and frictional drag due to the hydrofoils increase. A brief discussion on this issue will later be addressed in chapter 6.

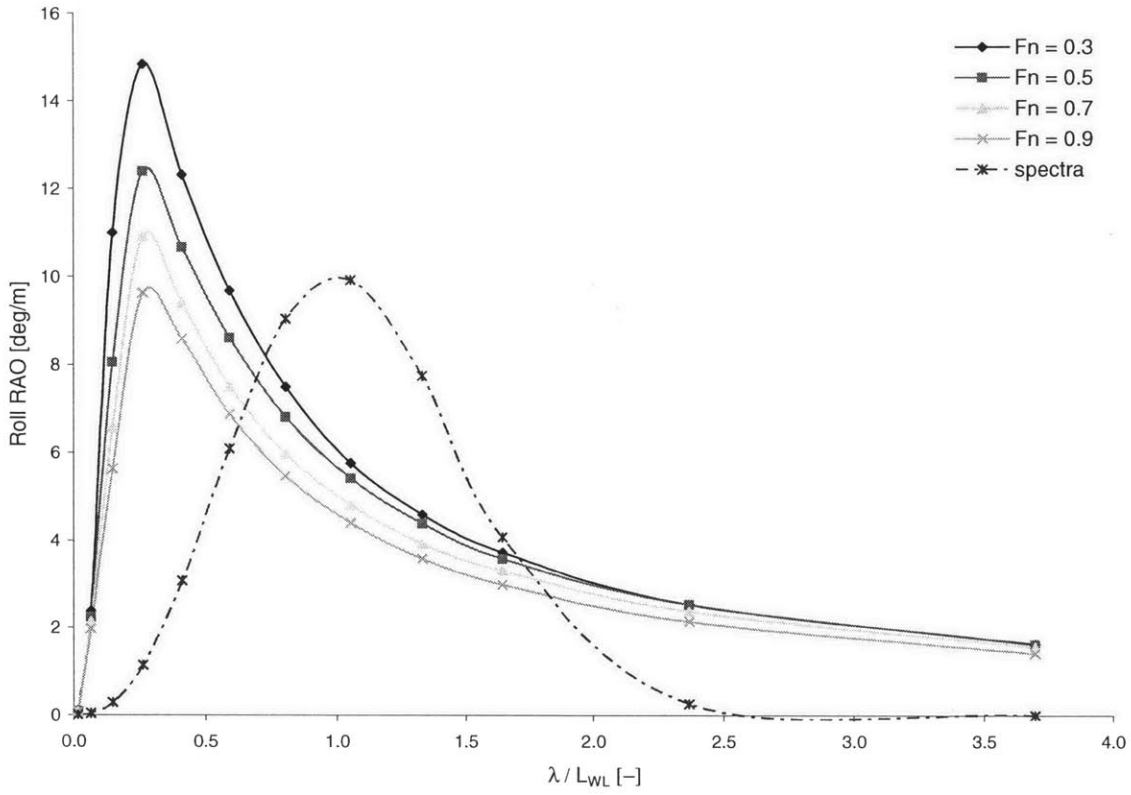

Figure 25: Roll RAOs, β=090° and χ_{FOIL}=midship, S=8 m^2, varying forward speeds

We kept the hydrofoil planform area S and the locations of the hydrofoils constant while we varied the ship forward speed and the wave heading β. A linear increase in forward speed U is capable of giving additional linear reduction in roll RAO. Figure 25 and Figure 26 show the effect of the forward speed for β=090° and β=105° cases. As will be seen in the following graphs, the roll RAO reduction pattern is similar for all wave heading cases.

The relative reduction is approximately 18% between Fn=0.3 and Fn=0.5. Then, the reduction ratio will stay around 10% as the speed step gets higher.

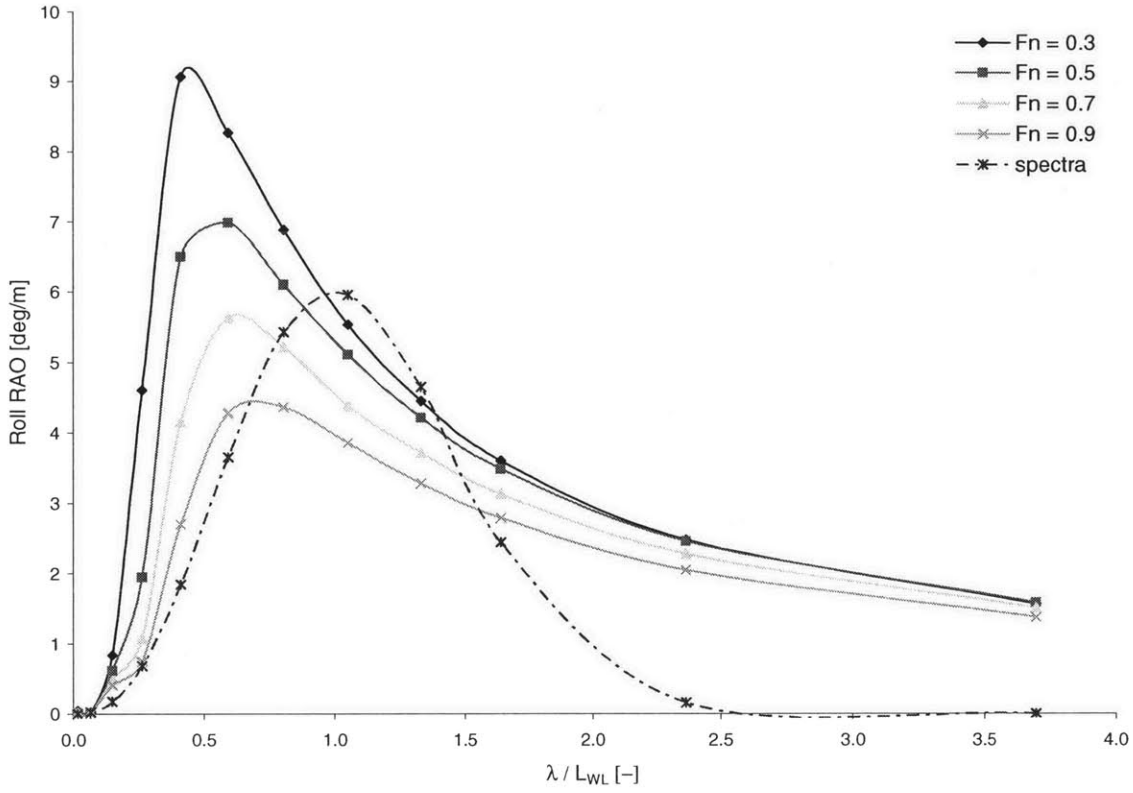

Figure 26: Roll RAOs, β=105° and χ_{FOIL}=midship, S=8 m^2, varying forward speeds

Increased speed results in smoother RAO graphs, more reduced RAO and response values around resonant frequency. The dependence of roll damping and restoring terms, when hydrofoils attached, to the forward speed can be seen explicitly in equations (66)-(70).

As β gets higher (from 090 up to 150), the relative reduction ratio increases in a remarkable way. For β=090° case, the relative reduction in RAO between Fn=0.3 and Fn=0.9 was approximately 35%. For β=105° case, the same ratio became almost 50%. This is valid for other wave headings.

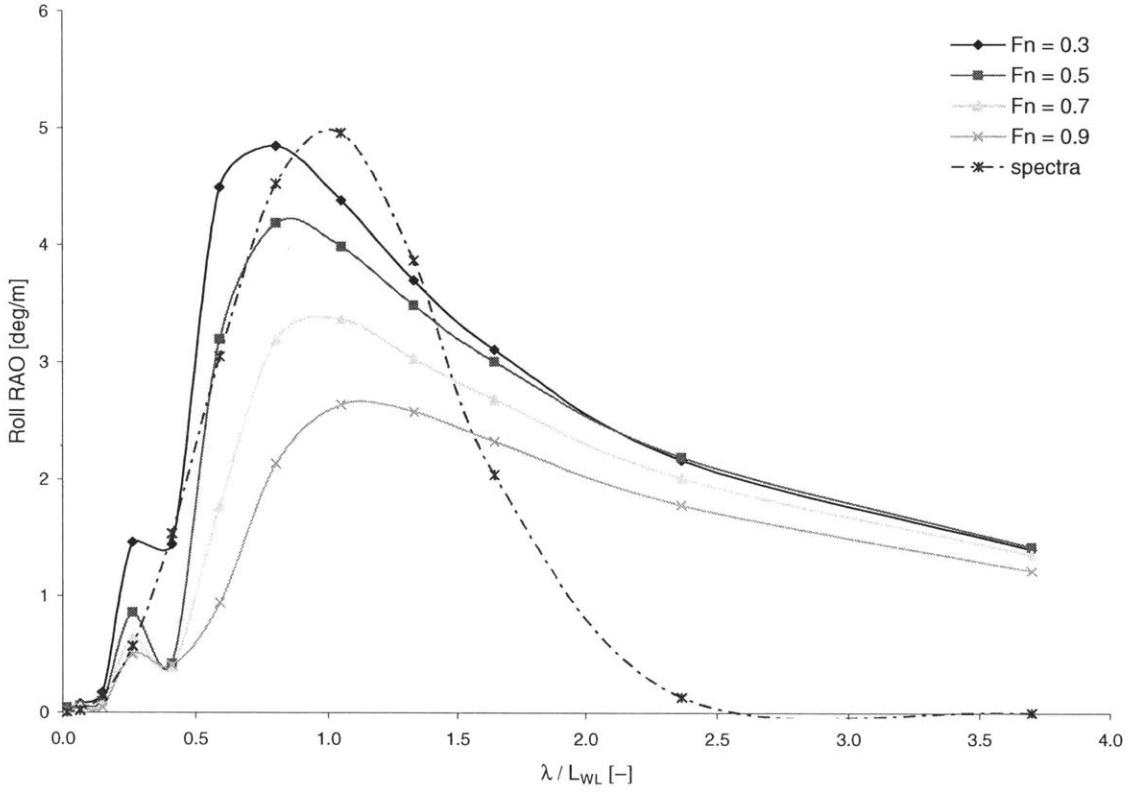

Figure 27: Roll RAOs, β=120° and χ_{FOIL}=midship, S=8 m^2, varying forward speeds

The absolute reductions in roll RAOs for all wave heading β situations are remarkable. More importantly, the relative reduction for different forward speed steps is also quite remarkable. As we have seen in the previous section, relative reduction decreases as we increase the hydrofoil planform area S. But here, the relative reduction stays almost constant for all speed steps and wave heading variations.

The easiest conclusion from these graphs is: Higher speed increases the effectiveness of this system. The faster the ship advances, the more effective the roll reduction system is.

5. Active Roll Control with Hydrofoils

In previous chapter, all important parameters in roll reduction system with passive hydrofoils were investigated. We saw that use of hydrofoils attached to the ship under the hull gives significant reduction on roll RAO and response for all wave headings. We also saw that increased forward speed and hydrofoil planform area give better results. The midship location appeared to be the best longitudinal position of the hydrofoils, with an area ratio of 2%.

We can calculate the instantaneous anti-rolling moment generated by a hydrofoil pair using Prandtl's lifting line theory as following

$$M = y_{foil} \cdot \rho U^2 S \pi \frac{AR}{AR+2} (\alpha_{port} - \alpha_{starbord}) \tag{119}$$

As seen in (119), the effective moment is the difference of two moments generated by each hydrofoil. The α values are the effective angles of attack of the hydrofoils and defined previously as (59)

$$\alpha(t) = \alpha_0 - \xi_5(t) + \frac{\frac{\partial \phi_I}{\partial z} - \dot{\xi}_3(t) - y_{foil}\dot{\xi}_4(t) + x_{foil}\dot{\xi}_5(t)}{U + \dot{\xi}_1(t) - \frac{\partial \phi_I}{\partial x}} \tag{120}$$

In passive (fixed) hydrofoil system, we do not have any capability to change / control the time dependent effective angle of attack, meaning that we can not determine the magnitude of anti-rolling moment for any time step. The idea behind the active roll control system is very basic. If we can change the effective angles of attack of the hydrofoil in an effective way, then we can get more anti-rolling moment whenever it is required.

$$\alpha(t)_{final} = \alpha(t) + C_1 \cdot \xi_4(t) + C_2 \cdot \dot{\xi}_4(t) \tag{121}$$

If we introduce two new terms to the final time dependent effective angle of attack, we can change its final value as it gives the most possible anti-rolling moment. Think that α_{port} and $\alpha_{starbord}$ has opposite signs: In moment equation (119) they are canceling their effects out to some extent, and the remaining is the moment we are looking for. But here they actually add

up and give more instantaneous anti-rolling moment since C_1 and C_2 term can be chosen such that the result will be additive. In the equation (121), C_1 is comparable in size to restoring moment term whereas C_2 is to damping term. Thus, C_1 is multiplied by the instantaneous roll angle; C_2 is multiplied by the instantaneous roll angular velocity.

Using a similar approach as for passive foils, the active control contributions to the equation of motion for roll are determined as follows

$$\omega^2 (I + A_{44})\Xi_4 + i\omega(B_{44} + \sum_{i=1}^{2} y_i^2 \cdot \frac{F}{U} + \sum_{i=1}^{2} y_i \cdot C_1 \cdot F)\Xi_4 + i\omega(\sum_{i=1}^{2} y_i \cdot \frac{F}{U})\Xi_3 - i\omega(\sum_{i=1}^{2} y_i \cdot x_i \cdot \frac{F}{U})\Xi_5 + \ldots$$
$$\ldots + (C_{44} + \sum_{i=1}^{2} y_i \cdot C_2 \cdot F)\Xi_4 + (\sum_{i=1}^{2} y_i \cdot F)\Xi_5 = X_4 + \sum_{i=1}^{2} \frac{i\omega}{U} \cdot y_i \cdot F \cdot e^{-kT - ik(x_i \cos\beta + y_i \sin\beta)} \quad (122)$$

where $F = \dfrac{\pi\rho SU^2 AR}{AR + 2}$.

Now; we can control the equation of motion of roll to some degree since we can choose what C_1 and C_2 are instantaneously.

In an explicit way, we can show the effects of these new coefficients on roll equation of motion as follows

$$B_{44}^{\ with\_foil} = B_{44} + \sum_{i=1}^{2} y_i^{\,2} \cdot \frac{F}{U} + \sum_{i=1}^{2} y_i \cdot C_{1_i} \cdot F \quad (123)$$

$$C_{44}^{\ with\_foil} = C_{44} + \sum_{i=1}^{2} y_i \cdot C_{2_i} \cdot F \quad (124)$$

The contribution from the new terms with coefficients are controllable and significant since they directly contribute to the damping and restoring main terms, resulting decreased RAOs.

The determination of instantaneous values of C_1 and C_2 coefficients is up to the control command unit of the active control mechanism. Here, in this thesis, it is enough to investigate whether we can get less roll RAO values provided that appropriate C_1 and C_2 coefficients are used. During active control runs, the C_1 and C_2 coefficients were kept constant at a

predetermined value. As we can see in Figure 28, Figure 29, and Figure 30 for various wave headings, the additional reduction in roll RAO is quite remarkable.

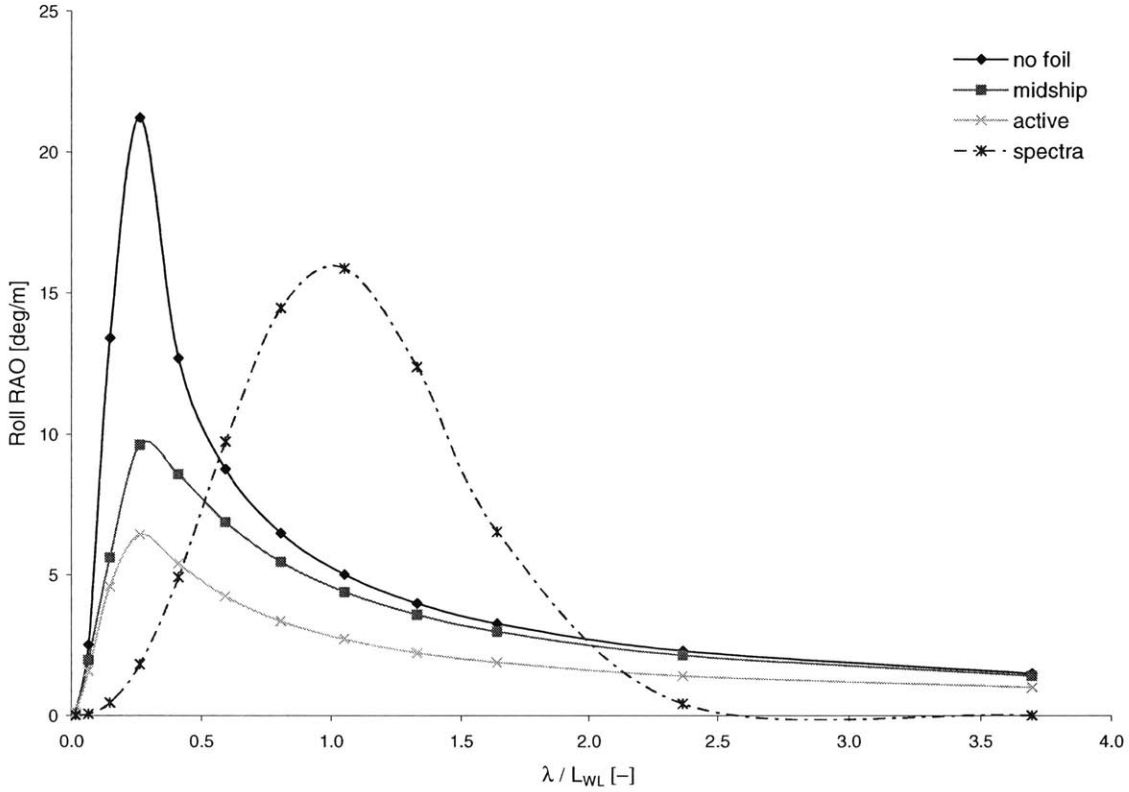

Figure 28: Roll RAOs, β=090° and χ_{FOIL}=midship, S=8 m^2, Fn=0.9, active and passive foil comparison

To investigate the active control effect on roll motion, the optimum pair of hydrofoils in passive roll system was used as a base point. Then, determining the effective angle of attack α and its phase are the only task to have active control mechanism to be effective.

The relative reduction is even more significant as the wave heading β tends from 90° to 150°. The relative reduction term here means the reduction ratio of roll RAO when the RAO values with passive hydrofoil system and the RAO values with active control system are compared.

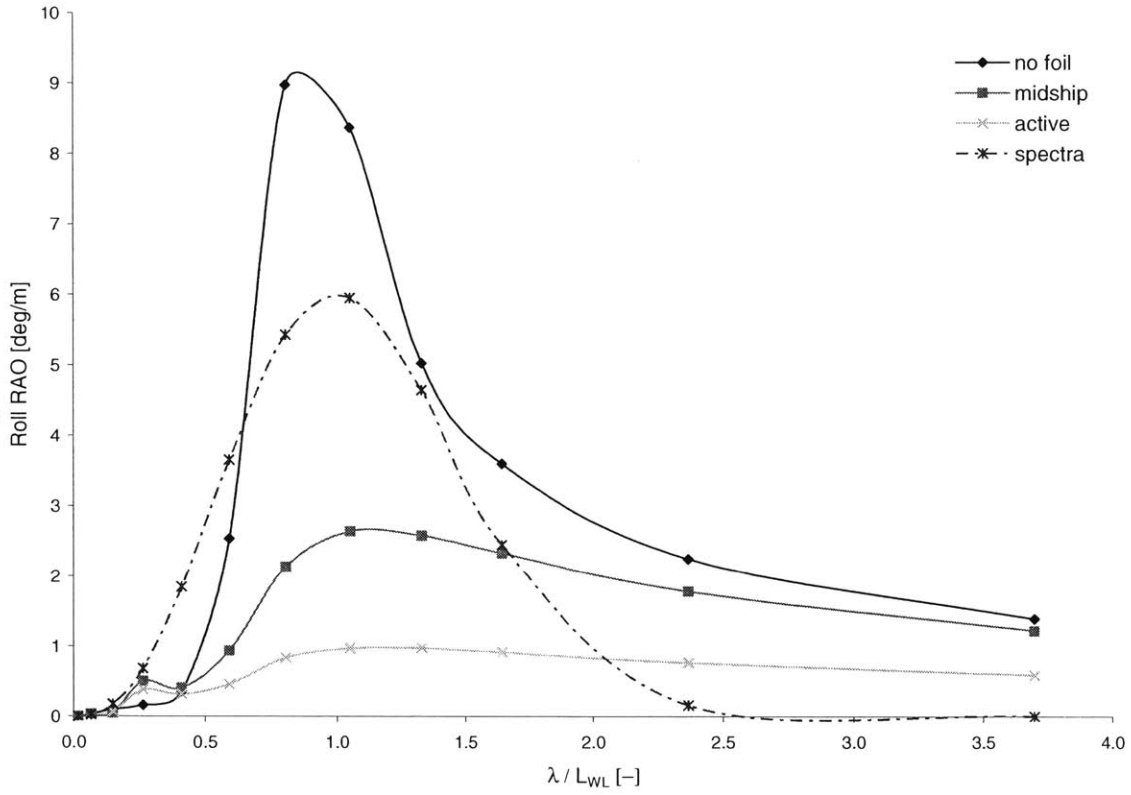

Figure 29: Roll RAOs, β=120° and χ_{FOIL}=midship, S=8 m^2, Fn=0.9, active and passive foil comparison

For the resonant frequency at roll, the above-defined relative reduction values (the reduction between the case with passive hydrofoil and the case with active hydrofoil) and absolute reduction (reduction between the case without any hydrofoil and the case with active control hydrofoil) are:

Wave heading β (°)	Relative reduction (%)	Absolute reduction (%)
090	35	69
105	62	89
120	65	90
135	69	91
150	75	94

The values above were achieved at the highest speed carried out for this study, Fn: 0.9. For lower speed runs, the relative reduction and the absolute reduction decrease slightly but still remarkable. These values depend on the C_1 and C_2 coefficients chosen: This means that the

reduction can be higher or lower according to the applied coefficients. The aim here was not finding the best possible coefficients but proving that remarkable additional reduction can be achieved when reasonable coefficients applied to the system.

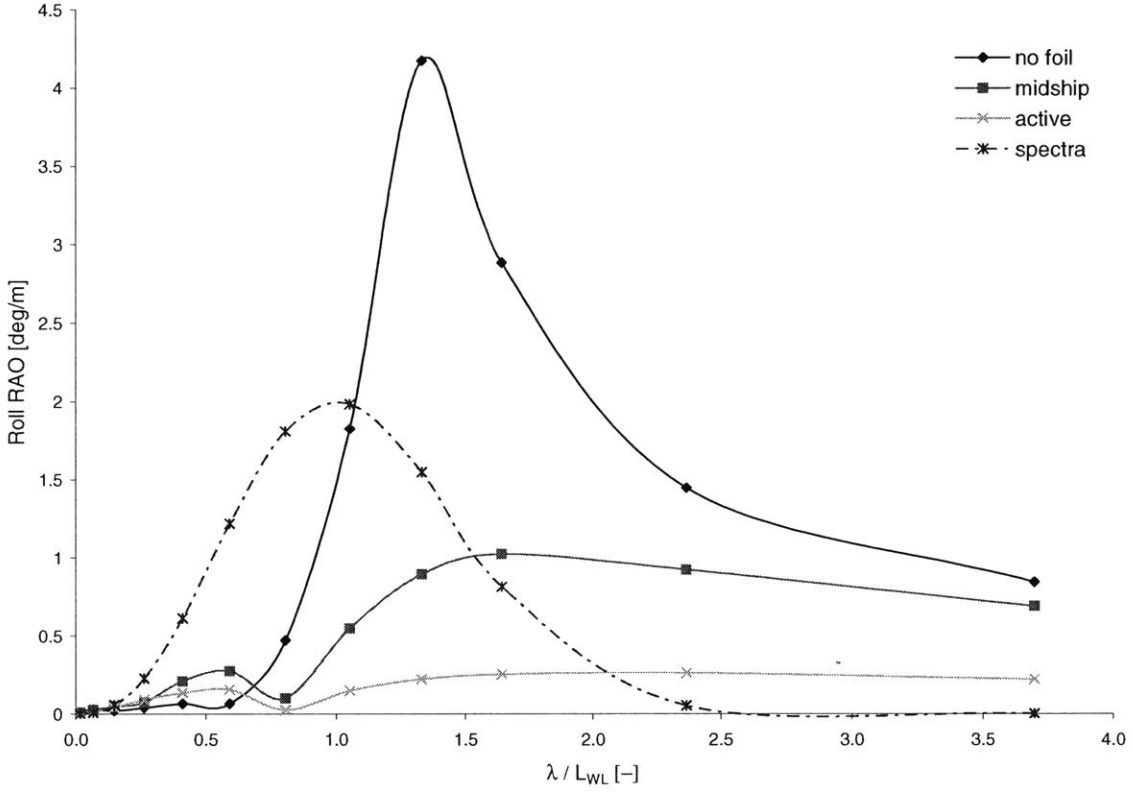

Figure 30: Roll RAOs, β=150° and χ_{FOIL}=midship, S=8 m^2, Fn=0.9, active and passive foil comparison

The best thing is to achieve the significant elimination of roll peak around resonant frequency. This is valid even for 090°-120° wave heading interval where the roll excitation forces attain their maximum values.

Figure 31 summarizes the active control effect at Fn: 0.9. Slightly less reduction in values with similar reduction patterns were achieved for other speed steps.

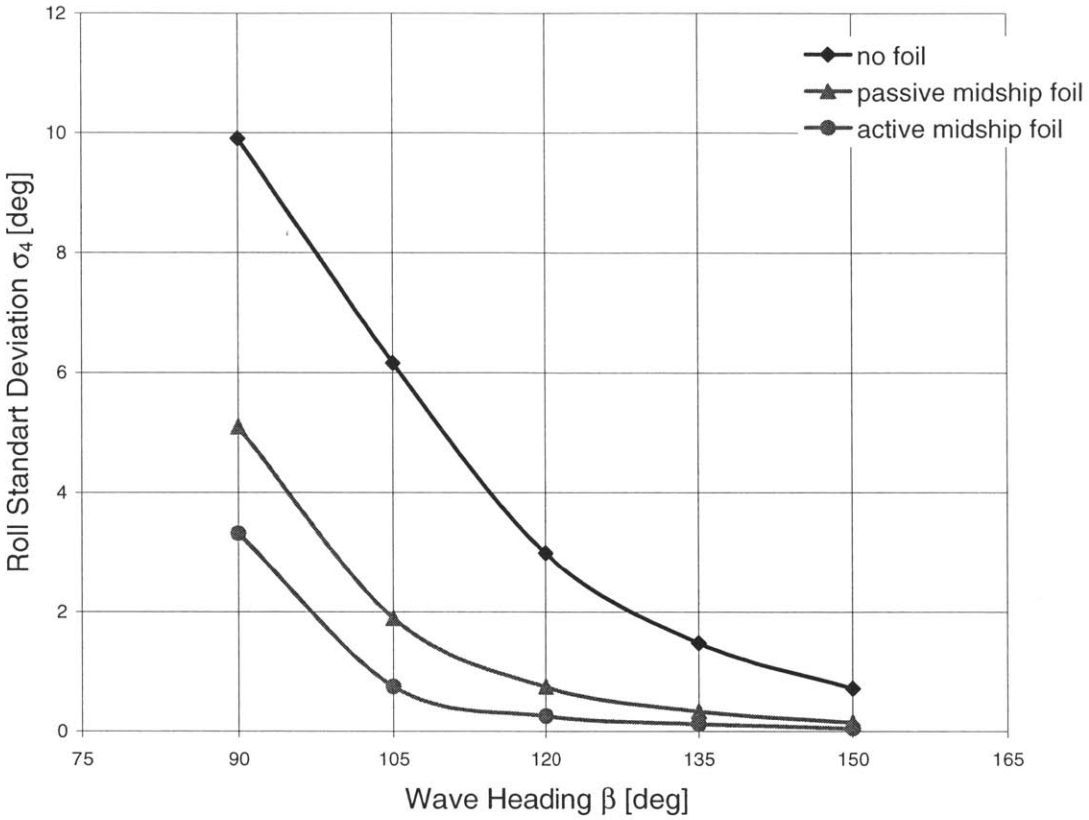

Figure 31: Roll Standard Deviation comparison for passive and active hydrofoil conditions, χ_{FOIL}=midship, S=8 m^2, Fn=0.9

6. Results, Discussions and Conclusions

6.1. General

The numerical stability of the time-domain Rankine Panel Method SWAN-2 used in this thesis is proven to be robust. Within linear theory, we can depend on the results of seakeeping runs carried out for this study.

Since SWAN-2 does not include viscous effects, especially for roll damping, the roll RAO reduction presented in this thesis can not be absolutely accurate. But without any hesitation one can depend on the relative decreases in roll RAOs. The goal of this thesis is not to determine the absolute reductions that can be achieved but to investigate the passive and active roll reduction mechanisms with hydrofoils and the influence of speed, planform area and the location on these systems. The following sections briefly explain the results of passive and active roll reduction system with hydrofoils studied in this thesis.

6.2. Passive Hydrofoil Roll Control Results

The influences of the foil planform area S, longitudinal foil position χ_{foil}, vessel forward speed U and wave heading β on the roll RAO were investigated in chapter 4. The complete set of results for the SWAN-2 simulations carried out in order to investigate the effect of these parameters is given in Appendices A-C.

From the results in chapter 4, it is unquestionable that the use of hydrofoils as roll reduction mechanism is quite effective for all cases studied. It was seen that the hydrofoil positioned at midship is the best motion damper in roll. The roll motion RAOs are significantly reduced by introducing a foil at this longitudinal position. From a hydrodynamic point of view, a passive motion damping lifting appendage should thus be positioned near the midship. A hydrofoil near the stern will have some effect on roll, but as a roll motion damper, it will have poor effect compared to the case with a hydrofoil positioned at midship in general.
The past studies showed that the selection of longitudinal position of hydrofoils is quite important in similar motion reduction systems for heave and pitch. The main reason is that the

longitudinal distance from midship is the moment arm for pitch moment due to hydrofoil lift force. With analogy to this, the lateral distance from the centerline is the moment arm for roll moment created by the lift force from hydrofoils. But as explained earlier, it is not feasible to vary this lateral position due to the ship beam. Since the midship location causes the minimum additional excitation and it is the most suitable for structural reasons, we can conclude that it is best to choose midship location if a hydrofoil roll reduction system such as the introduced one will be employed.

An increase in the foil planform area S will strengthen the reductions of the RAO peaks, but as the foil size increases, the relative reduction in the roll RAO peak will decrease. At some point, increasing the foil size will thus not affect the RAOs significantly. The selection of foil size will be a compromise between gain in roll motion damping and the increased drag the lifting appendages introduce.

When a lifting appendage is included, the effect of increased vessel speed is more pronounced due to the U^2 dependence of the hydrofoil lift force. It was shown that the increased vessel speed will lead to an additional significant reduction of roll RAOs, making this roll reduction system much more effective at higher speeds.

When increasing the vessel speed, two effects will alter the seakeeping characteristics of the vessel in roll, independent of lifting appendages. The frequency of encounter effect will shift the resonant frequency of the heave and pitch RAOs towards longer wavelengths. For high vessel speeds, this indicates that the resonant peak of the RAOs may be in a frequency range where there normally is little energy in the wave spectrum. An increase in the vessel speed also introduces lifting effects from the hull itself in the transom area.

A reduction in the wave heading β, away from oblique sea, will have an exact same effect as a speed reduction for roll. Due to the frequency of encounter effect, a reduction in β will shift the peak of the roll RAO towards longer wavelengths. It will also reduce the exciting force, and thus the peak of the RAOs slightly. Whether a heading change results in an increase or a

decrease of the heave and pitch responses is however dependent upon the mean wave period of the wave spectrum.

The roll RAOs of the vessel without lifting appendages present peaks at a value of λ/L_{WL} of 0.25-1.25 dependent upon speed. These values correspond to 2.5-12.5 λ/B_{WL}, where BWL stands for the beam at design waterline. For the same vessel speed, roll RAO peaks at nearly the same wavelength when hydrofoils are used, with peak magnitudes less than the cases without any hydrofoils.

We saw in section 2.7.2 that the damping coefficient and excitation force of roll equations of motion change (increase) when the hydrofoils are attached to the hull.

$$B_{44}^{\,with\_foil} = B_{44} + \sum_{i=1}^{2} y_i^{\,2} \cdot \frac{F}{U}$$

$$X_4^{\,with\_foil} = X_4 + \sum_{i=1}^{2} \frac{i\omega}{U} \cdot y_i \cdot F \cdot e^{-k \cdot T - ik(x_i \cdot \cos\beta + y_i \cdot \sin\beta)} \quad \text{where } F = \frac{\pi \rho S U^2 AR}{2 + AR}.$$

These terms are basically enough to figure out the effects of ship forward speed, longitudinal and lateral position of hydrofoils, and the planform area on roll reduction.

Since the B_{44} term includes U, there is direct relation between the damping force and the forward speed U. The excitation term also includes U, but the increase of excitation due to hydrofoils is small compared to the increase of damping due to the hydrofoils. This explains why this system is more effective at higher speeds.

The B_{44} term also includes the hydrofoil planform area S, building another direct relation between damping and hydrofoil planform area. But one should keep in mind that it is generally not feasible to increase the planform area more than to some extent, unless you decrease the AR. It is clear that the relative effect of increasing S will decrease since F term is directly related to $\frac{AR}{2 + AR}$.

The excitation term reveals the optimum longitudinal location of hydrofoils. The hydrofoils located at midship cause minimum additional excitation, or in an explicit way, minimum total roll excitation. Instead, the hydrofoils located rear of midship will increase the total excitation slightly, causing higher roll RAO compared to the case with midship hydrofoils. Actually, looking at damping and excitation term, one can easily see that one of the most important terms is y_{foil} since it is the moment arm term in roll moment. The B_{44} term is proportional to the y_{foil}^2, and the excitation term is to the y_{foil}. But it is not generally feasible to vary this term since we do not want our hydrofoils extend beyond the beam. Best thing to do is to choose the most upper limit for y_{foil} that the beam of the ship allows.

6.3. Active Hydrofoil Roll Control Results

Having all the optimum results from passive roll control system, an active control mechanism was experimented. The capability of controlling the coefficients resulted in a very effective roll control mechanism. The absolute and relative reduction for all speed, planform area and wave heading condition were quite remarkable.

A limit of $\pm 15°$ for effective angle of attack was employed in order to estimate the anti-rolling moment as true as possible in linear terms. Whenever the effective angle of attack goes beyond this limit, the lift force becomes zero resulting into no moment.

The active control runs were performed keeping C_1 and C_2 terms constant, not time dependent, during runs. Since the effective angle of attack is time dependent, time dependent coefficients can be input in the mechanism that will likely more effective in motion reduction. But for this study it was enough to show that even with constant values of coefficients the active control mechanism is quite effective.

Appendix D includes all the results of runs on active control study.

6.4. Conclusions

The passive and active hydrofoil roll control systems were found to be very effective mechanisms in reducing the roll motion. The roll response will most likely be largest in beam seas, with and without the influence of a motion damping foil.

A passive roll control system consisting of hydrofoils will give the best performance if the hydrofoils are positioned near midship, one on port side and the other on starboard side.

In this position, increasing foil size will result in reducing roll response. The relative reduction decreases as the foil size get bigger. The optimum ratio (S_{FOIL}/A_{WP}) for the ship studied is around 0.02. The bigger ratios will result in less additional reduction but more viscous resistance. From a resistance point of view, a lifting appendage used for motion damping should be as small as possible. It is shown in [2] that the only resistance component that changes significantly with foil size is the added frictional and induced drag introduced by the foil. The induced drag from a lifting appendage is more or less independent of foil size if the foil is an effective motion damper.

The forward speed has a considerable influence on the effectiveness of both active and passive roll reduction system. The faster the ship is, the more reduction you get.

Based on the conclusions above, a foil with planform area $S=8m^2$ positioned at midship will be the best selection for roll motion damping and the ship resistance. For modest seas, the frictional and induced drags due to these hydrofoils are negligible compared to the bare hull resistance. For rough sea states, the drag due to the hydrofoils become significant and should be taken into account.

The primary results showed that the active roll control mechanism experimented here is more effective than the passive one for all cases. The further study on active motion control will be carried out.

7. References & Bibliography

[1] Abbot, I.H. &Von Doenhoff, A.E. *Theory of wing sections,* Dover Publications, Inc. New York.

[2] Borgen, Henning. The Influence of Lifting Appendages on a High Speed Monohull, MIT Masters Thesis, 2001.

[3] Boston Marine Consulting Inc. *SWAN-2 2001 theory manual.*

[4] Boston Marine Consulting Inc. *SWAN-2 2001 user manual.*

[5] Faltinsen, O.M. *Sea Loads on Ships and Offshore Structures,* Cambridge University Press, 1990.

[6] Katz, J., Plotkin, A. Low Speed Aerodynamics From Wing Theory to Panel Methods, 1991.

[7] Kring, D.C. *Time Domain Ship Motions by a Three-Dimensional Rankine Panel Method*, PhD thesis, MIT, Cambridge MA, 1994.

[8] Kring, D.C., Huang, Y., Sclavounos, P.D., Vada, T. & Braathen, A. *Nonlinear Ship Motions and Wave Induced Loads by a Rankine Panel Method*, 21st Symposium on Naval Hydrodynamics, Trondheim, 1996.

[9] Kring, D.C., Mantzaris, D.A., Tcheou, G.B. & Sclavounos, P.D. *A Time-Domain Seakeeping Simulation for Fast Ships*, FAST97 conference, Sydney, Australia, 1997.

[10] Lewis, Edward V. *Principles of Naval Architecture*, Volume II – "Resistance, Propulsion and Vibration" chapter 5, 1988.

[11] Lewis, Edward V. *Principles of Naval Architecture*, Volume III – "Motion in Waves and Controllability" chapter 8, 1989.

[12] Lloyd, A.R.J.M. *Seakeeping: Ship behavior in Rough Weather*, 1989.

[13] Moran, J. *Introduction to Theoretical and Computational Aerodynamics*, John Whiley & Sons Inc., 1984.

[14] Nakos, D.E. & Sclavounos, P.D. *Stability Analysis of Panel Methods for Free-Surface Flows With Forward Speed*, 17th Symposium of Naval Hydrodynamics, The Hague, The Netherlands, 1988.

[15] Nakos, D.E. & Sclavounos, P.D. *On Steady and Unsteady Ship Wave Patterns,* Journal of Fluid Mechanics vol. 215, 1990.

[16] Nakos, D.E. & Sclavounos, P.D. *Ship Motions by a Three-Dimensional Rankine Panel Method,* Massachusetts institute of technology.

[17] Nakos, D.E. *Ship Wave Patterns and Motions by a Three Dimensional Rankine Panel Method*, PhD thesis, MIT, Cambridge MA, 1990.

[18] Nakos, D.E. *Stability of Transient Gravity Waves on a Discrete Free Surface*, MIT report, 1993

[19] Nakos, D.E., Kring, D.C. & Sclavounos, P.D. *Rankine Panel Methods for Transient Free Surface Flows,* 6th International Conference on Numerical Ship Hydrodynamics, Iowa City, 1993

[20] Newman, J.N. *Marine Hydrodynamics*, The MIT Press, Cambridge MA, 1977.

[21] Sclavounos, P.D., Nakos, D.E. & Huang, Y. *Seakeeping and Wave Induced Loads on Ships With Flare by a Rankine Panel Method*, 6th International Conference on Numerical Ship Hydrodynamics, Iowa City, 1993.

[22] Sclavounos, P.D. *Responses of Marine Structures to Sea Loads,* Class Notes Course 13.022, Massachusetts Institute of Technology.

[23] Sclavounos, P.D. *Computation of Wave Ship Interactions*, Advances in marine hydrodynamics, Computational Mechanics Publications, 1995.

[24] Sclavounos, P.D. & Huang, Y. *Rudder Winglets on Sailing Yachts,* Massachusetts Institute of Technology.

[25] Triantafyllou,M.S., Chryssostomidis C. *Environment Description, Force Prediction and Statistics for Design Applications in Ocean Engineering*, Department of Ocean Engineering, MIT, Cambridge, MA, USA, 1980.

[26] Vada, T. & Nakos, D.E., *Time-marching Schemes for Ship Motion Simulations*, Eight International Workshop on Water Waves and Floating Bodies, 1993

8. Nomenclature

$\Phi(\vec{x},t)$	Total velocity potential	[-]
$\phi_I(\vec{x},t)$	Incident wave velocity potential	[-]
$\phi_0(\vec{x})$	Basis flow velocity potential	[-]
$\phi(\vec{x},t)$	Disturbance flow velocity potential	[-]
$\psi(\vec{x},t)$	Impulsive velocity potential	[-]
$\varphi(\vec{x},t)$	Residual velocity potential	[-]
$\zeta(\vec{x},t)$	Free surface elevation	[m]
$\zeta_0(\vec{x})$	Basis flow free surface elevation	[m]
$\vec{x}$	Position vector	[m]
$\vec{n}$	Surface normal vector	[-]
∇	Differential operator = $\frac{\partial}{\partial x}+\frac{\partial}{\partial y}+\frac{\partial}{\partial z}$	[-]
$\Re$	Real part operator	[-]
$\vec{V}(\vec{x},t)$	Fluid velocity vector	[m/s]
$\vec{V}_B(\vec{x},t)$	Hull surface velocity vector (rigid body)	[m/s]
ω_0	Absolute frequency of ambient waves	[rad/s]
ω	Frequency of encounter	[rad/s]
k	Wave number	[m^{-1}]
A	Wave amplitude	[m]
β	Wave heading	[rad]
V_P	Wave phase velocity	[m/s]
V_G	Wave group velocity	[m/s]
ε	Phase angle	[rad]
H	Water depth	[m]
g	Acceleration due to gravity	[m/s^2]
U	Vessel speed	[m/s]

p	Pressure	$[N/m^2]$
ρ	Density of seawater	$[kg/m^3]$
g	Acceleration due to gravity	$[m/s^2]$
M_{ij}	Inertia matrix	$[kg],[kgm^2]$
A_{ij}	Added mass matrix	$[kg],[kgm^2]$
B_{ij}	Damping matrix	$[Ns/m],[Nms]$
C_{ij}	Restoring coefficient matrix	$[N/m],[Nm/rad]$
X_i	Complex exciting force vector	$[N]$
ξ_j	Rigid body modes of motion	$[m]$, $[rad]$
$F_i(t)$	Hydrodynamic forces	$[N]$
F_{ex_i}	Complex exciting force divided by A	$[N]$
Ξ_j	Complex amplitude of the jth rigid body displacement mode	$[m]$
χ_j	Phase of the jth rigid body displacement mode	$[rad]$
σ_j	Standard deviation of the jth rigid body displacement mode	$[m]$
R_{TOT}	Total ship resistance	$[kN]$
R_{IF}	Ideal fluid resistance	$[kN]$
R_W	Wave resistance	$[kN]$
R_{IND}	Induced resistance	$[kN]$
$S_\zeta(\omega_0)$	Wave spectrum	$[m^2s]$
$H_{1/3}$	Significant wave height	$[m]$
T_1, T_2	Mean wave periods of wave spectrum	$[s]$
θ	Wave propagation direction in Kelvin Wake	$[deg]$
x_{foil}	Longitudinal position of foil	$[m]$
F_{3L}	Complex amplitude of foil lift force	$[N]$
F	Lifting line constant in the foil lift force	$[N]$
L	Lift force	$[N]$
D	Drag force	$[N]$

C_L	Lift coefficient	[-]
C_D	Drag coefficient	[-]
Γ	Foil circulation	[-]
c	Foil chord	$[m]$
s	Foil span	$[m]$
AR	Foil aspect ratio	[-]
α	Foil angle of attack	$[rad]$
S	Foil planform area	$[m^2]$
S_W	Wetted surface of foil	$[m^2]$
S_B	Wetted surface of hull	$[m^2]$
$\overline{S}_B$	Mean wetted surface of hull	$[m^2]$
T	Foil draft	$[m]$
Ω	Reduced frequency	[-]
FS	The free surface	
W	Free surface wake	
$G(\vec{x};\vec{\xi})$	The Green function	
$\vec{\xi}$	Position of Rankine Source	$[m]$
Re	Reynolds number	[-]
Fn	Froude number	[-]
F_h	Panel Froude number	[-]
h_x	Streamwise panel dimension	$[m]$
h_y	Transverse panel dimension	$[m]$
$B_j(\vec{x})$	Bi-quadratic spline coefficient	[-]
β	Non-dimensional time step	[-]
α	Panel aspect ratio	[-]
ν	Damping parameter	$[Ns/m]$
$\vec{\xi}$	Vessel displacement vector	$[m]$

$\vec{\alpha}$	Vessel centre angular displacement vector	$[rad]$
$\vec{\delta}$	Panel centre displacement vector	$[m]$
$\vec{F}_h$	SWAN-2 hydrodynamic force vector	$[N]$
$\vec{M}_h$	SWAN-2 hydrodynamic moment vector	$[Nm]$
$\vec{F}_{m_i}$	Memory force vector	[N], $[Nm]$

9. Appendix A: The Influence of Longitudinal Position of Hydrofoils

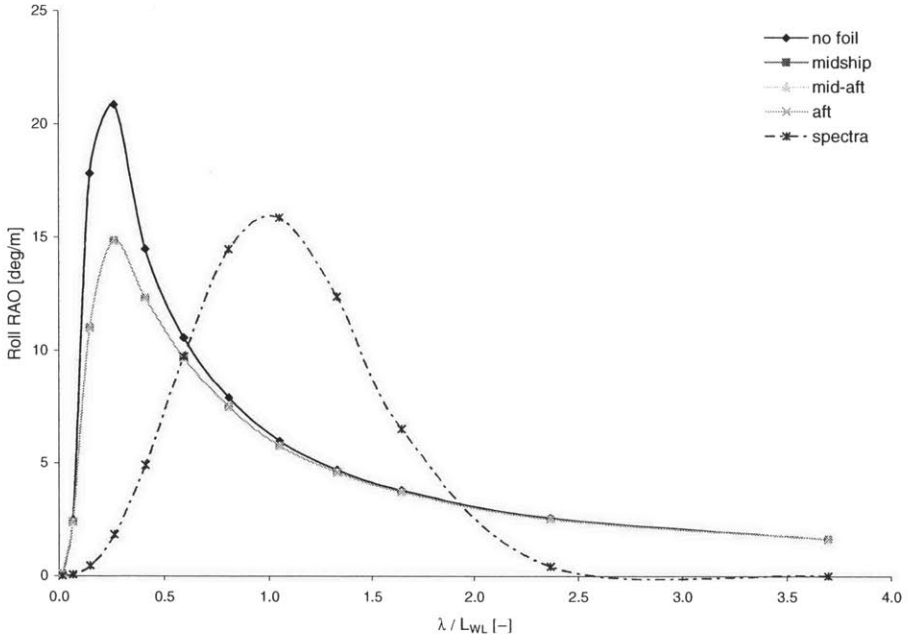

Figure 32: Roll RAO, Variation of Longitudinal Location, β =090°, S = 8 m^2, Fn = 0.3

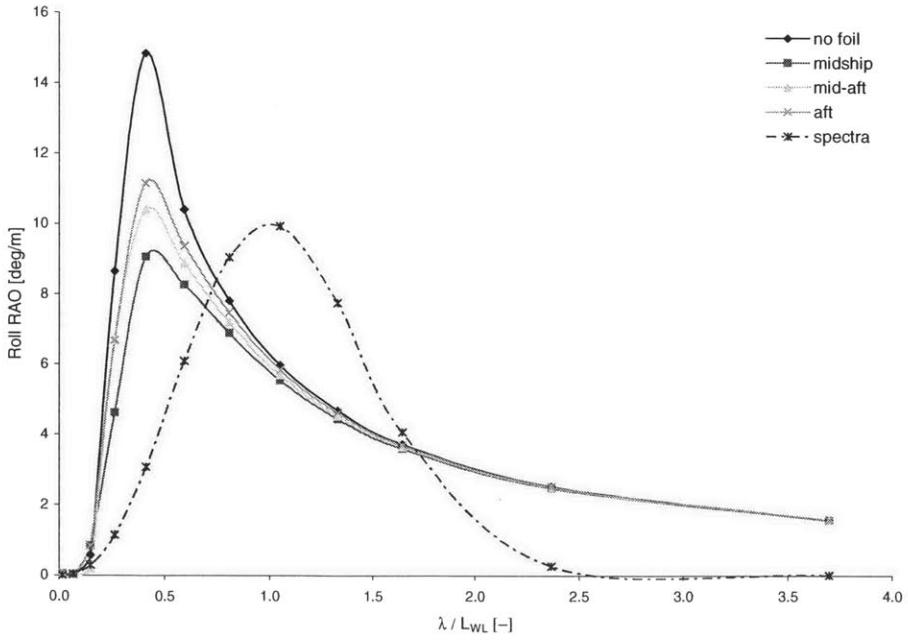

Figure 33: Roll RAO, Variation of Longitudinal Location, β =105°, S = 8 m^2, Fn = 0.3

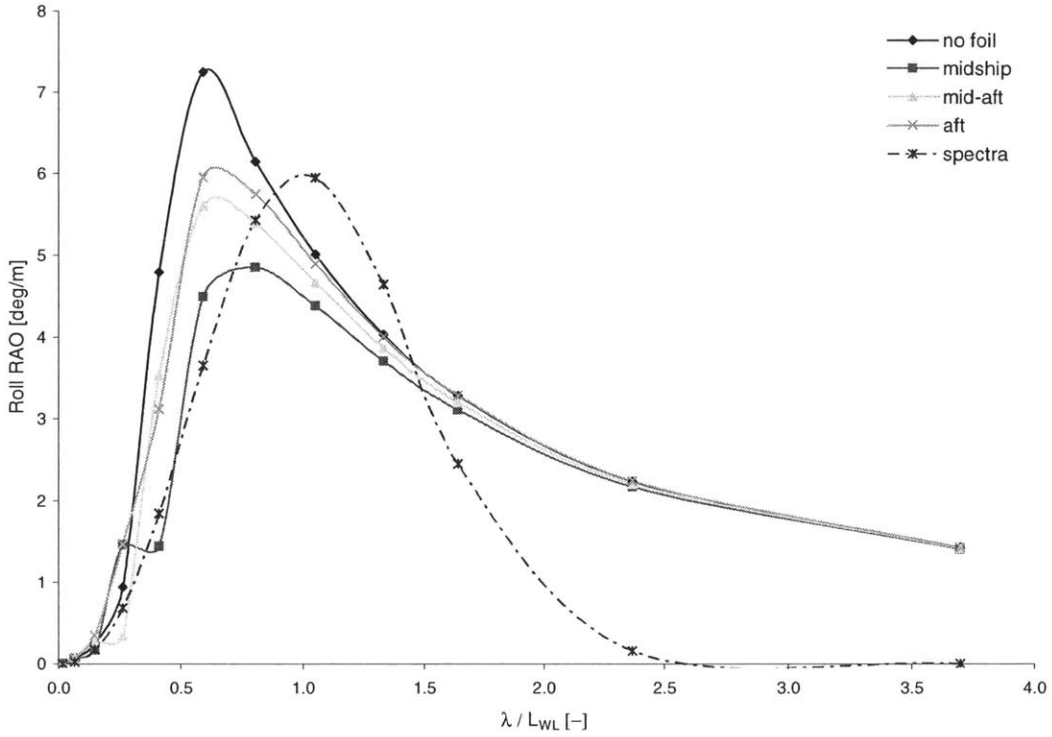

Figure 34: Roll RAO, Variation of Longitudinal Location, β =120°, S = 8 m², Fn = 0.3

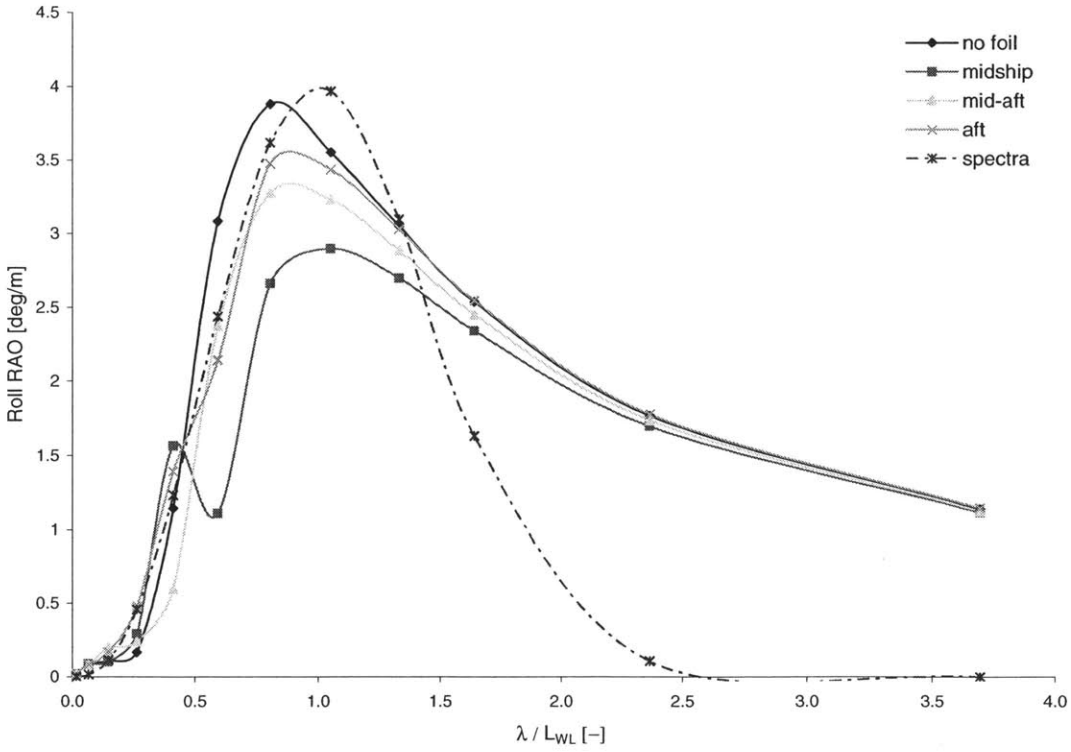

Figure 35: Roll RAO, Variation of Longitudinal Location, β =135°, S = 8 m², Fn = 0.3

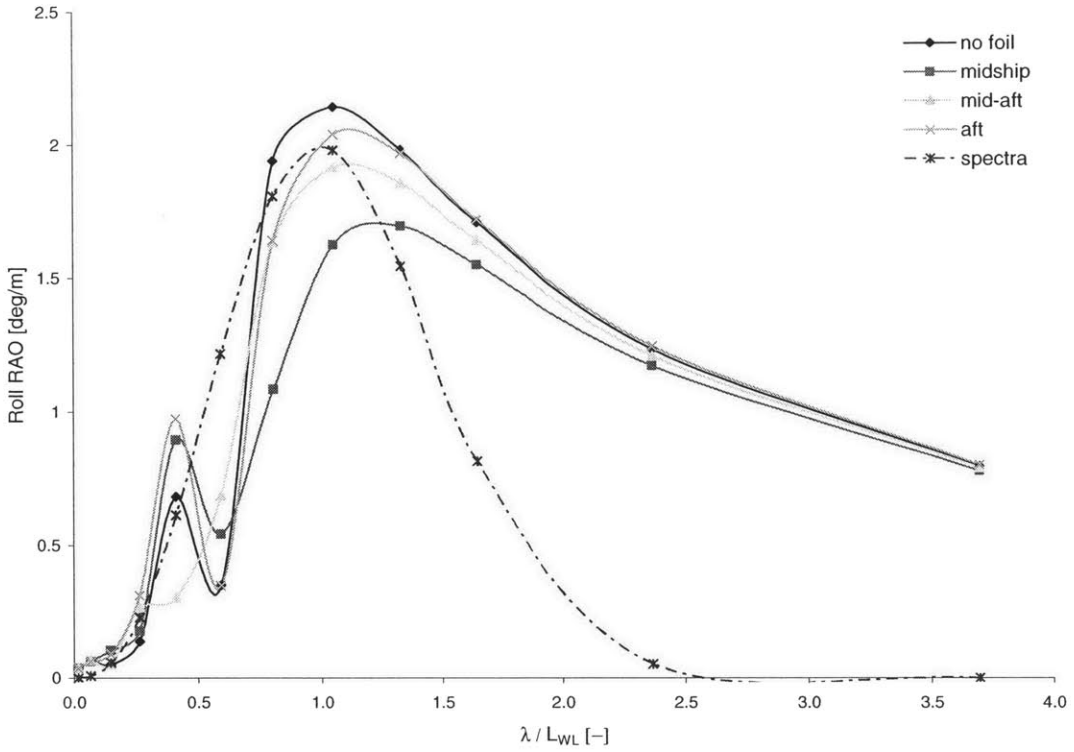

Figure 36: Roll RAO, Variation of Longitudinal Location, β =150°, S = 8 m², Fn = 0.3

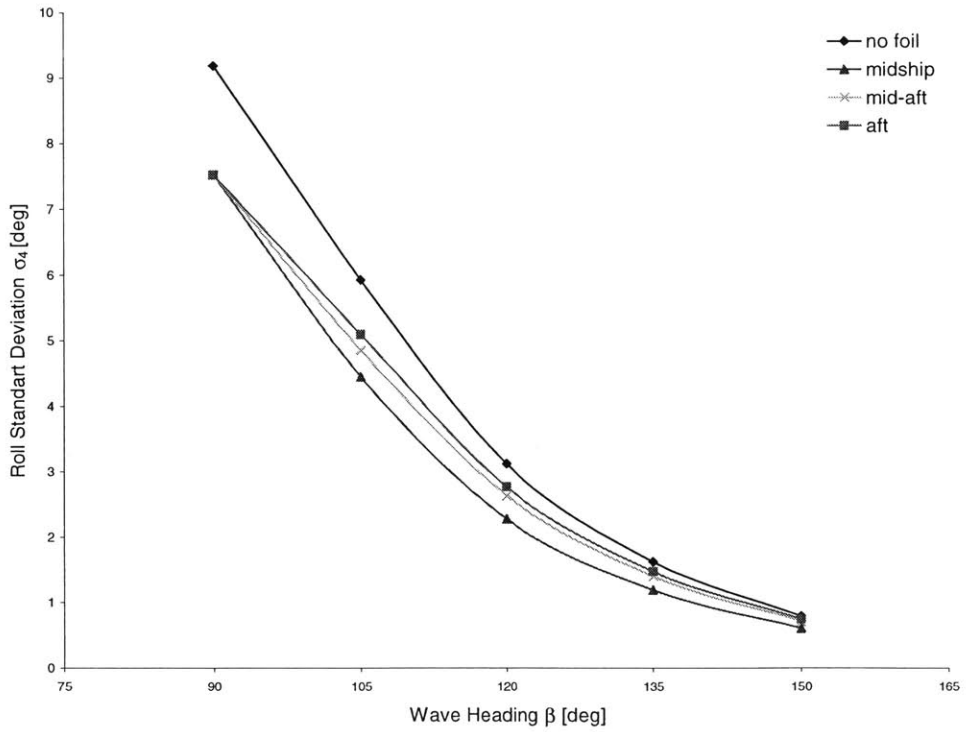

Figure 37: Roll Standard Deviation, varying β and χ Location, S = 8 m², Fn = 0.3

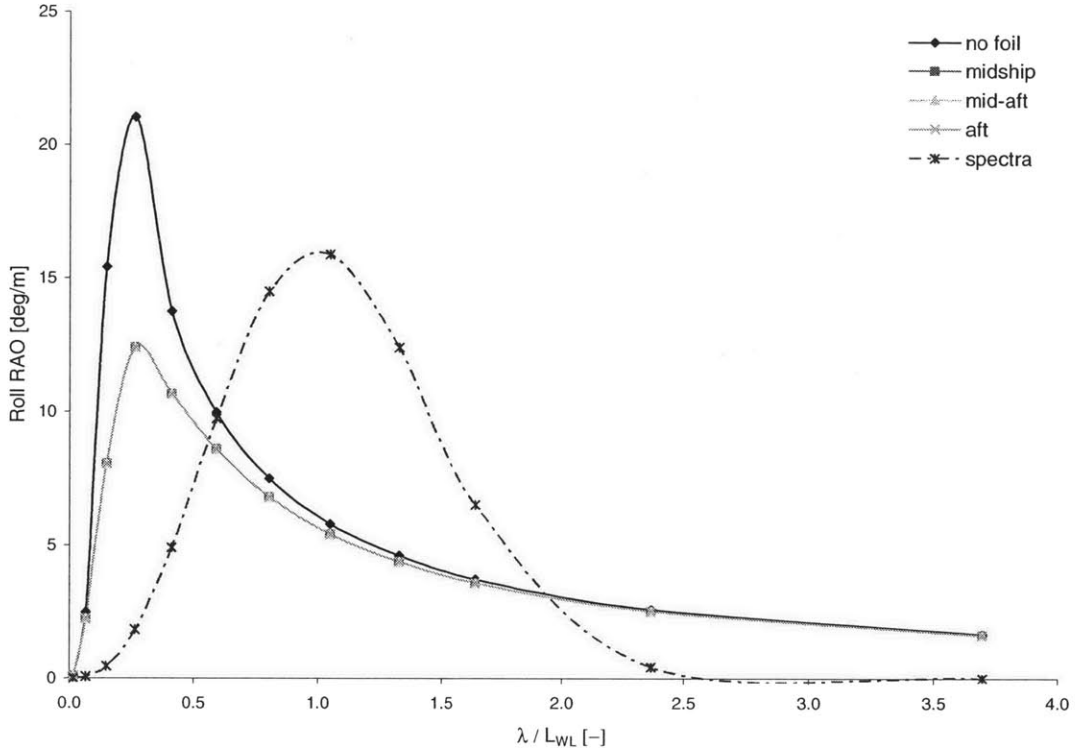

Figure 38: Roll RAO, Variation of Longitudinal Location, β =090°, S = 8 m², Fn = 0.5

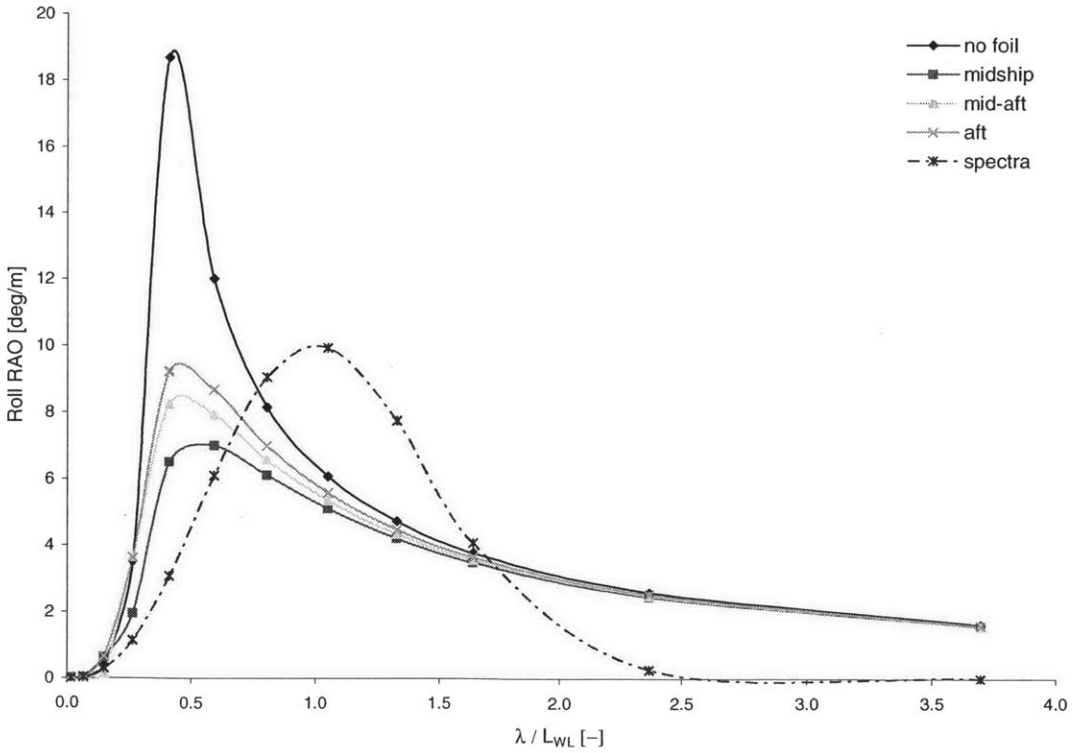

Figure 39: Roll RAO, Variation of Longitudinal Location, β =105°, S = 8 m², Fn = 0.5

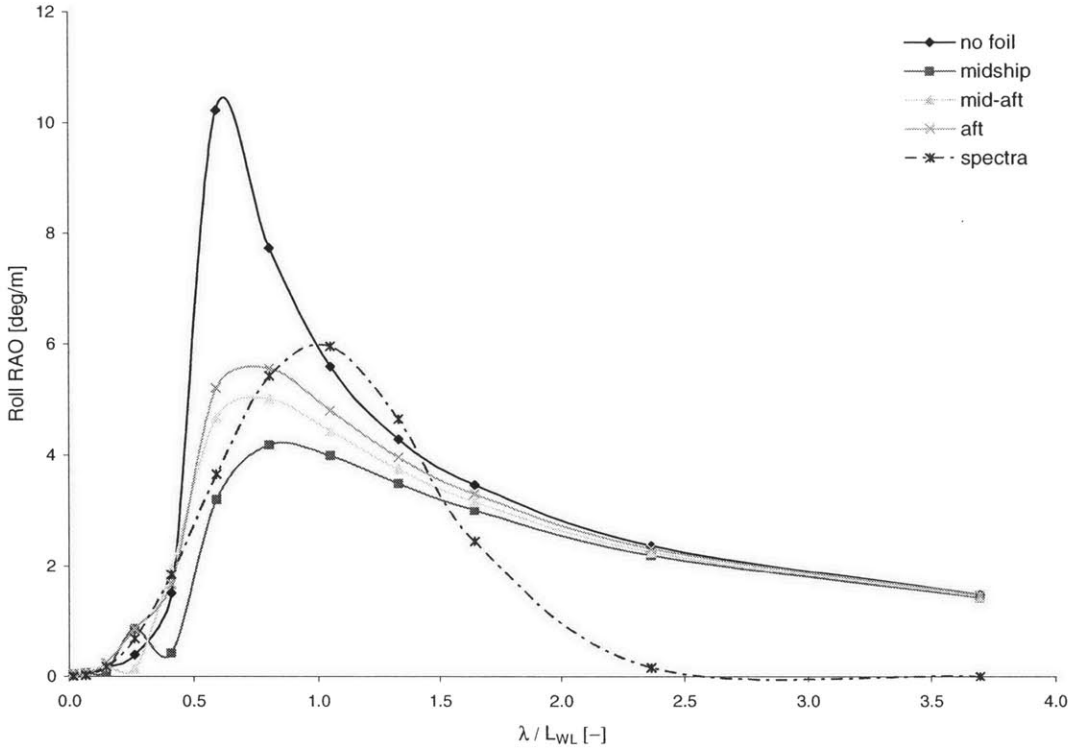

Figure 40: Roll RAO, Variation of Longitudinal Location, β =120°, S = 8 m^2, Fn = 0.5

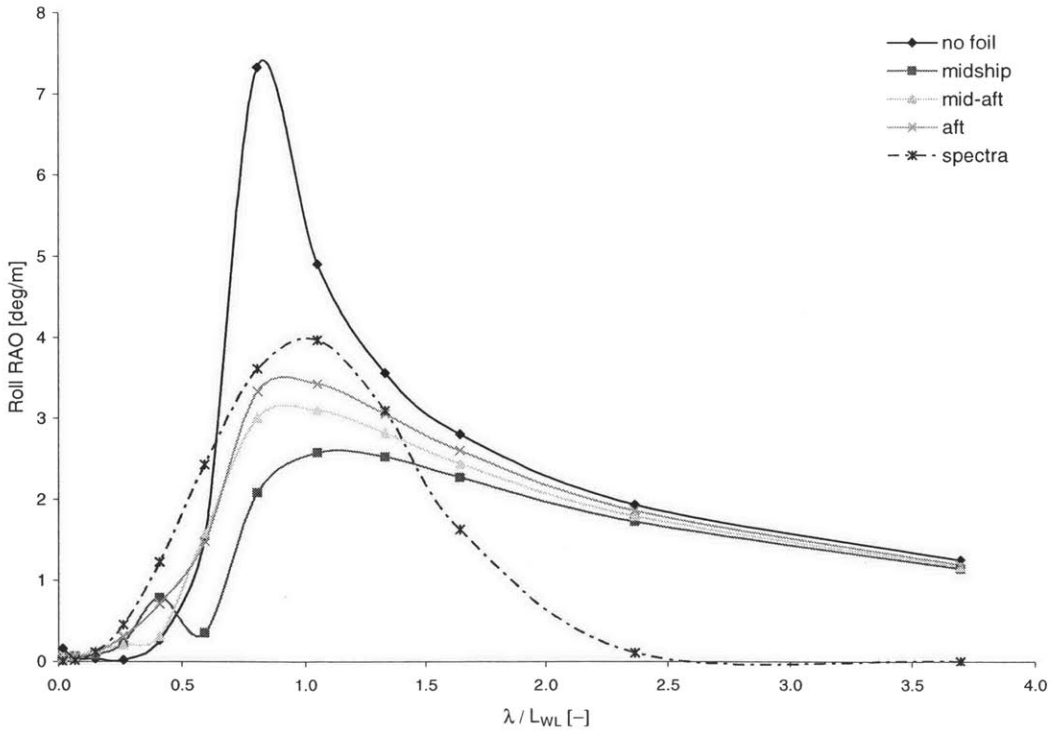

Figure 41: Roll RAO, Variation of Longitudinal Location, β =135°, S = 8 m^2, Fn = 0.5

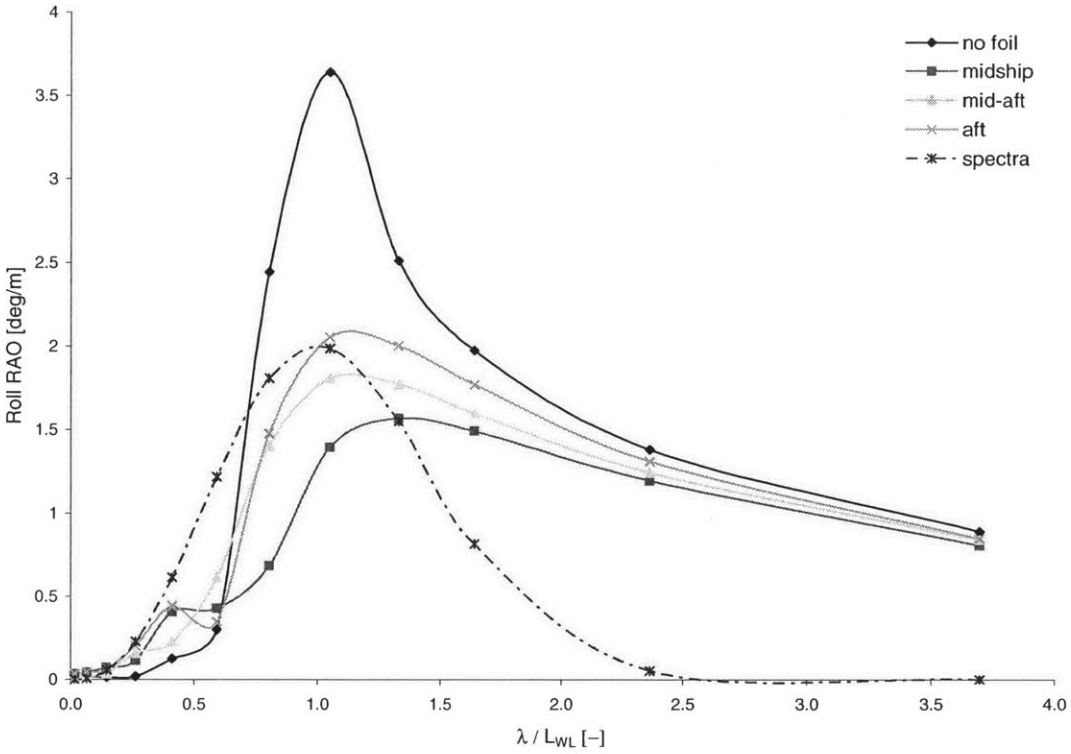

Figure 42: Roll RAO, Variation of Longitudinal Location, β =150°, S = 8 m², Fn = 0.5

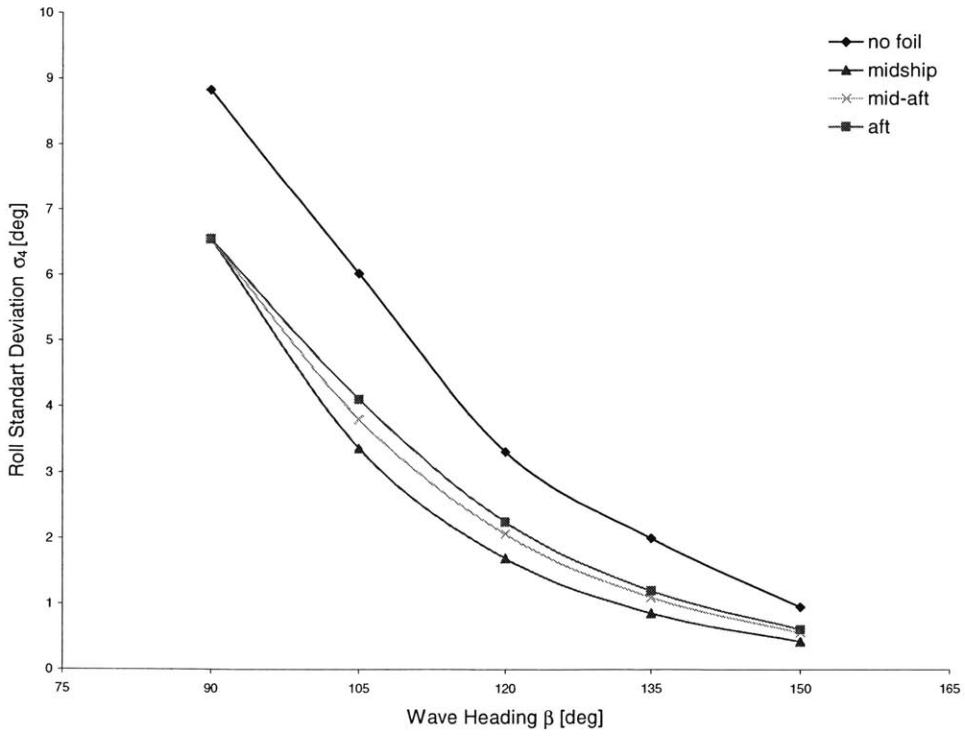

Figure 43: Roll Standard Deviation, varying β and χ Location, S = 8 m², Fn = 0.5

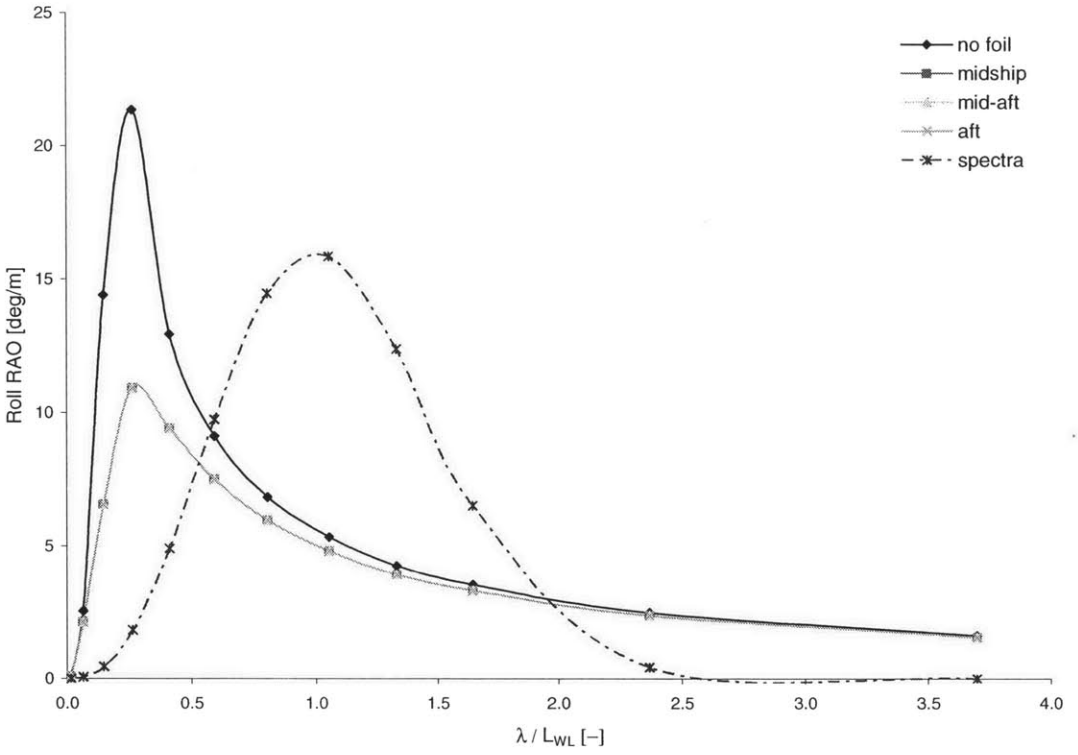

Figure 44: Roll RAO, Variation of Longitudinal Location, β =090°, S = 8 m^2, Fn = 0.7

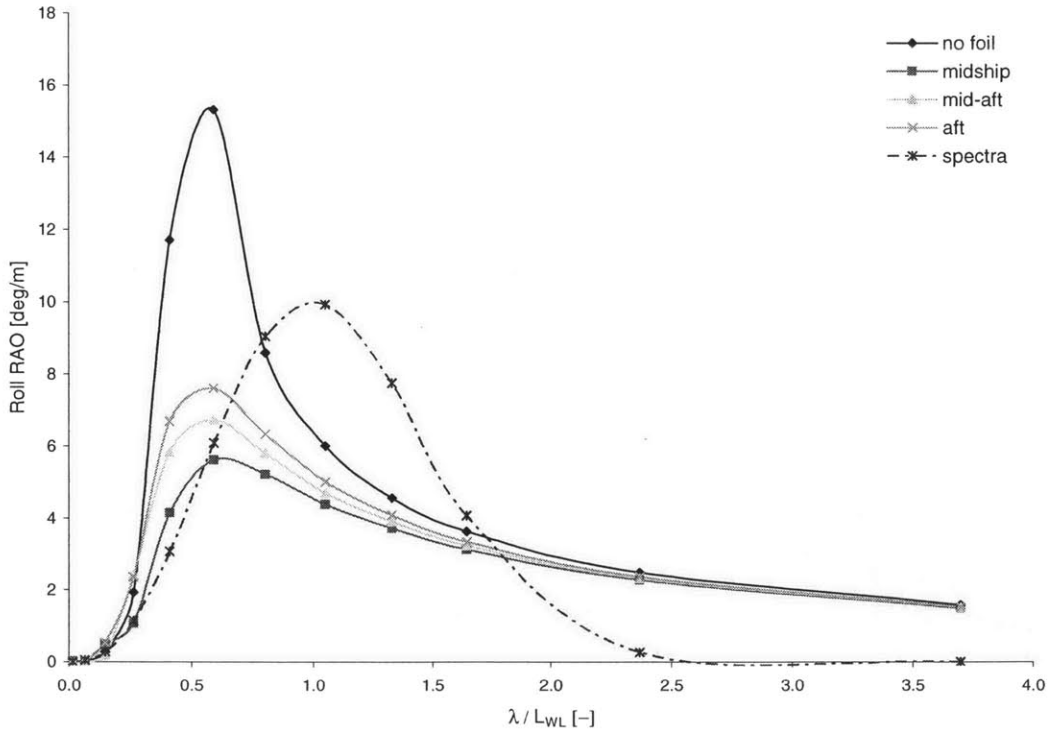

Figure 45: Roll RAO, Variation of Longitudinal Location, β =105°, S = 8 m^2, Fn = 0.7

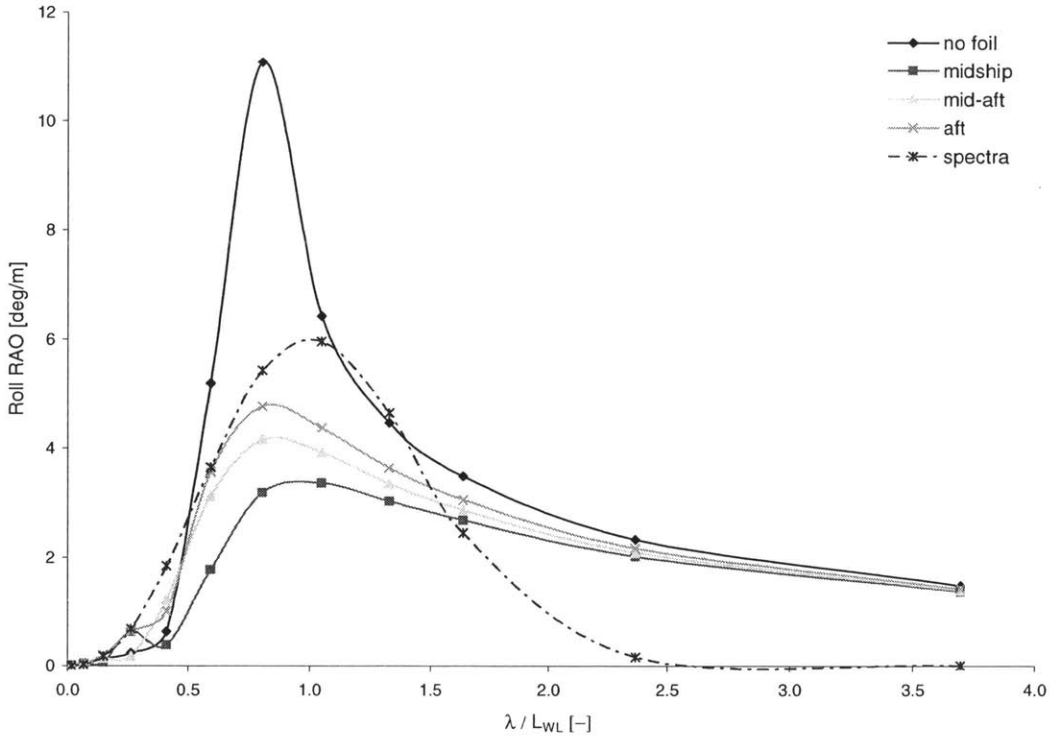

Figure 46: Roll RAO, Variation of Longitudinal Location, β =120°, S = 8 m², Fn = 0.7

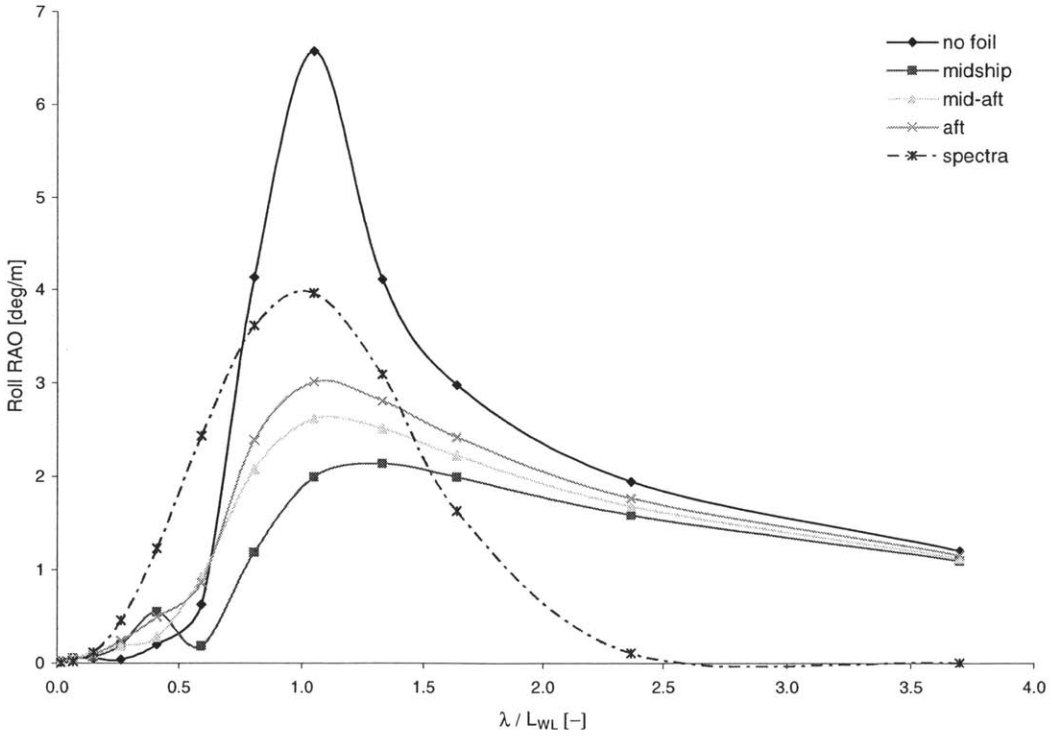

Figure 47: Roll RAO, Variation of Longitudinal Location, β =135°, S = 8 m², Fn = 0.7

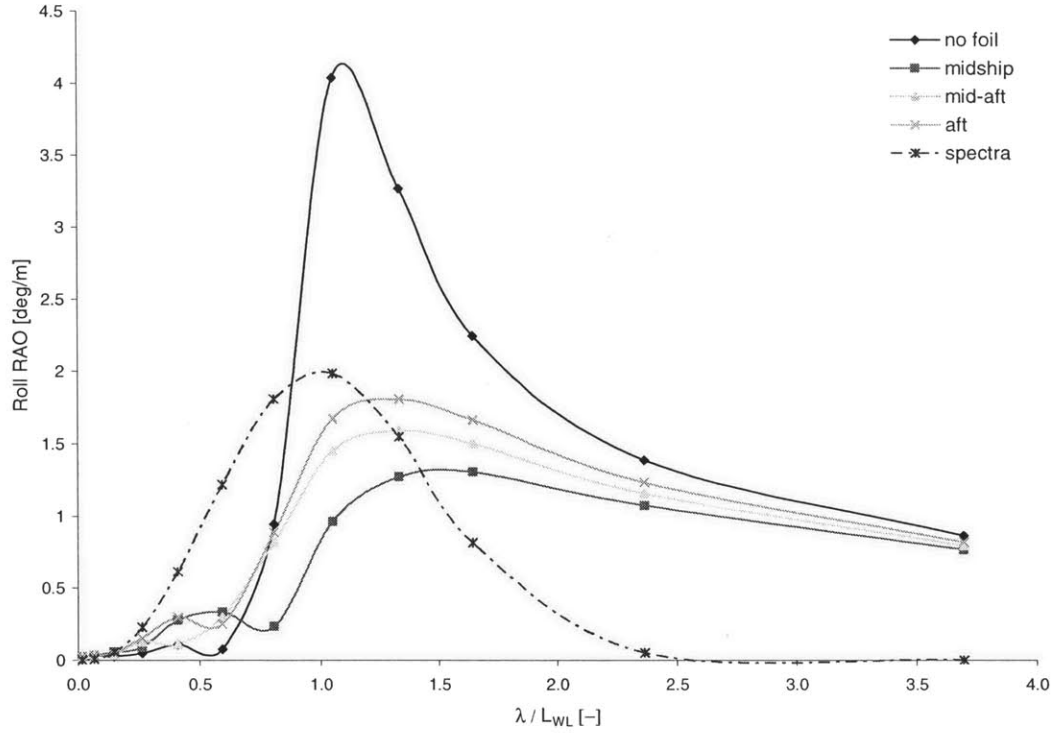

Figure 48: Roll RAO, Variation of Longitudinal Location, β =150°, S = 8 m², Fn = 0.7

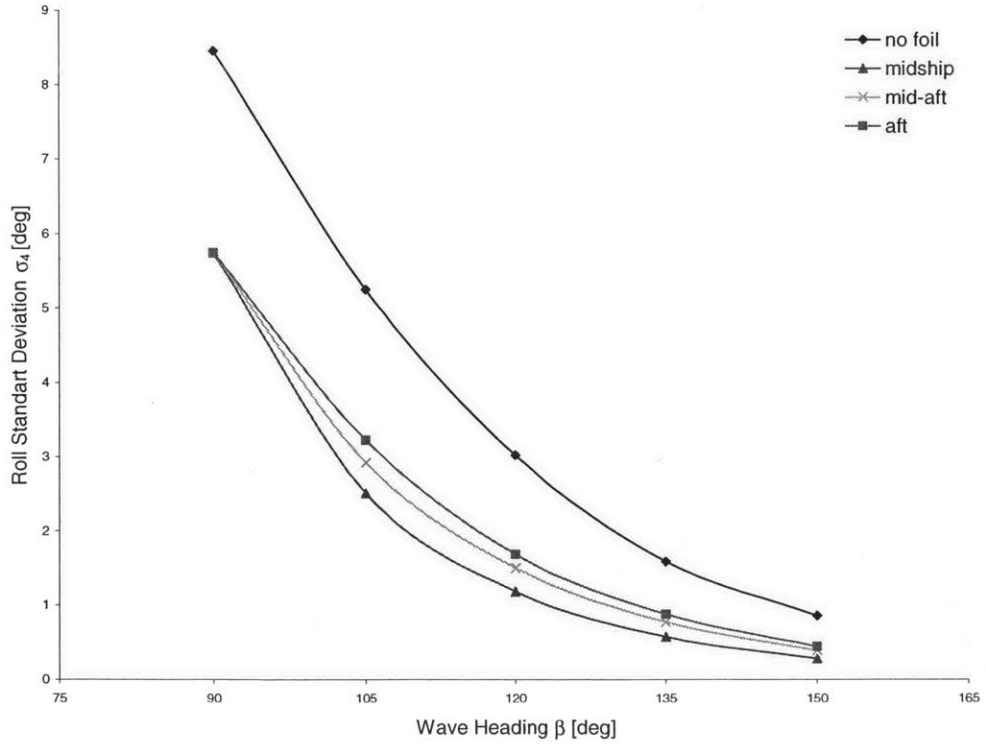

Figure 49: Roll Standard Deviation, varying β and χ Location, S = 8 m², Fn = 0.7

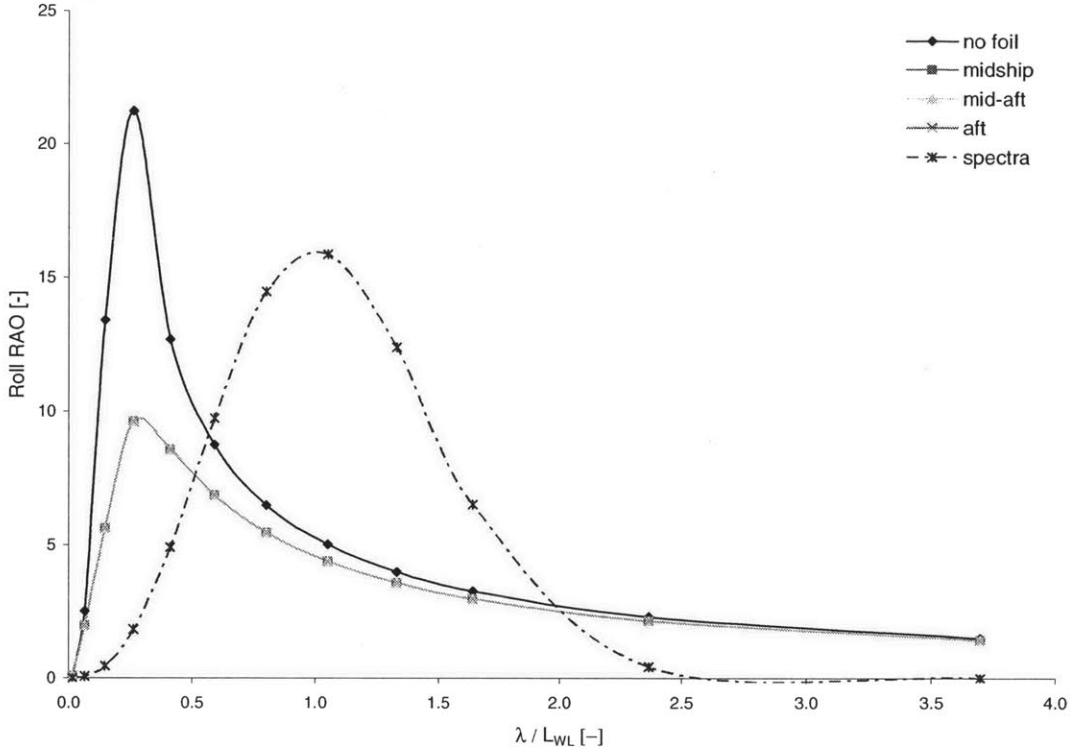

Figure 50: Roll RAO, Variation of Longitudinal Location, β =090°, S = 8 m², Fn = 0.9

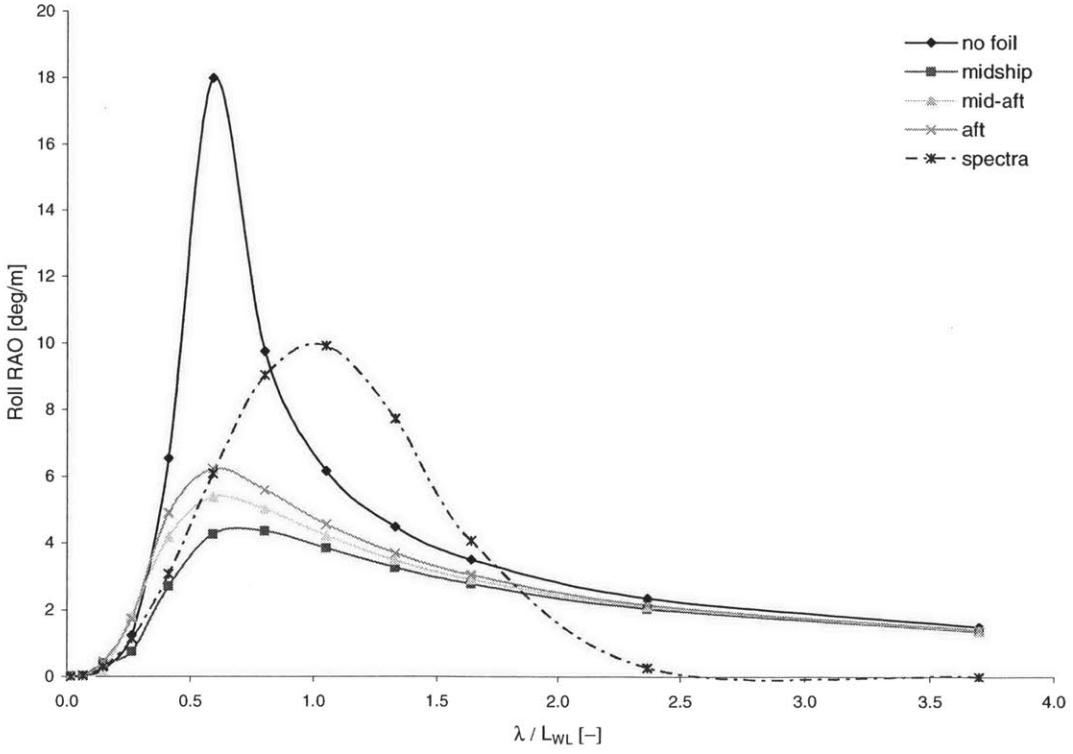

Figure 51: Roll RAO, Variation of Longitudinal Location, β =105°, S = 8 m², Fn = 0.9

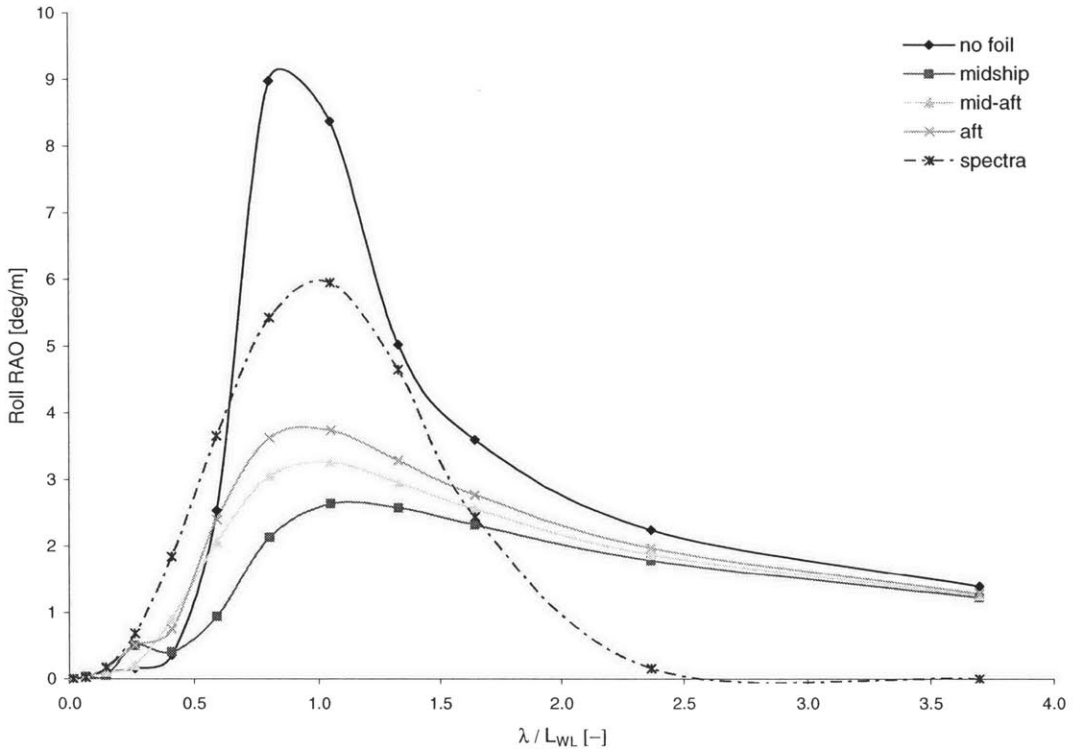

Figure 52: Roll RAO, Variation of Longitudinal Location, β =120°, S = 8 m², Fn = 0.9

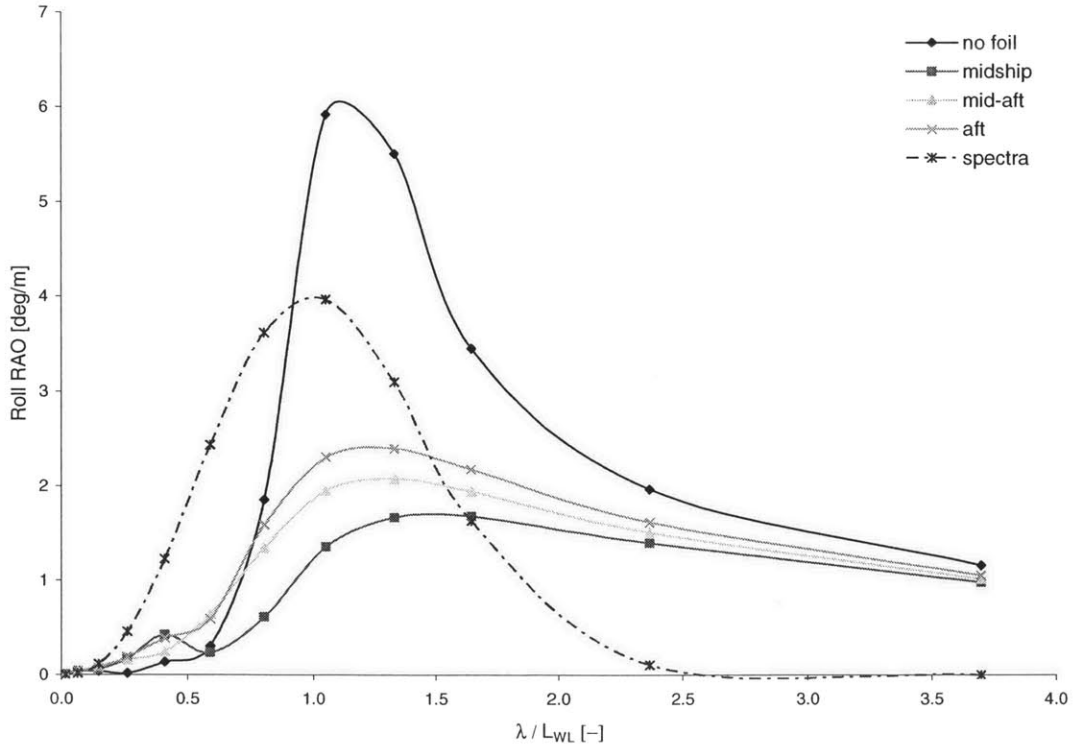

Figure 53: Roll RAO, Variation of Longitudinal Location, β =135°, S = 8 m², Fn = 0.9

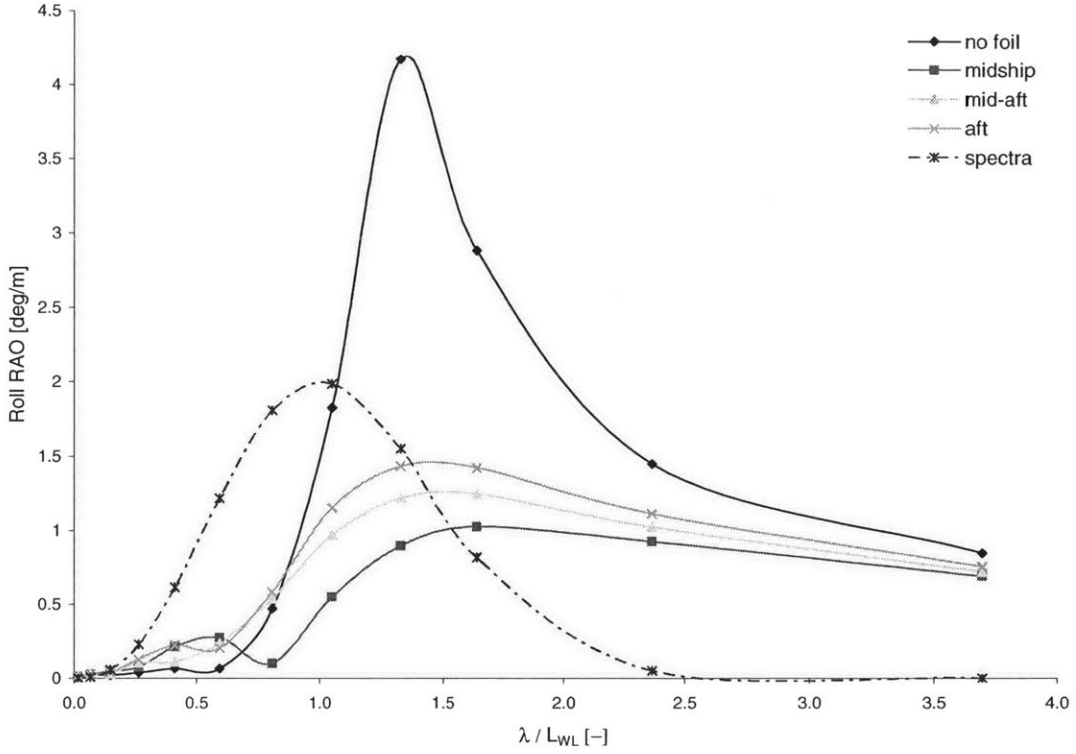

Figure 54: Roll RAO, Variation of Longitudinal Location, β =150°, S = 8 m², Fn = 0.9

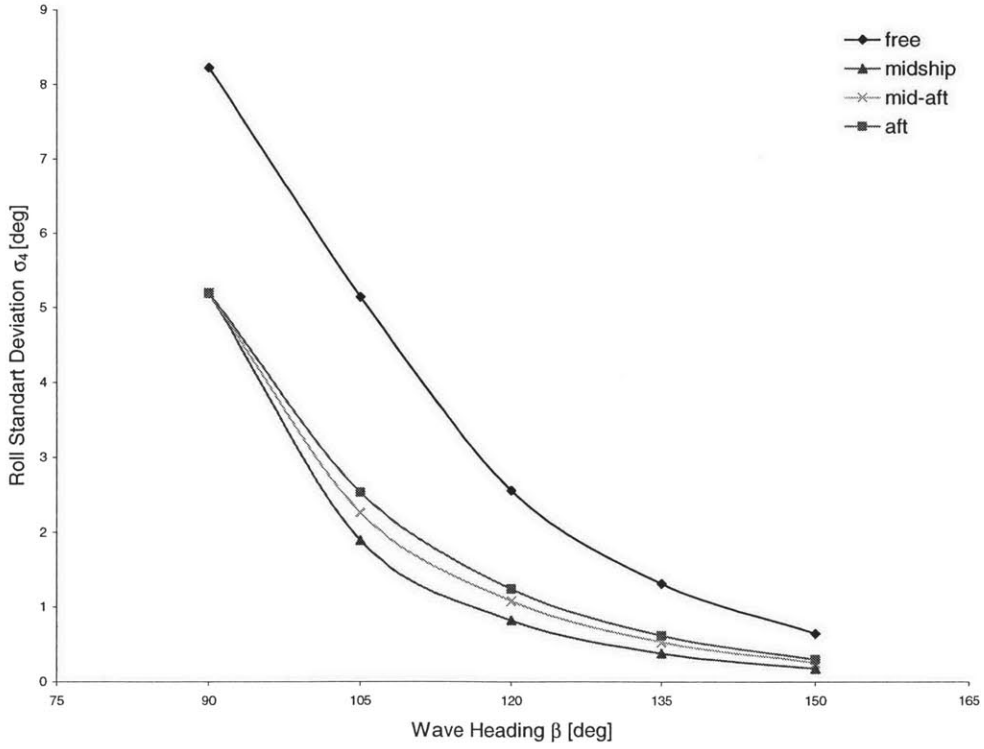

Figure 55: Roll Standard Deviation, varying β and χ Location, S = 8 m², Fn = 0.9

10. Appendix B: The Influence of Hydrofoil Planform Area [S]

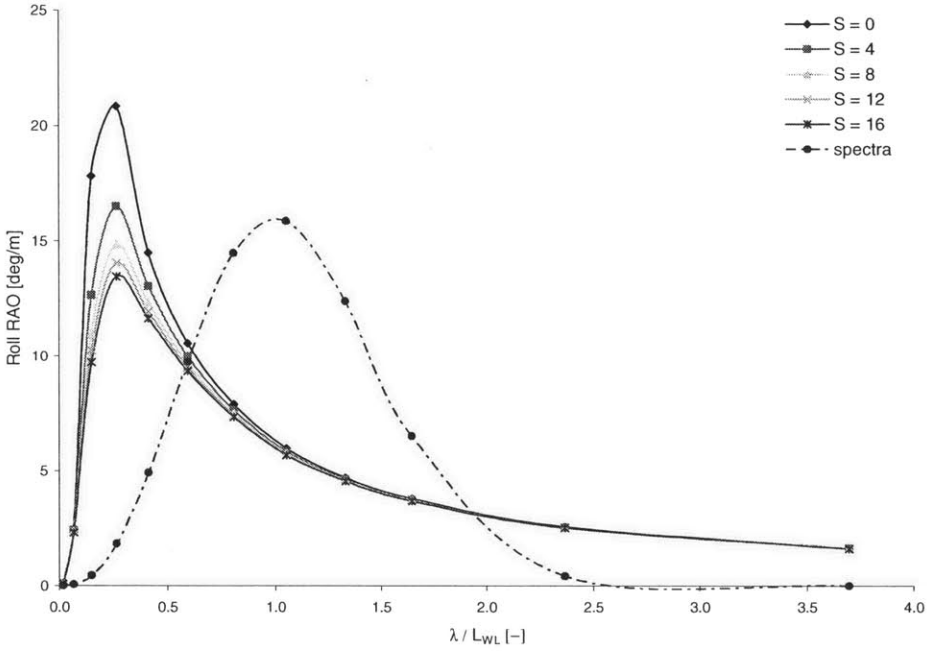

Figure 56: Roll RAOs, Fn = 0.3, β=090° and χ_{foil}=midship, varying S [m^2]

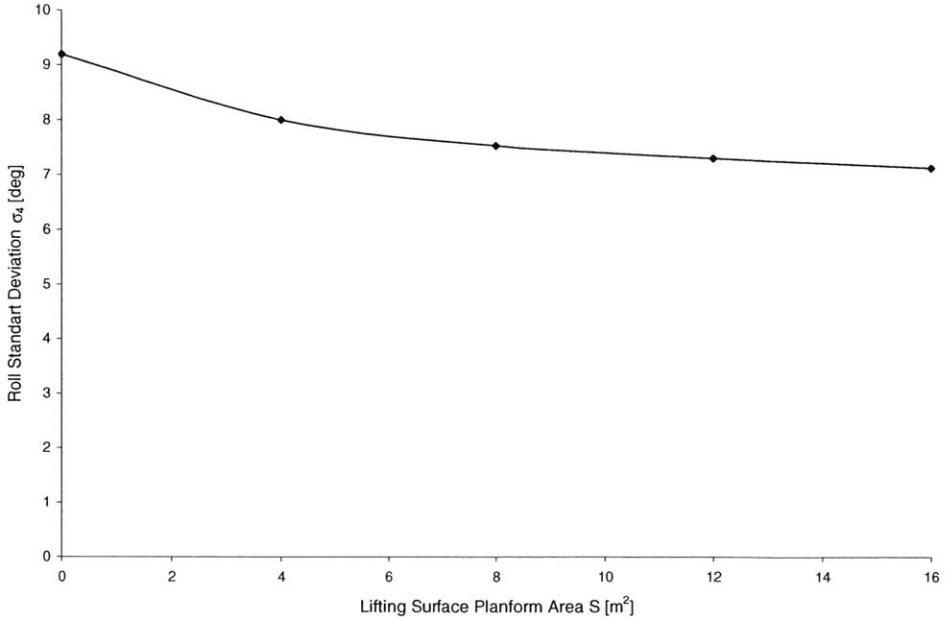

Figure 57: Roll Standard Deviation, Fn = 0.3, β=090° and χ_{foil}=midship, varying S [m^2]

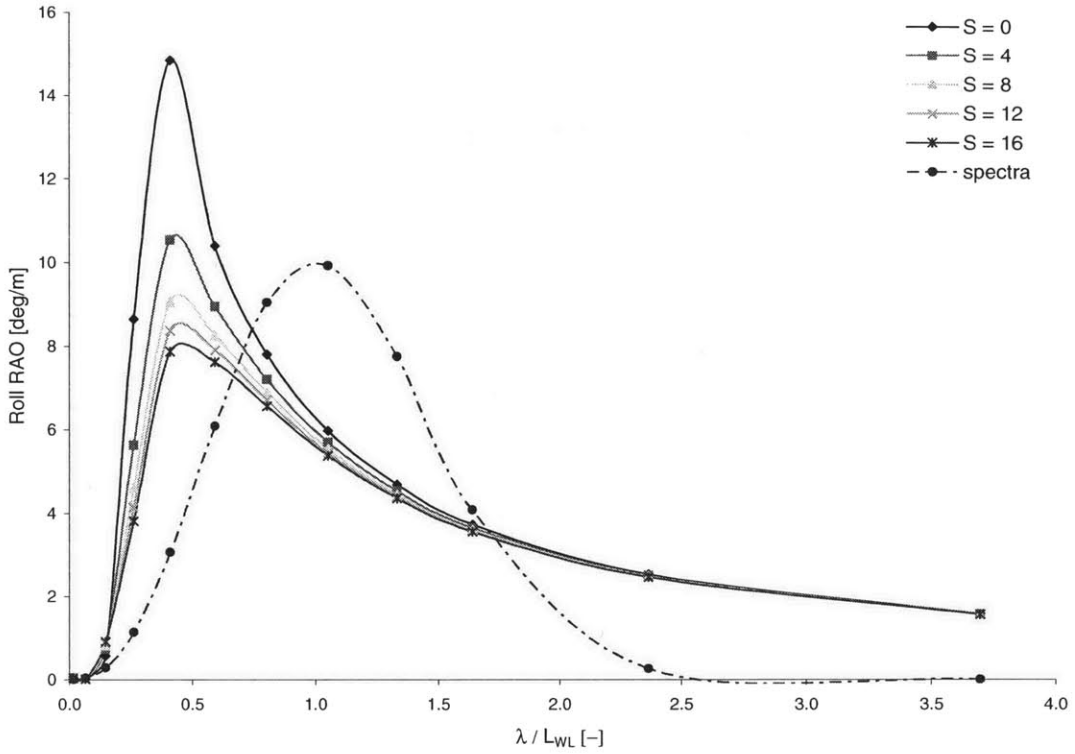

Figure 58: Roll RAOs, Fn = 0.3, β=105° and χ_{foil}=midship, varying S [m^2]

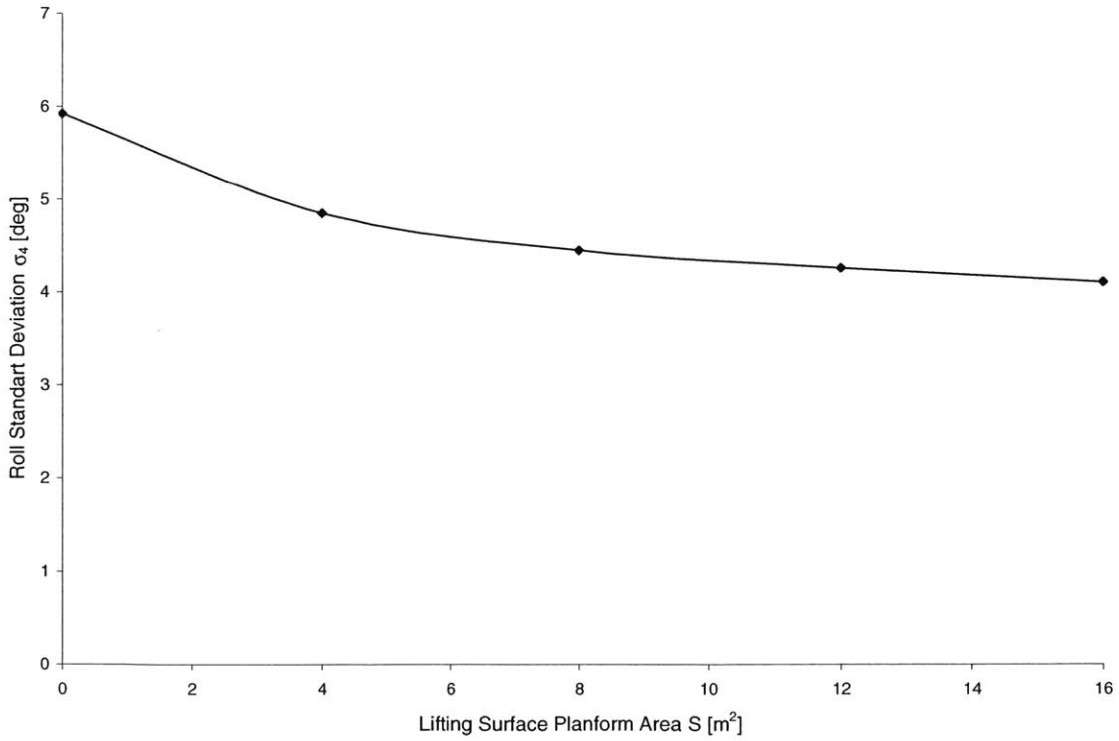

Figure 59: Roll Standard Deviation, Fn = 0.3, β=105° and χ_{foil}=midship, varying S [m^2]

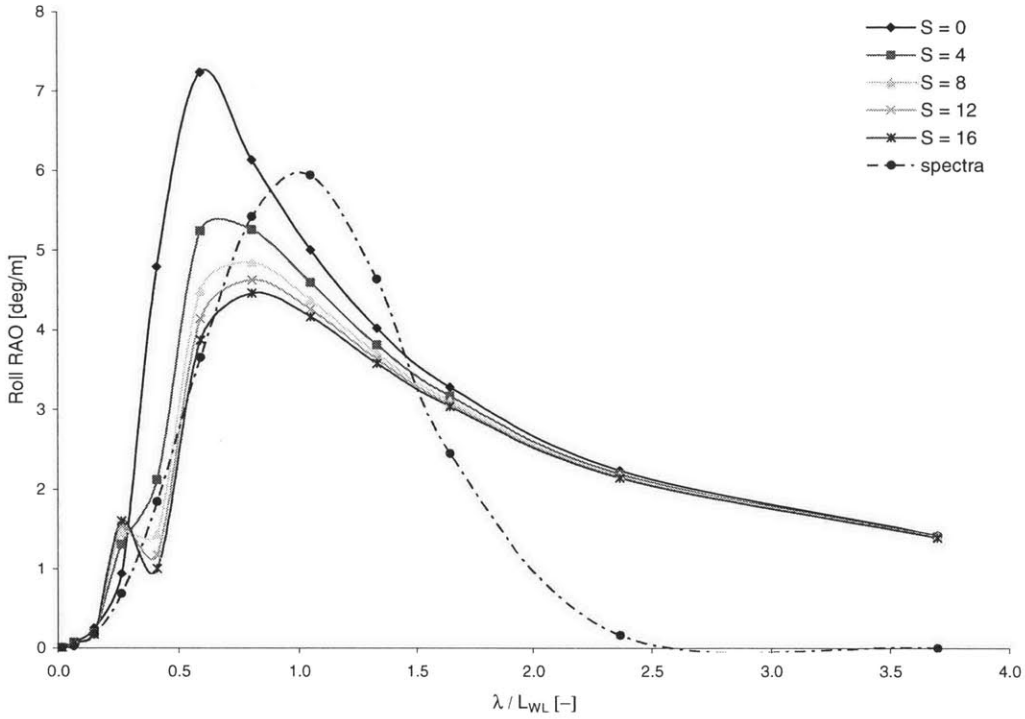

Figure 60: Roll RAOs, Fn = 0.3, β=120° and χ_{foil}=midship, varying S [m^2]

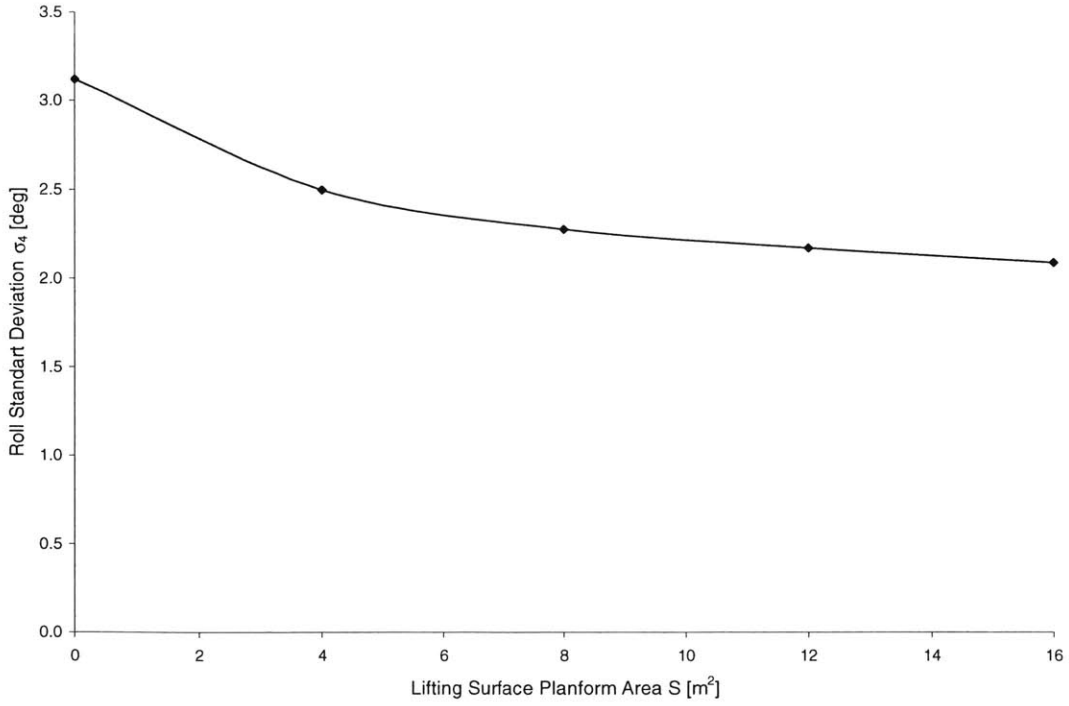

Figure 61: Roll Standard Deviation, Fn = 0.3, β=120° and χ_{foil}=midship, varying S [m^2]

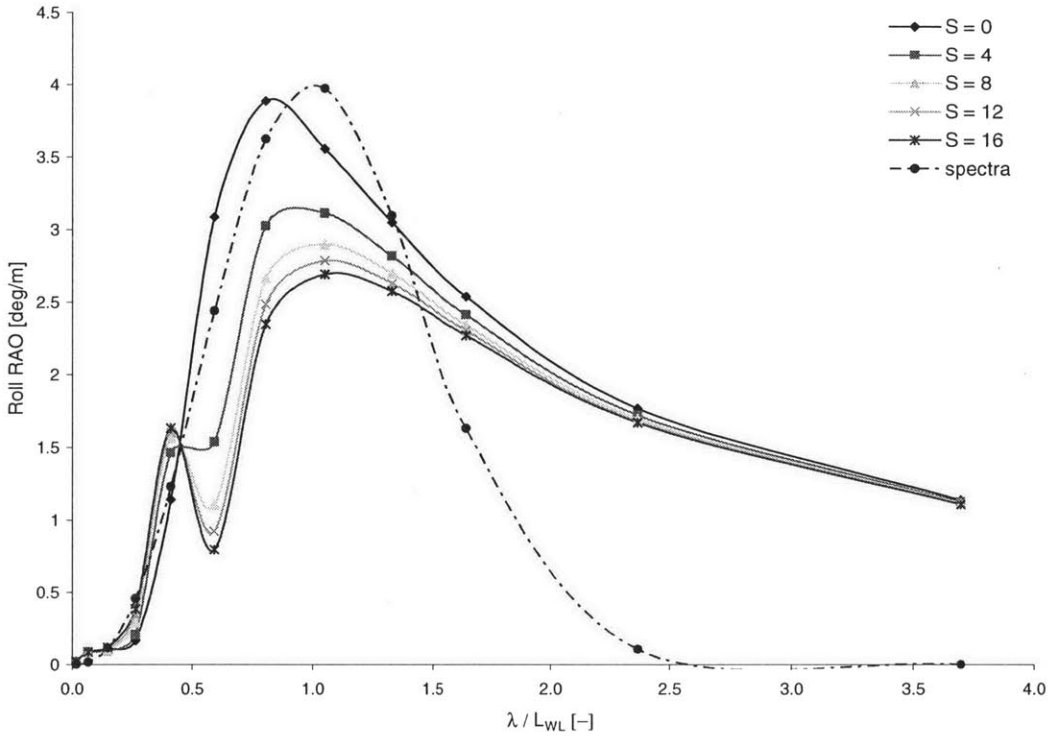

Figure 62: Roll RAOs, Fn = 0.3, β=135° and χ_{foil}=midship, varying S [m^2]

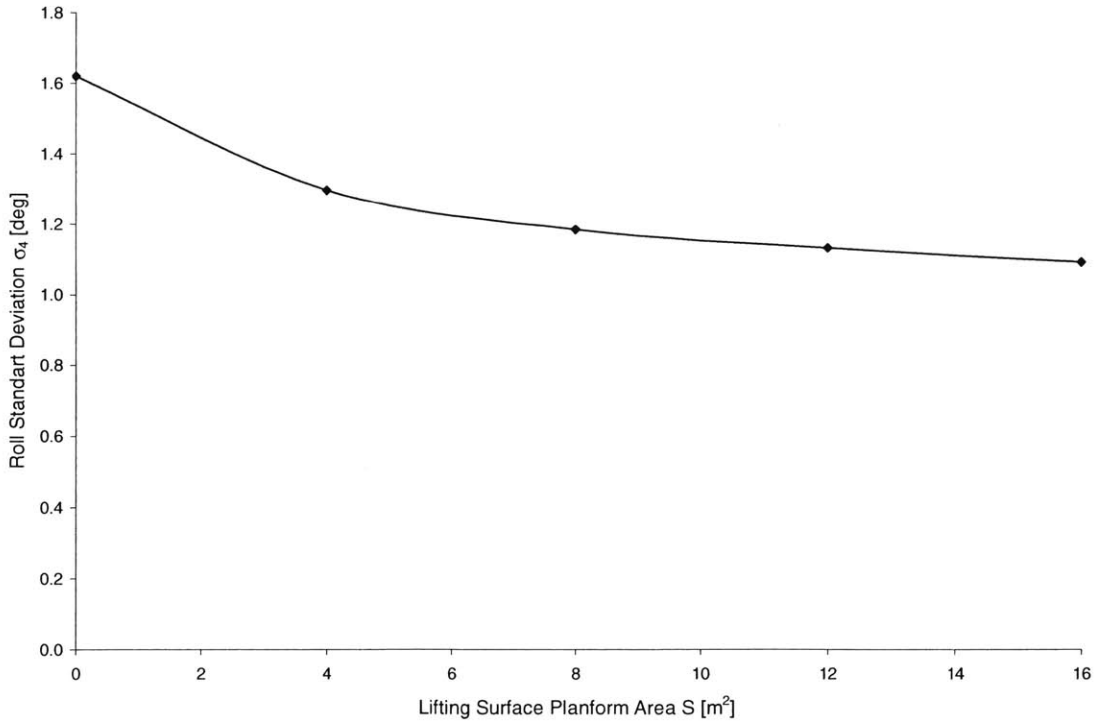

Figure 63: Roll Standard Deviation, Fn = 0.3, β=135° and χ_{foil}=midship, varying S [m^2]

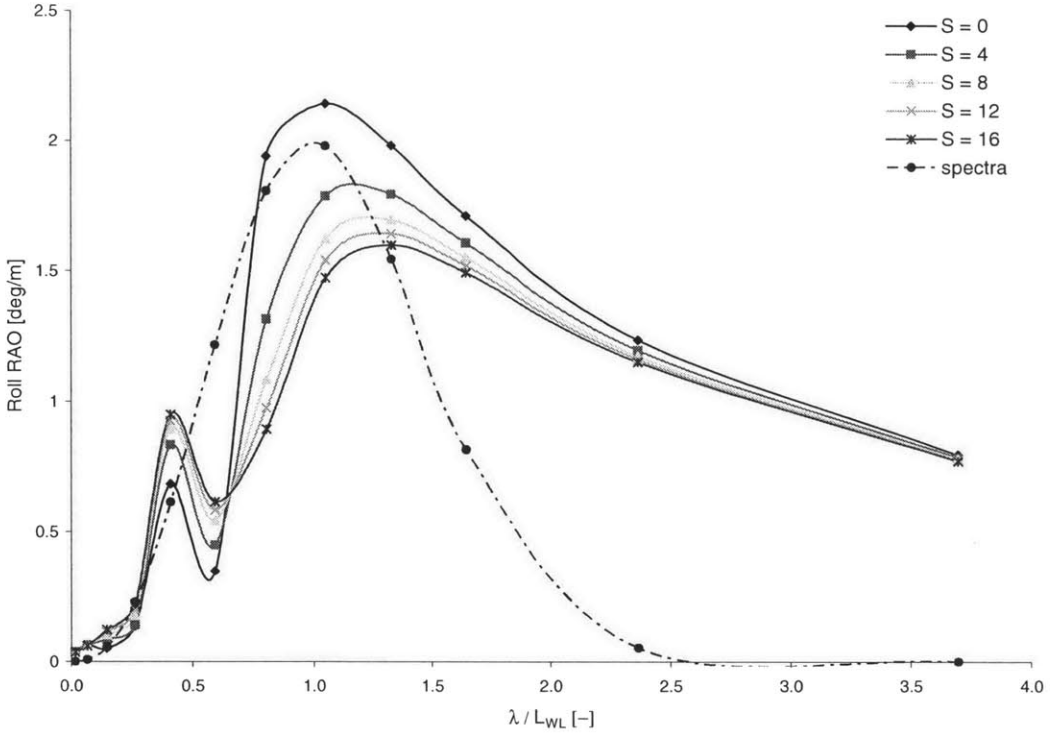

Figure 64: Roll RAOs, Fn = 0.3, β=150° and χ_{foil}=midship, varying S [m^2]

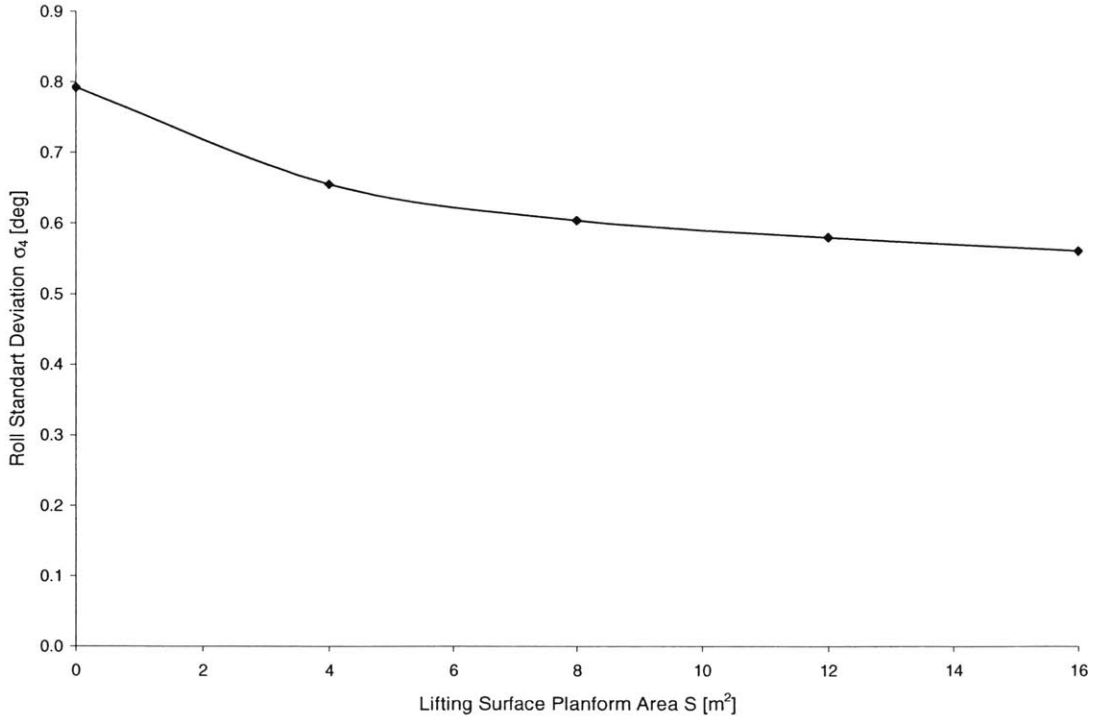

Figure 65: Roll Standard Deviation, Fn = 0.3, β=150° and χ_{foil}=midship, varying S [m^2]

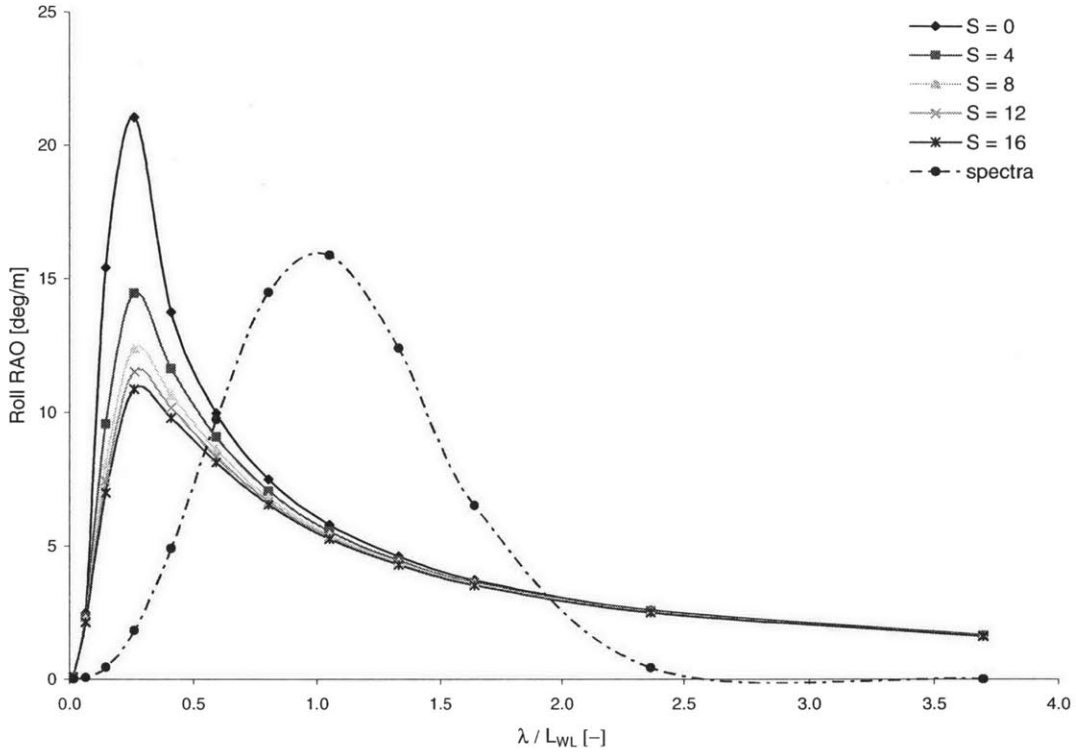

Figure 66: Roll RAOs, Fn = 0.5, β=090° and χ_{foil}=midship, varying S [m^2]

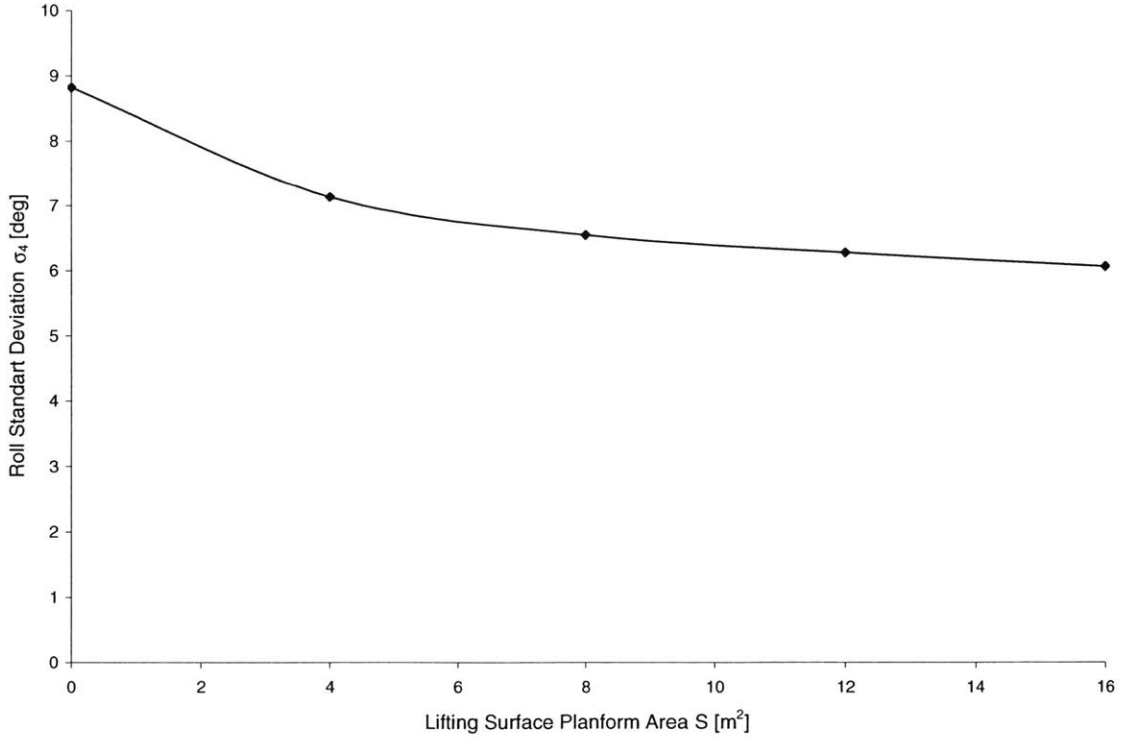

Figure 67: Roll Standard Deviation, Fn = 0.5, β=090° and χ_{foil}=midship, varying S [m^2]

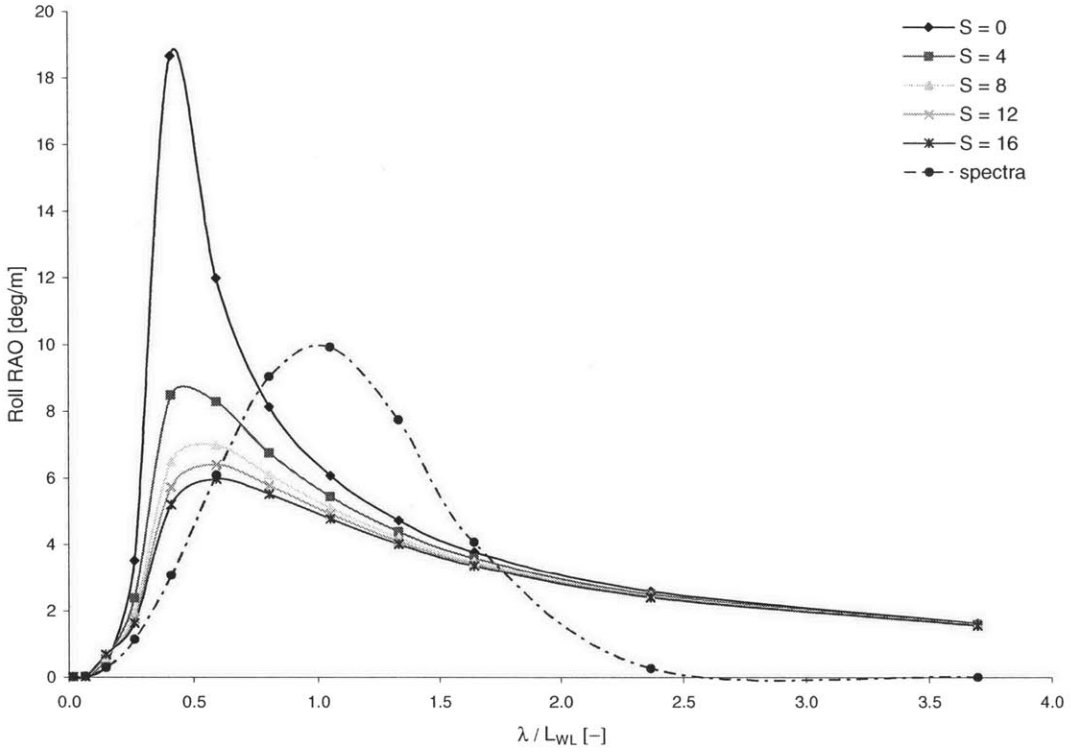

Figure 68: Roll RAOs, Fn = 0.5, β=105° and χ_{foil}=midship, varying S [m^2]

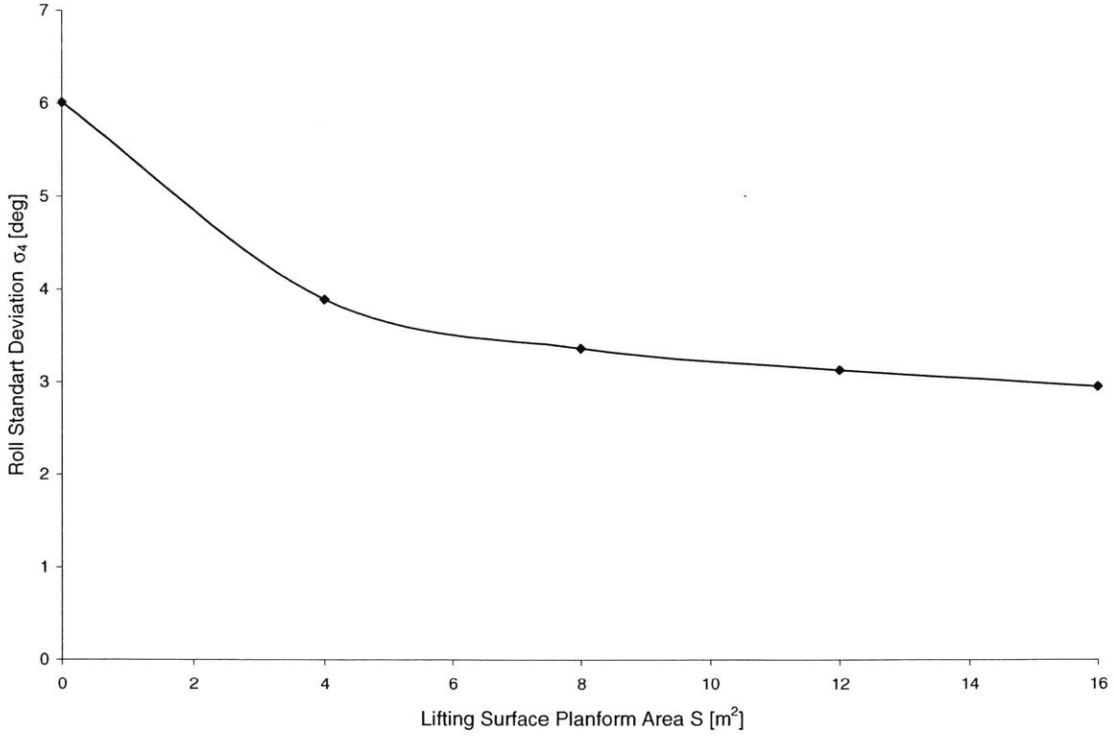

Figure 69: Roll Standard Deviation, Fn = 0.5, β=105° and χ_{foil}=midship, varying S [m^2]

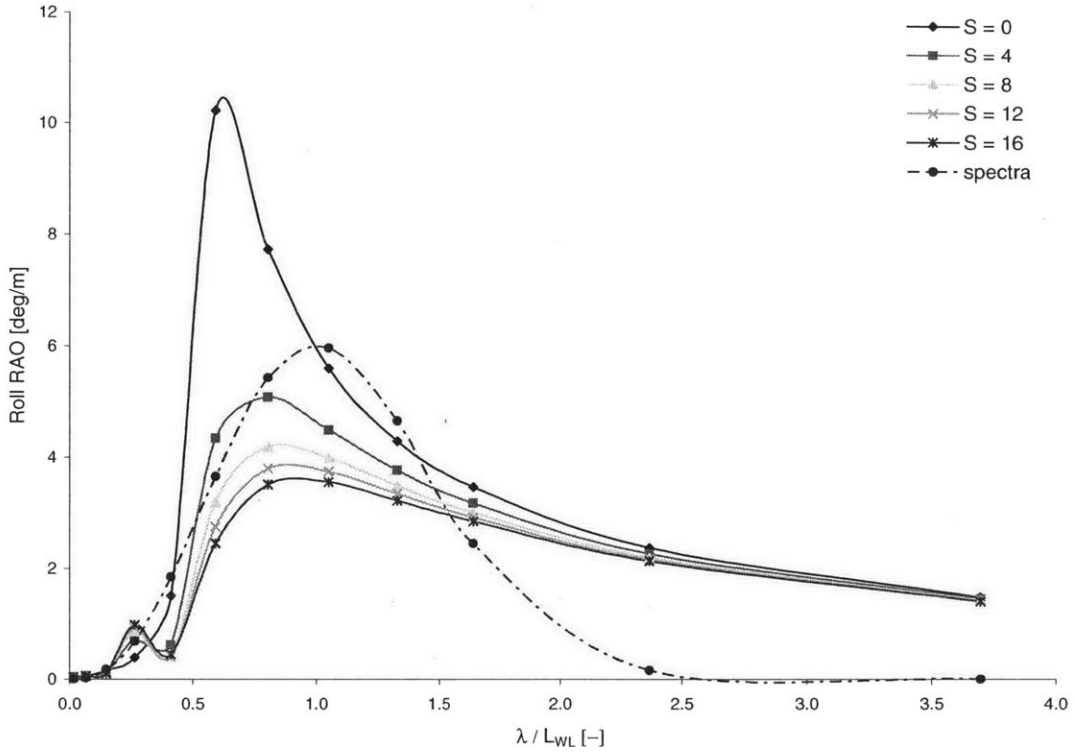

Figure 70: Roll RAOs, Fn = 0.5, β=120° and χ_{foil}=midship, varying S [m^2]

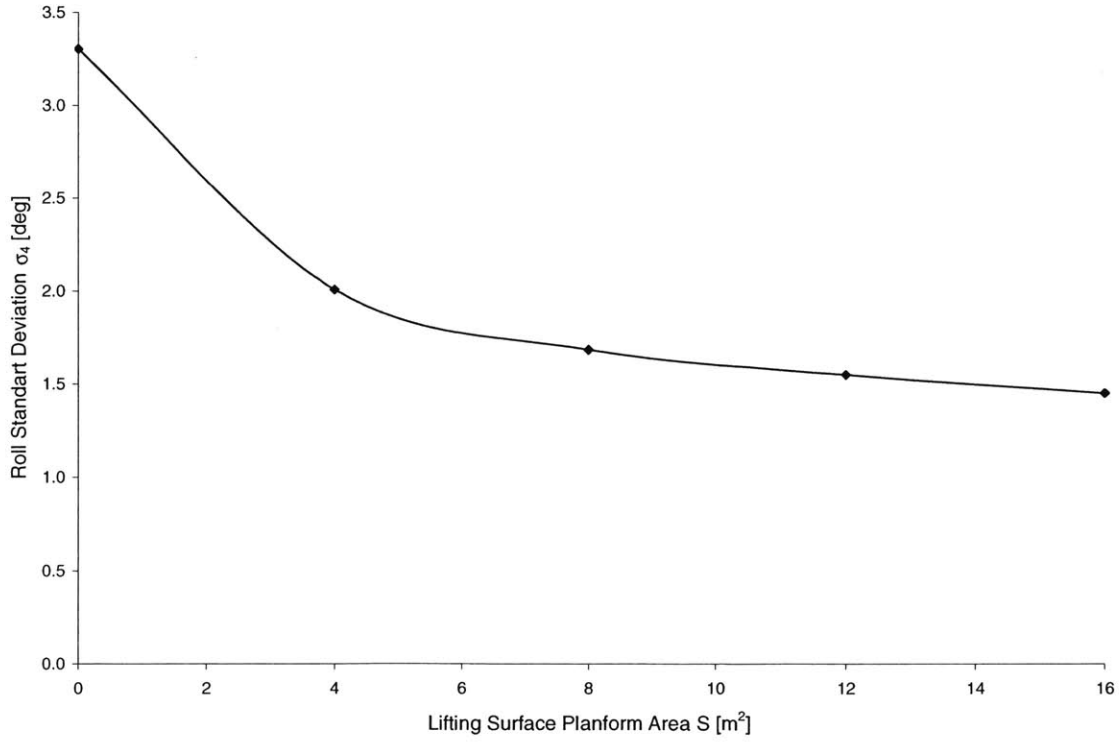

Figure 71: Roll Standard Deviation, Fn = 0.5, β=120° and χ_{foil}=midship, varying S [m^2]

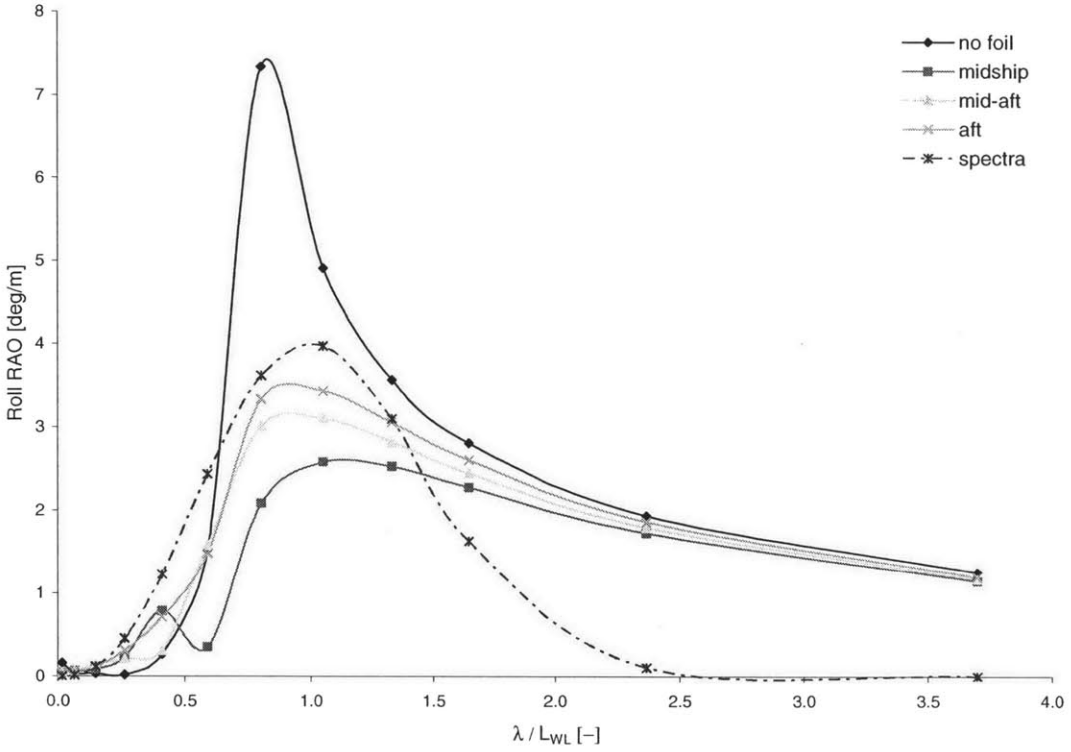

Figure 72: Roll RAOs, Fn = 0.5, β=135° and χ_{foil}=midship, varying S [m^2]

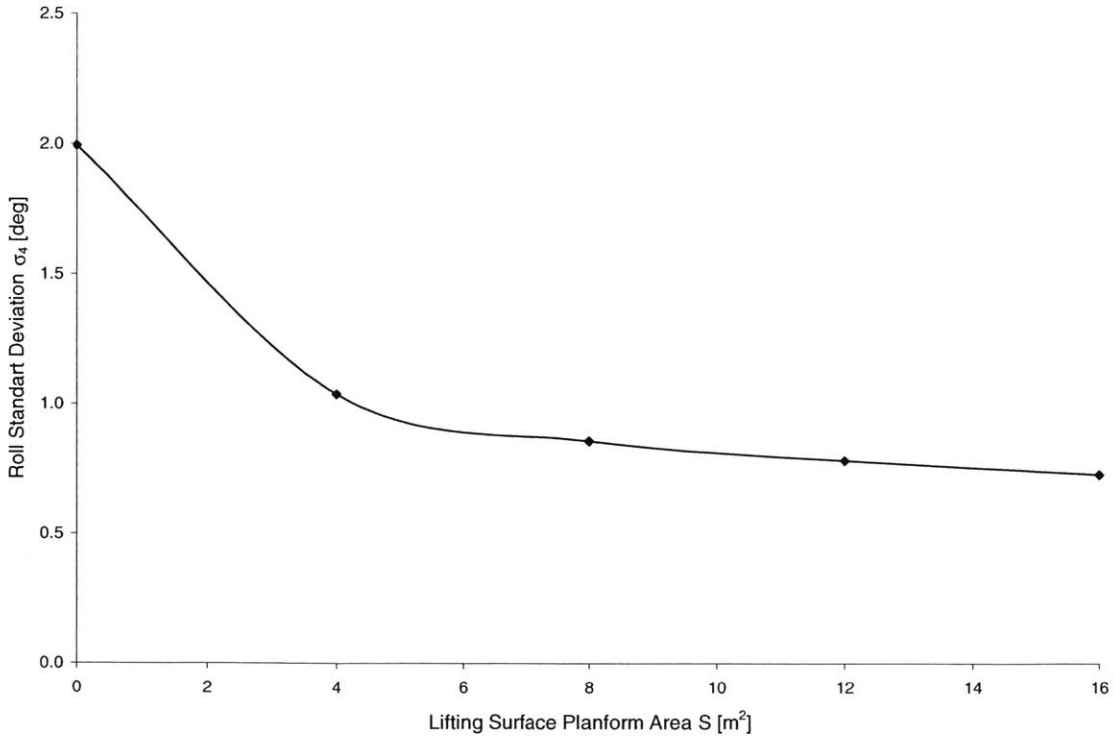

Figure 73: Roll Standard Deviation, Fn = 0.5, β=135° and χ_{foil}=midship, varying S [m^2]

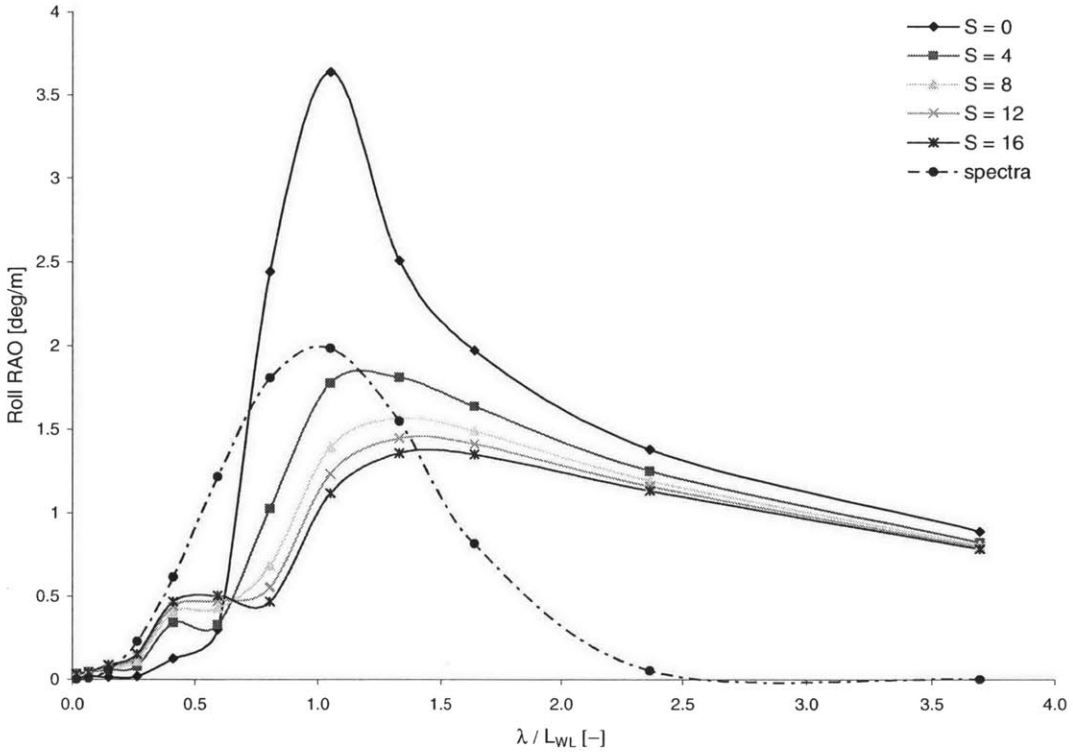

Figure 74: Roll RAOs, Fn = 0.5, β=150° and χ_{foil}=midship, varying S [m^2]

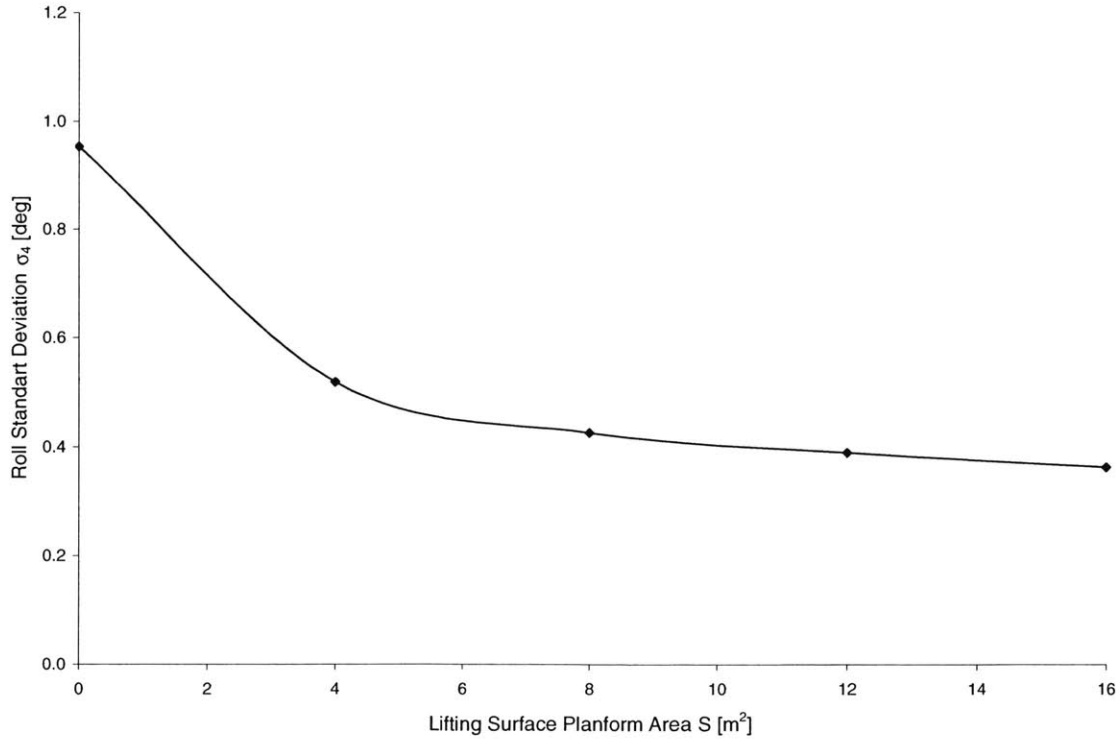

Figure 75: Roll Standard Deviation, Fn = 0.5, β=150° and χ_{foil}=midship, varying S [m^2]

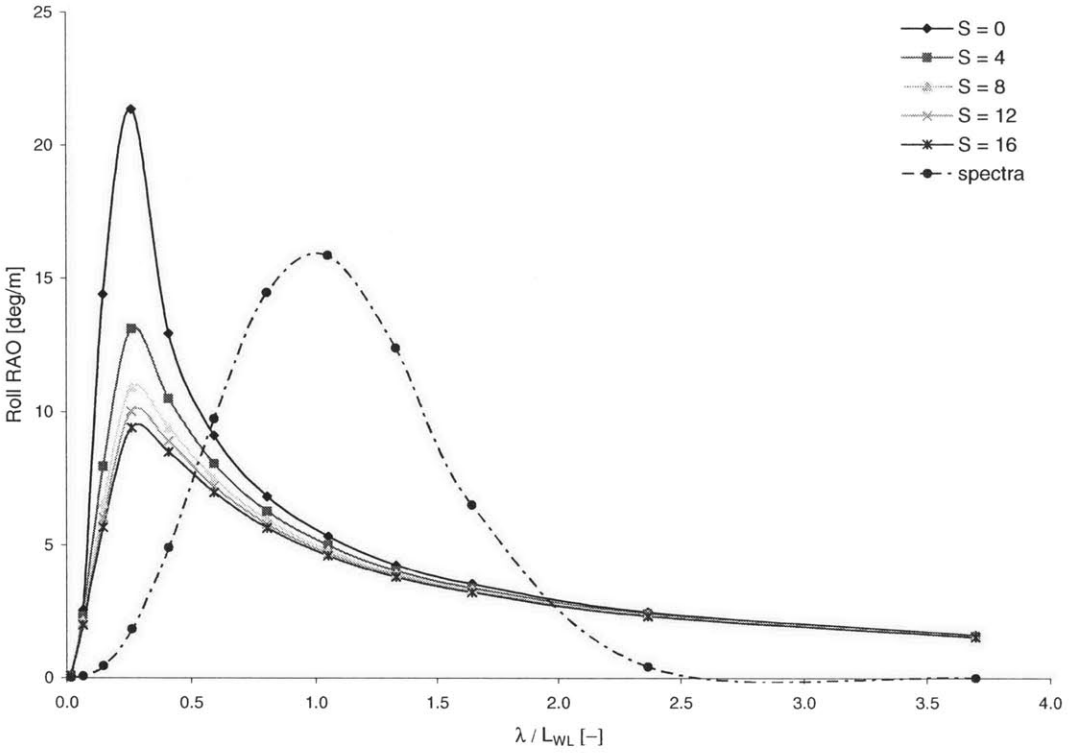

Figure 76: Roll RAOs, Fn = 0.7, β=090° and χ_{foil}=midship, varying S [m^2]

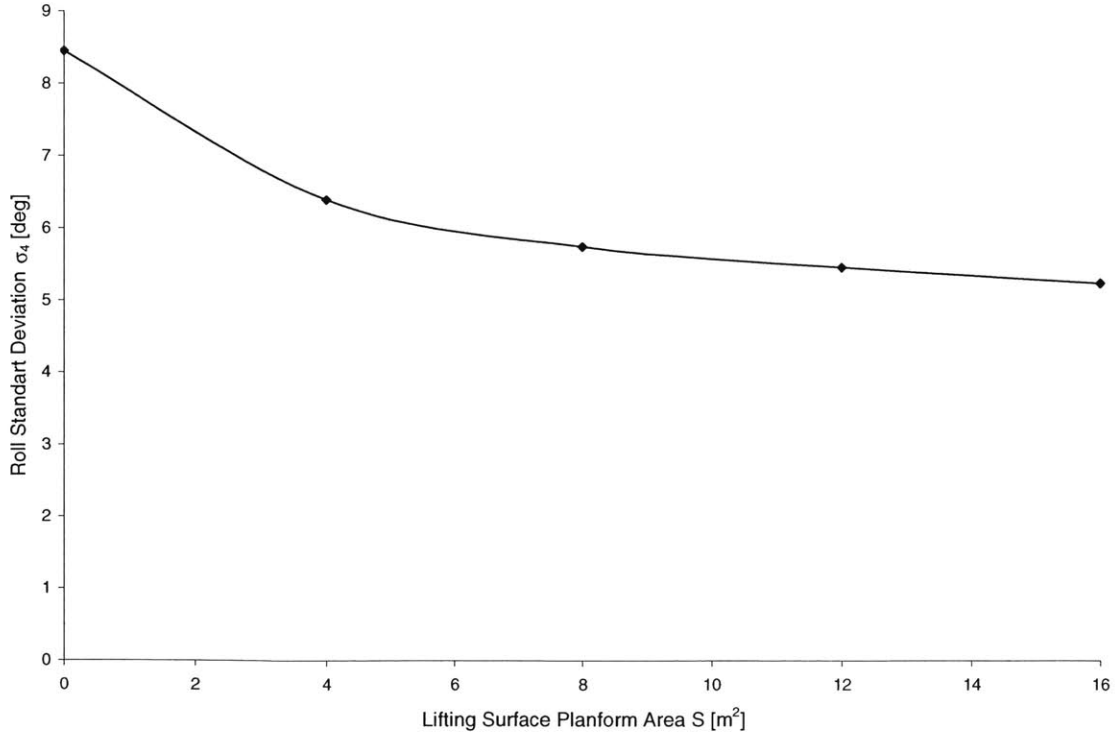

Figure 77: Roll Standard Deviation, Fn = 0.7, β=090° and χ_{foil}=midship, varying S [m^2]

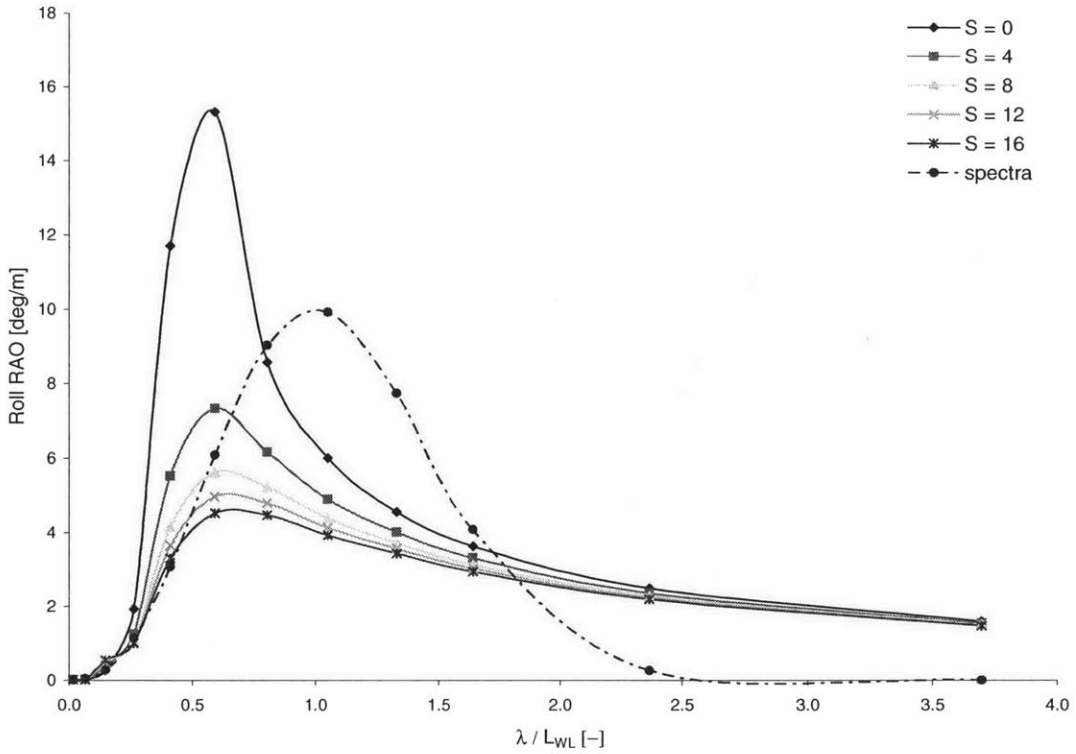

Figure 78: Roll RAOs, Fn = 0.7, β=105° and χ_{foil}=midship, varying S [m^2]

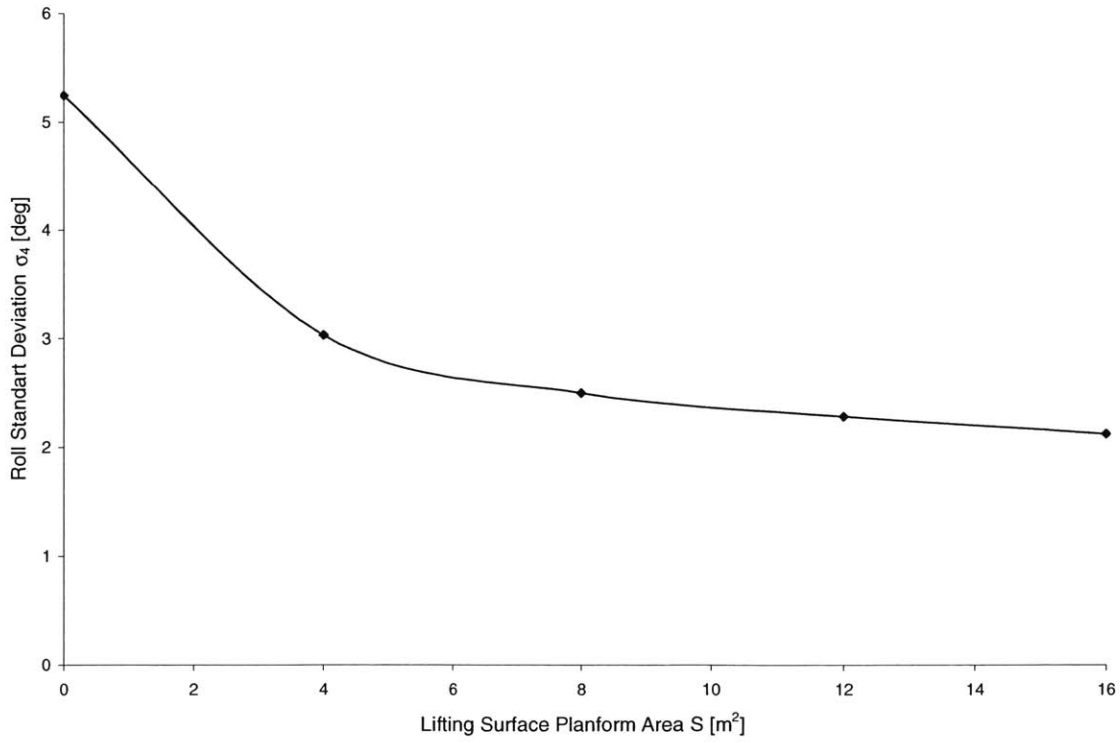

Figure 79: Roll Standard Deviation, Fn = 0.7, β=105° and χ_{foil}=midship, varying S [m^2]

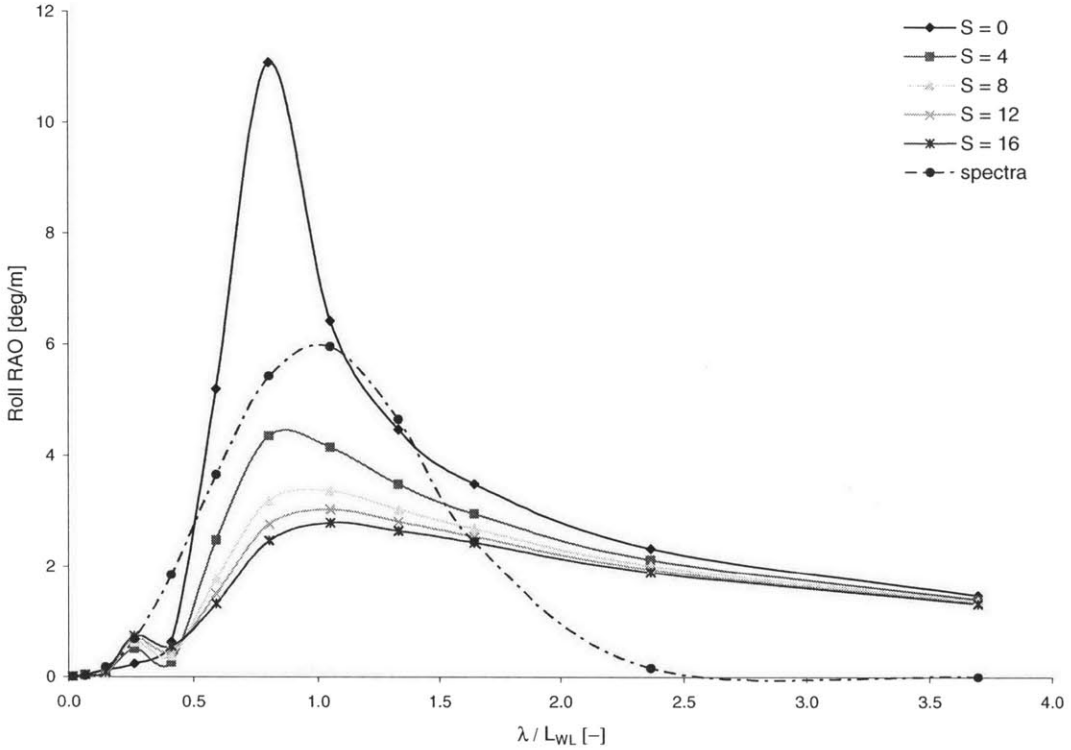

Figure 80: Roll RAOs, Fn = 0.7, β=120° and χ_{foil}=midship, varying S [m^2]

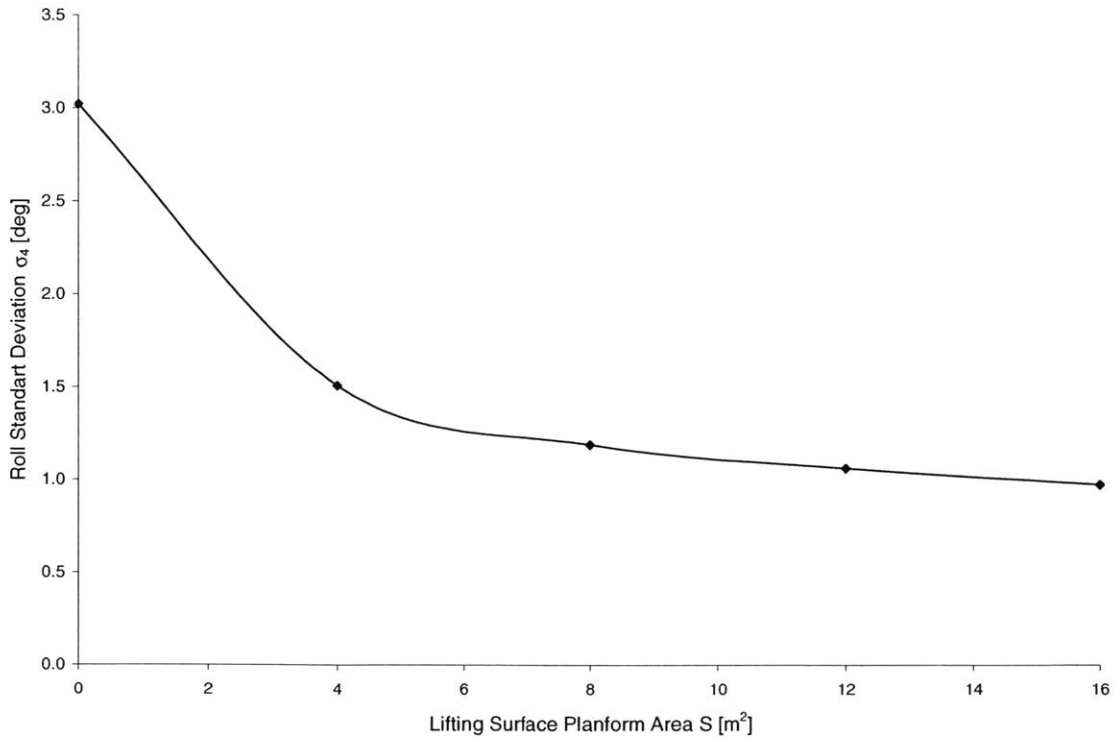

Figure 81: Roll Standard Deviation, Fn = 0.7, β=120° and χ_{foil}=midship, varying S [m^2]

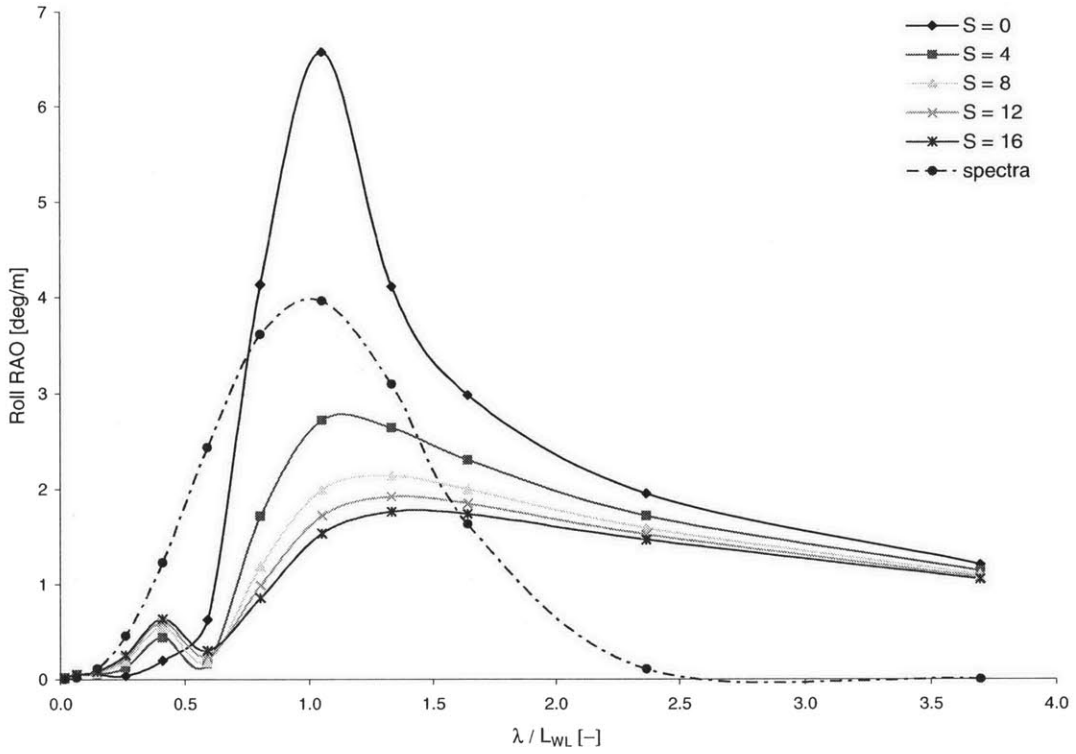

Figure 82: Roll RAOs, Fn = 0.7, β=135° and χ_{foil}=midship, varying S [m^2]

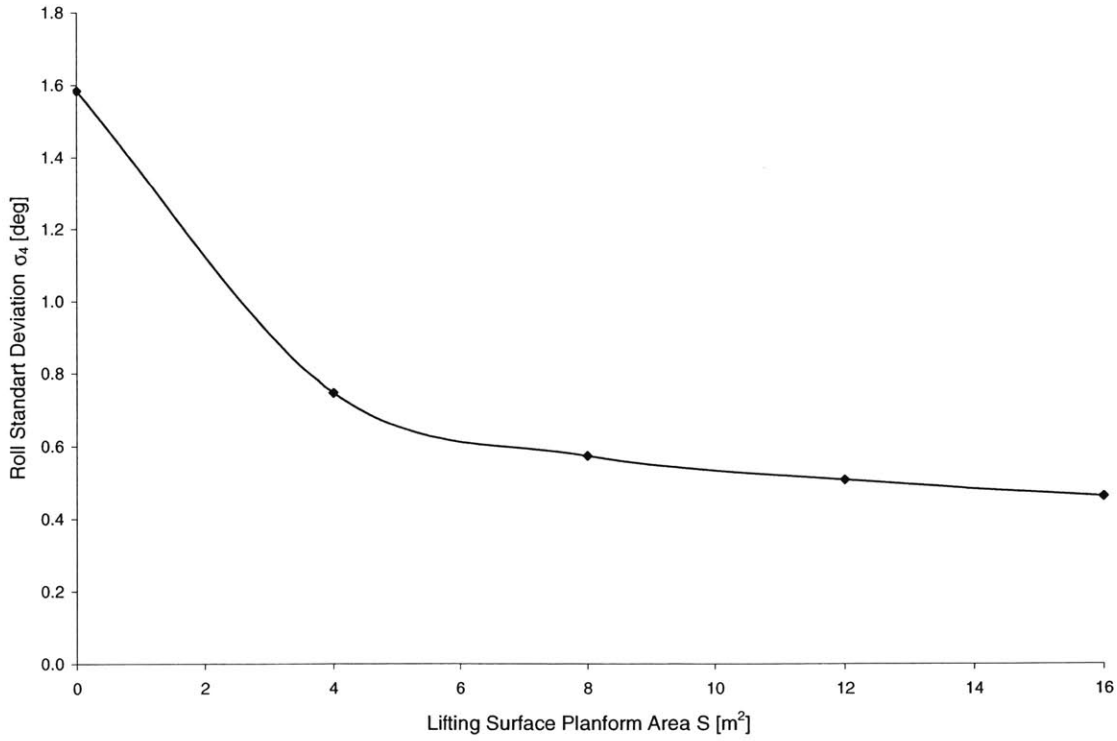

Figure 83: Roll Standard Deviation, Fn = 0.7, β=135° and χ_{foil}=midship, varying S [m^2]

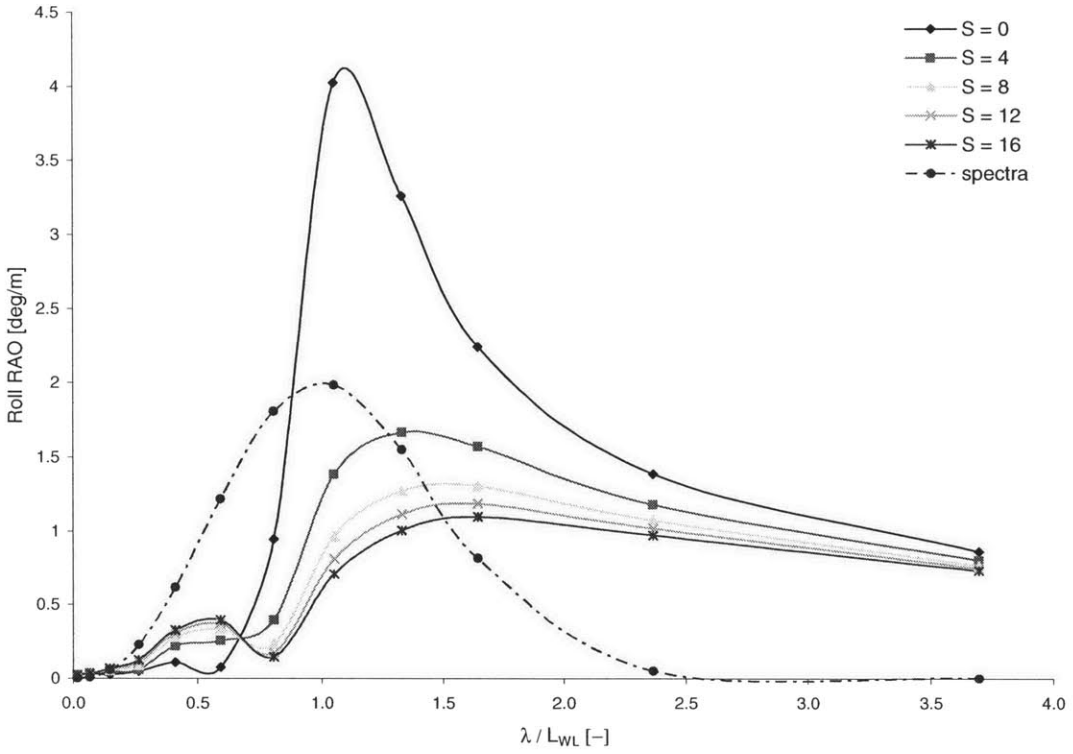

Figure 84: Roll RAOs, Fn = 0.7, β=150° and χ_{foil}=midship, varying S [m^2]

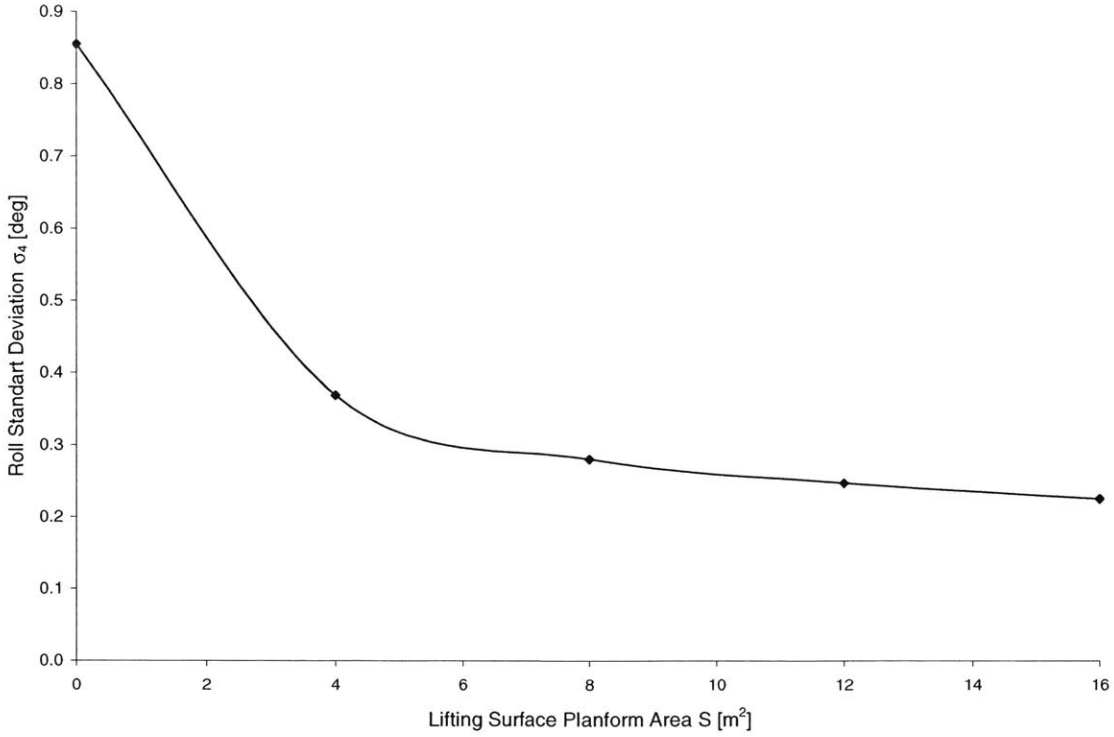

Figure 85: Roll Standard Deviation, Fn = 0.7, β=150° and χ_{foil}=midship, varying S [m^2]

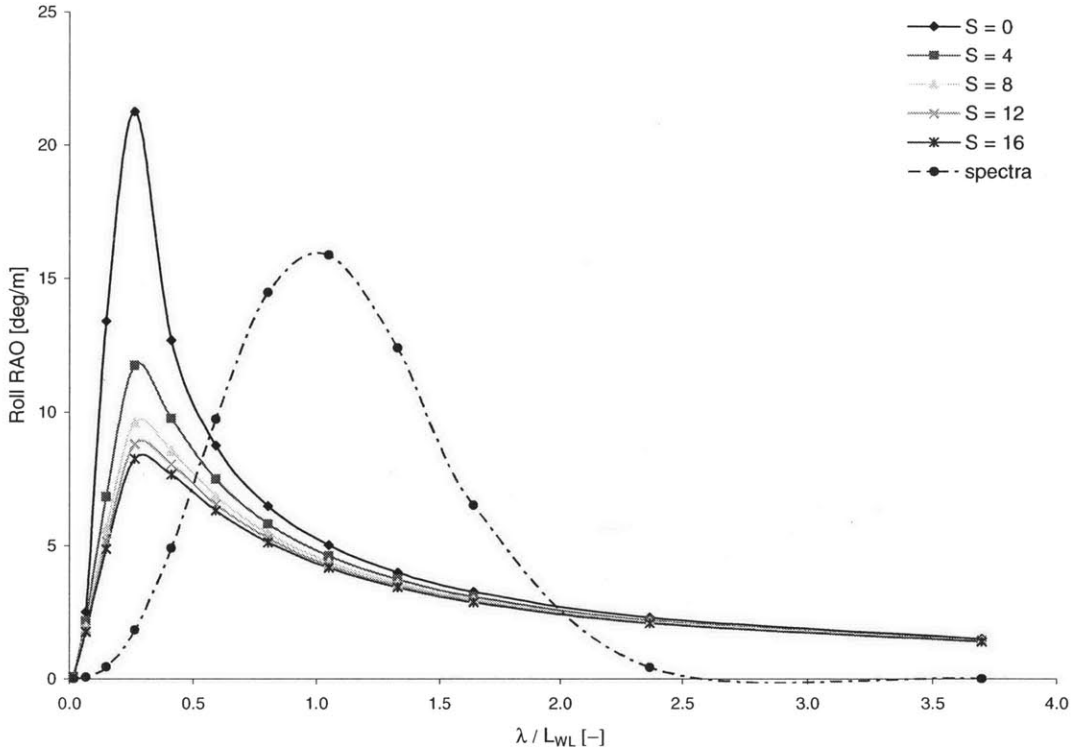

Figure 86: Roll RAOs, Fn = 0.9, β=090° and χ_{foil}=midship, varying S [m^2]

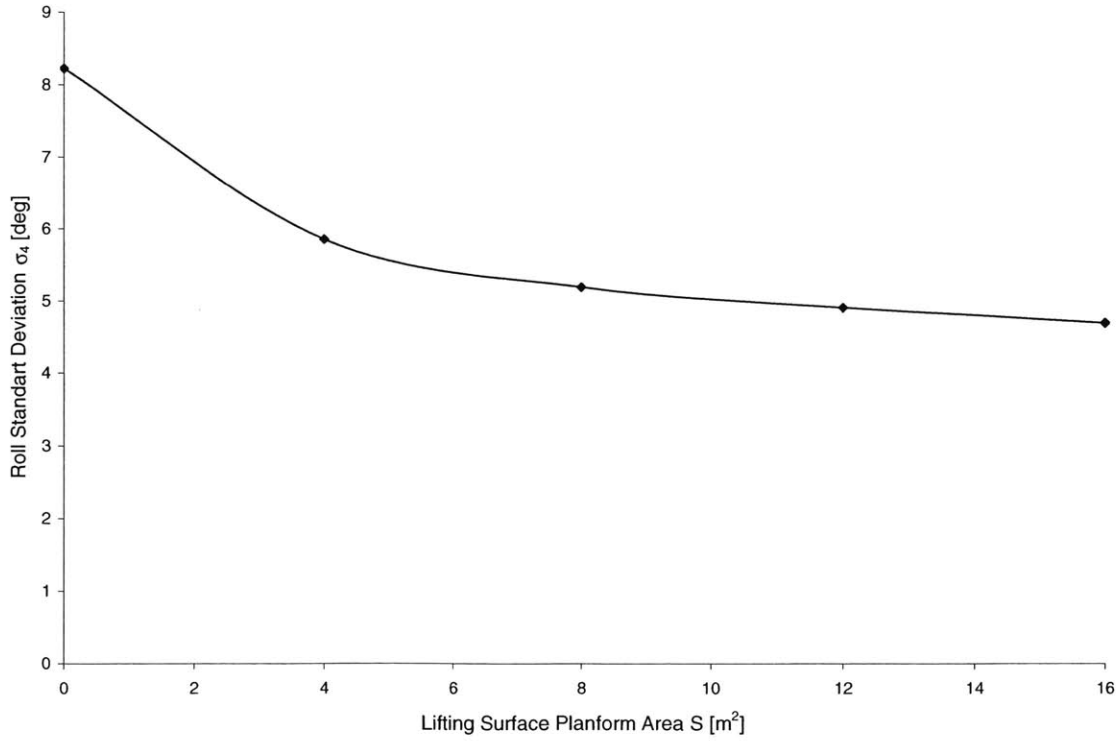

Figure 87: Roll Standard Deviation, Fn = 0.9, β=090° and χ_{foil}=midship, varying S [m^2]

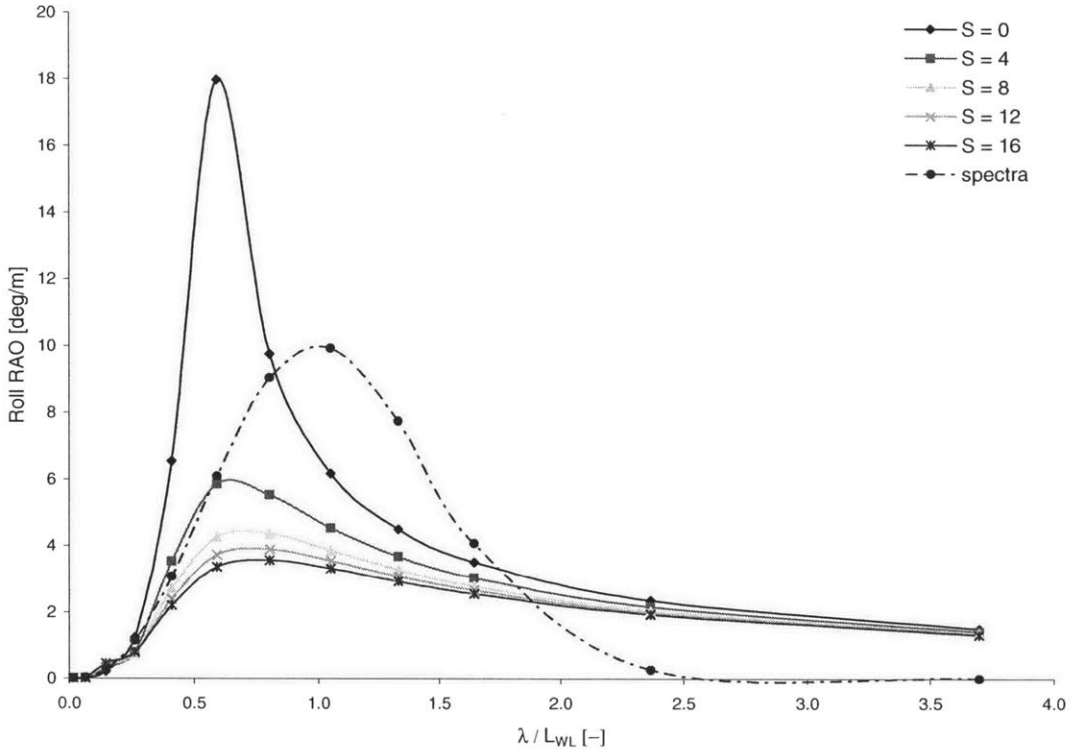

Figure 88: Roll RAOs, Fn = 0.9, β=105° and χ_{foil}=midship, varying S [m^2]

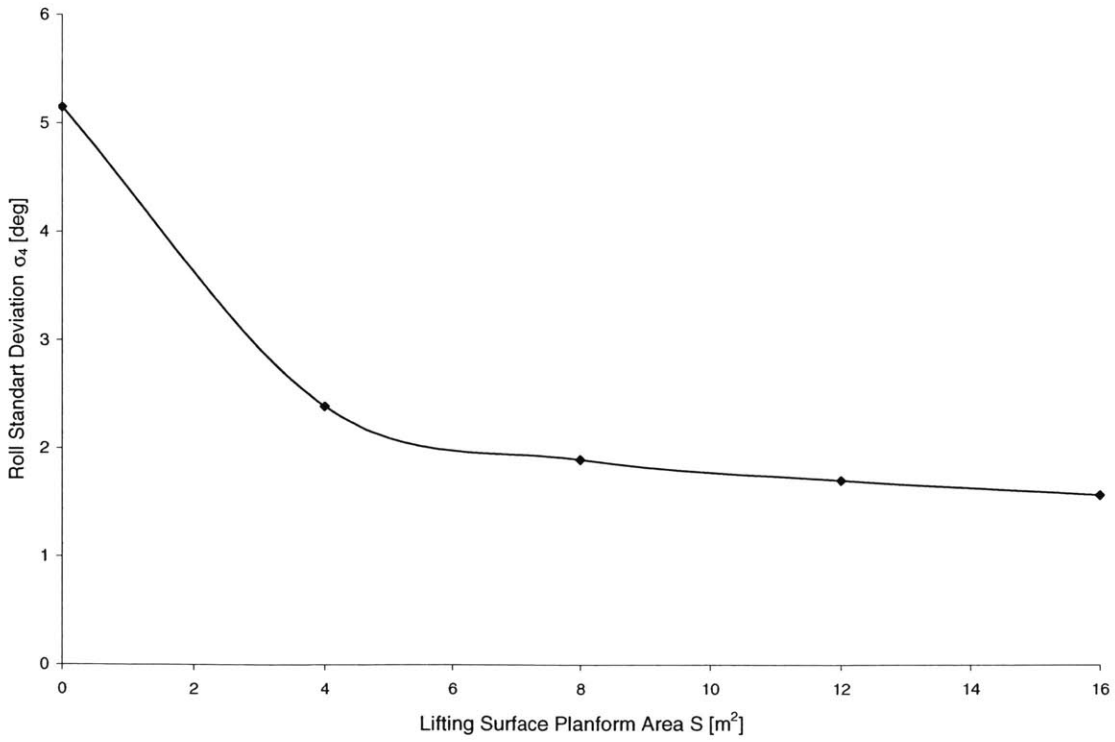

Figure 89: Roll Standard Deviation, Fn = 0.9, β=105° and χ_{foil}=midship, varying S [m^2]

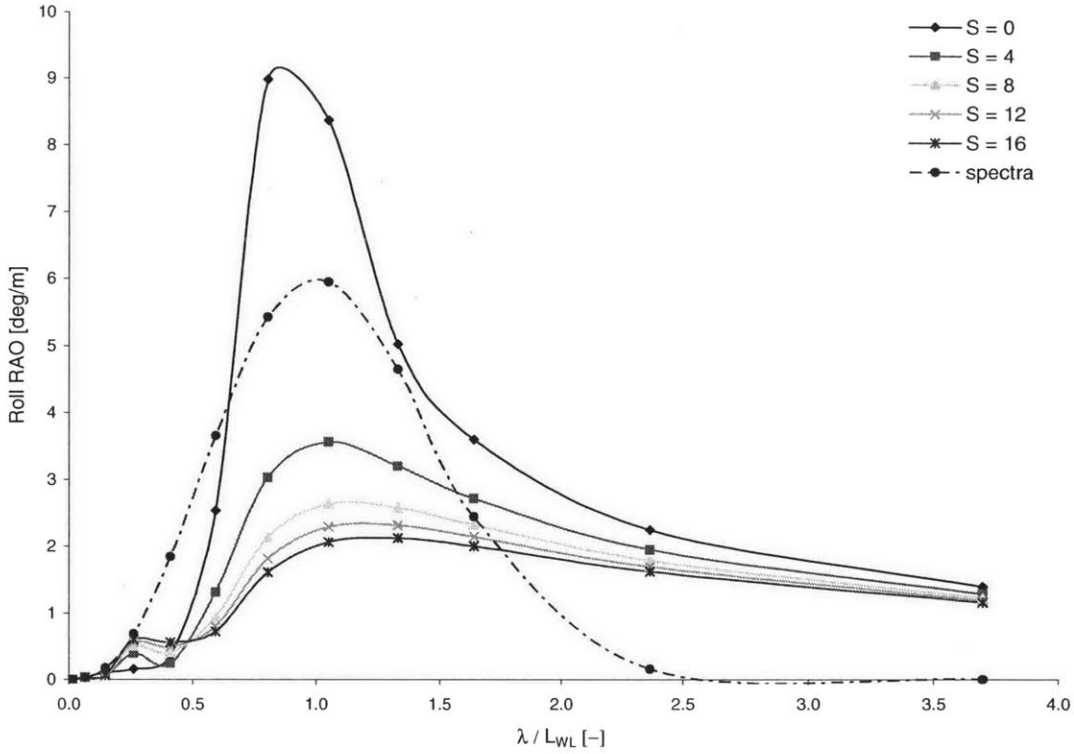

Figure 90: Roll RAOs, Fn = 0.9, β=120° and χ_{foil}=midship, varying S [m^2]

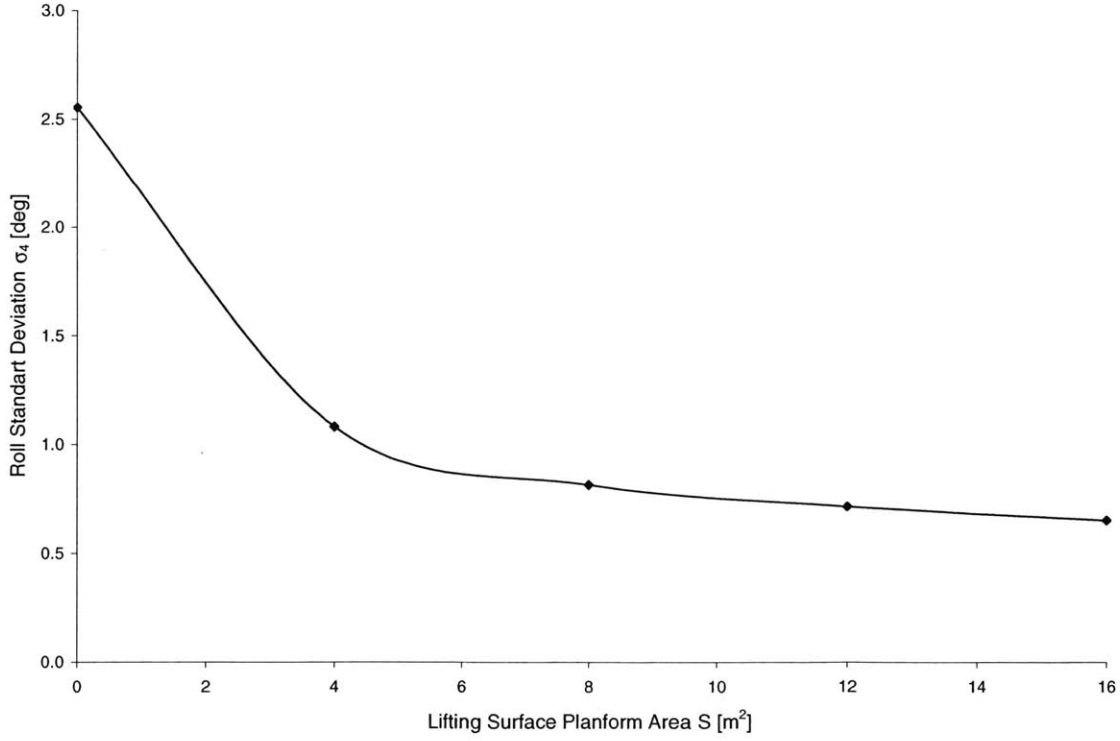

Figure 91: Roll Standard Deviation, Fn = 0.9, β=120° and χ_{foil}=midship, varying S [m^2]

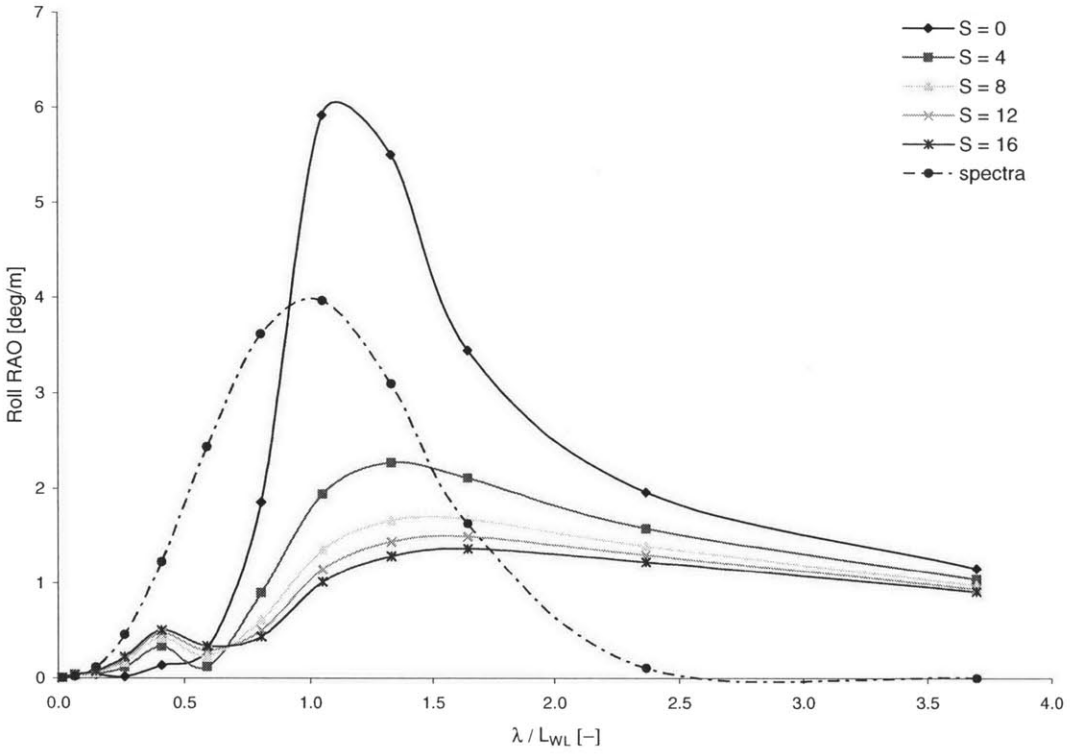

Figure 92: Roll RAOs, Fn = 0.9, β=135° and χ_{foil}=midship, varying S [m^2]

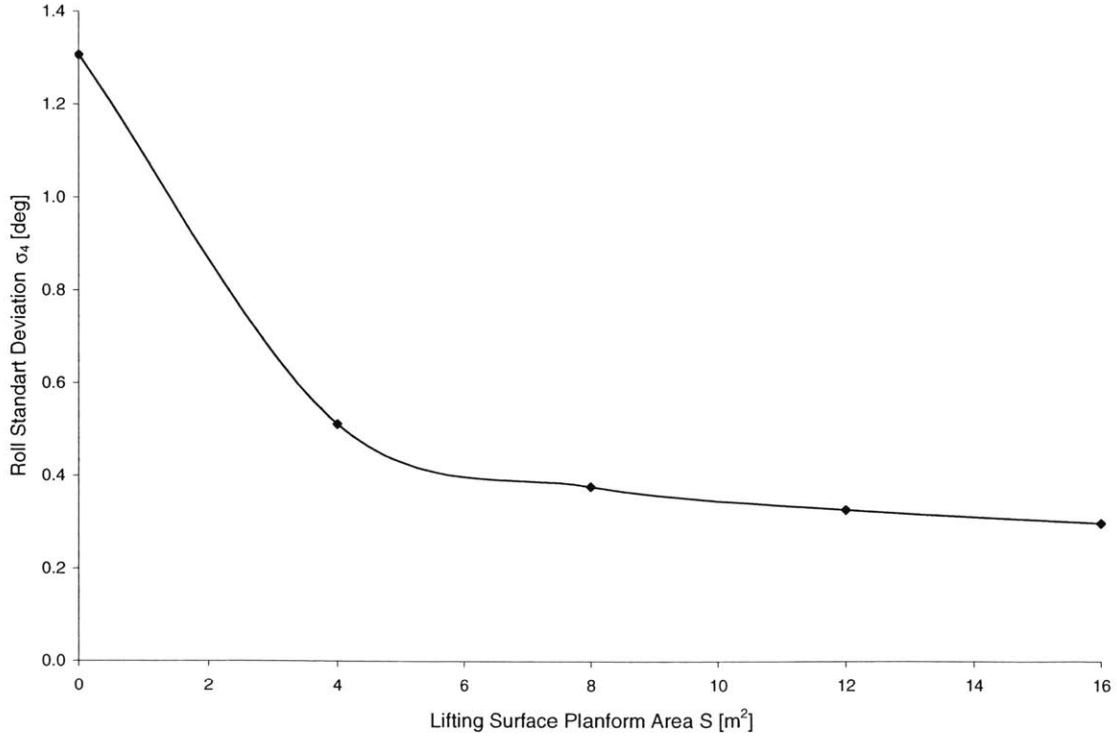

Figure 93: Roll Standard Deviation, Fn = 0.9, β=135° and χ_{foil}=midship, varying S [m^2]

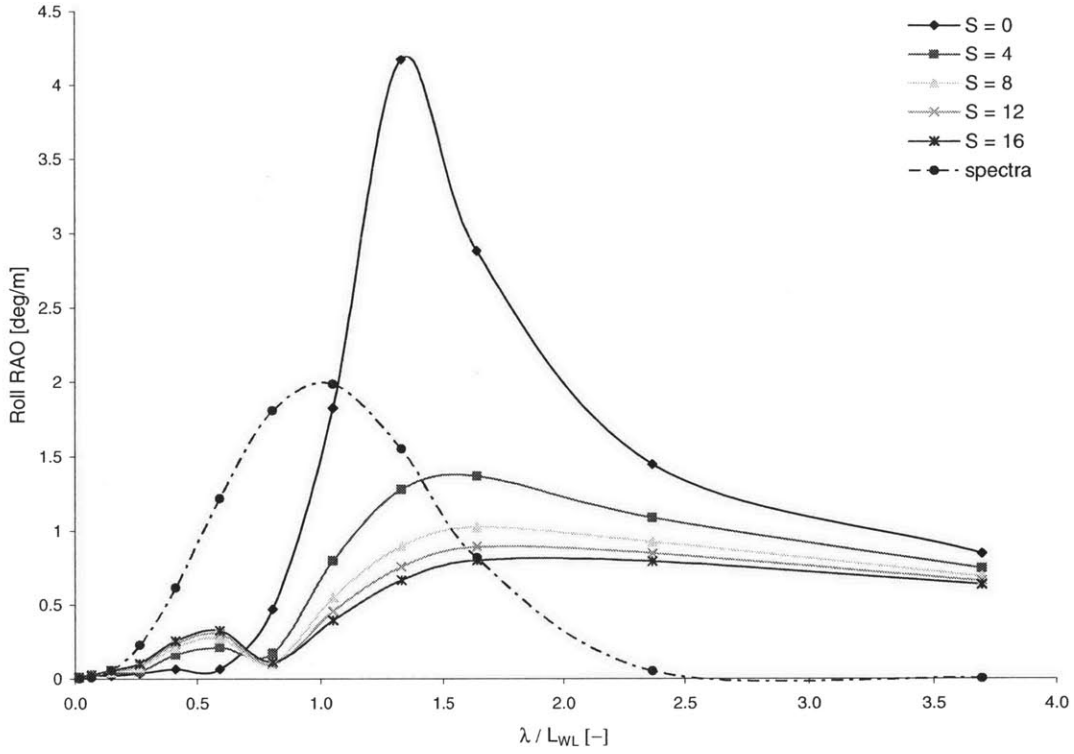

Figure 94: Roll RAOs, Fn = 0.9, β=150° and χ_{foil}=midship, varying S [m^2]

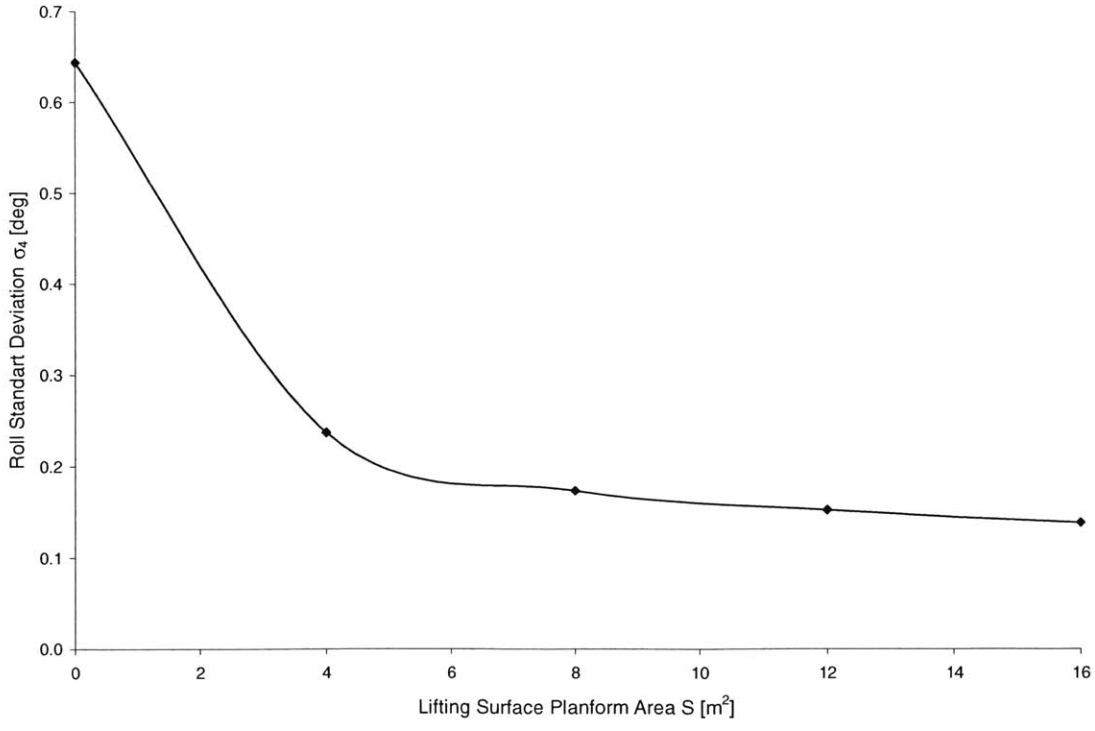

Figure 95: Roll Standard Deviation, Fn = 0.9, β=150° and χ_{foil}=midship, varying S [m^2]

11. Appendix C: The Influence of Ship Forward Speed

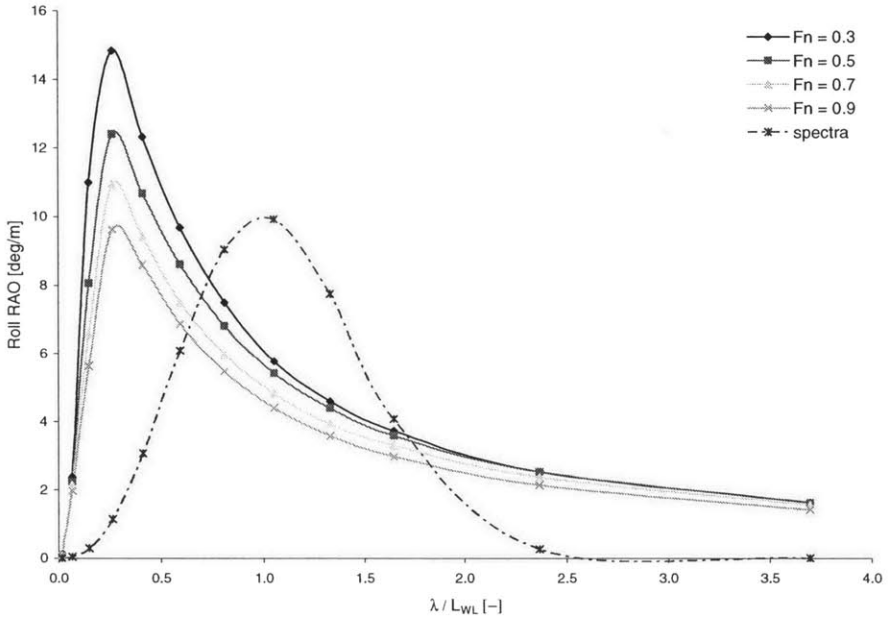

Figure 96: Roll RAOs, varying speed [Fn], β=090° and χ_{foil}=midship, S= 8 m^2

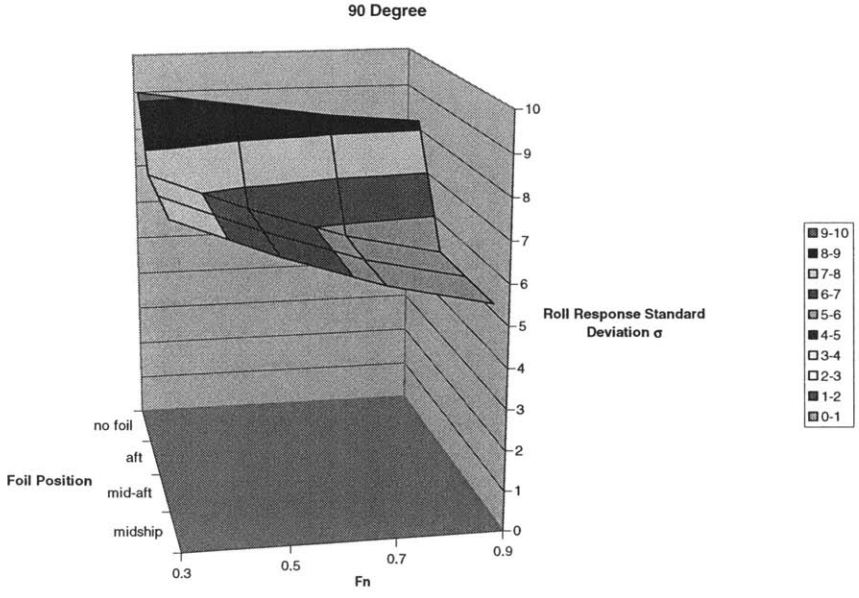

Figure 97: Roll Standard Deviation surface graph for varying vessel speed and hydrofoil longitudinal position, S=8 m^2, β=090°

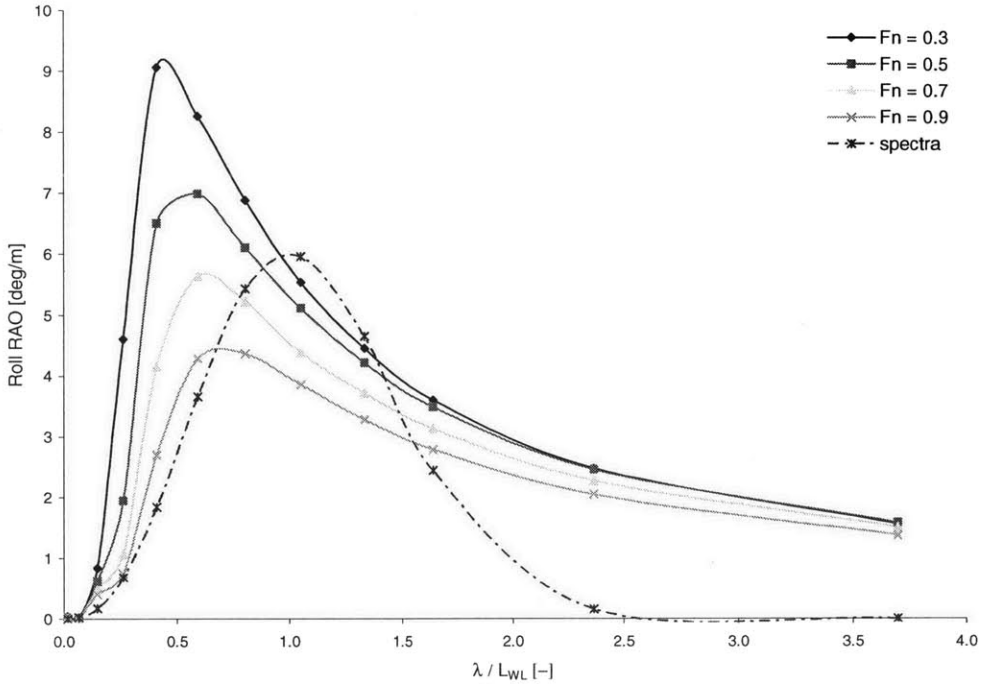

Figure 98: Roll RAOs, varying speed [Fn], β=105° and χ_{foil}=midship, S= 8 m^2

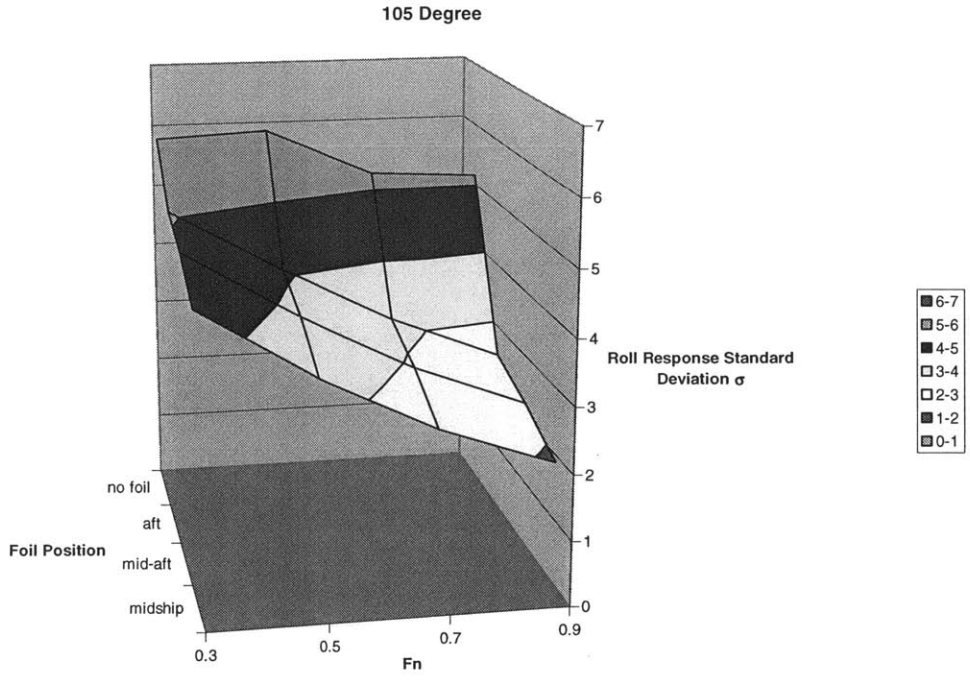

Figure 99: Roll Standard Deviation surface graph for varying vessel speed and hydrofoil longitudinal position, S=8 m^2, β=105°

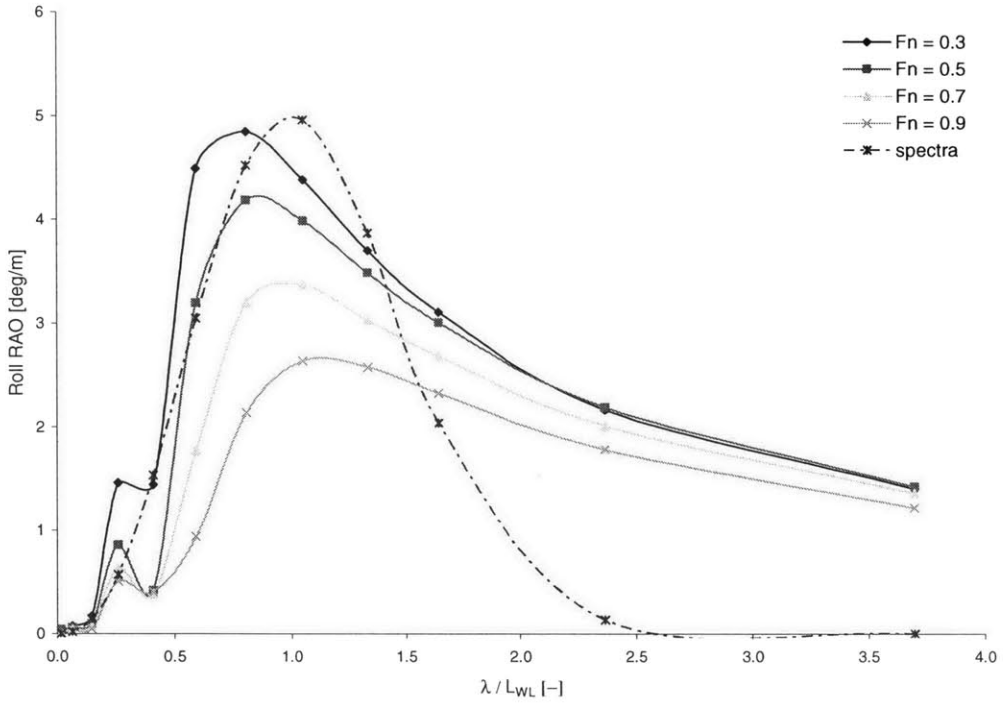

Figure 100: Roll RAOs, varying speed [Fn], β=120° and χ_{foil}=midship, S= 8 m^2

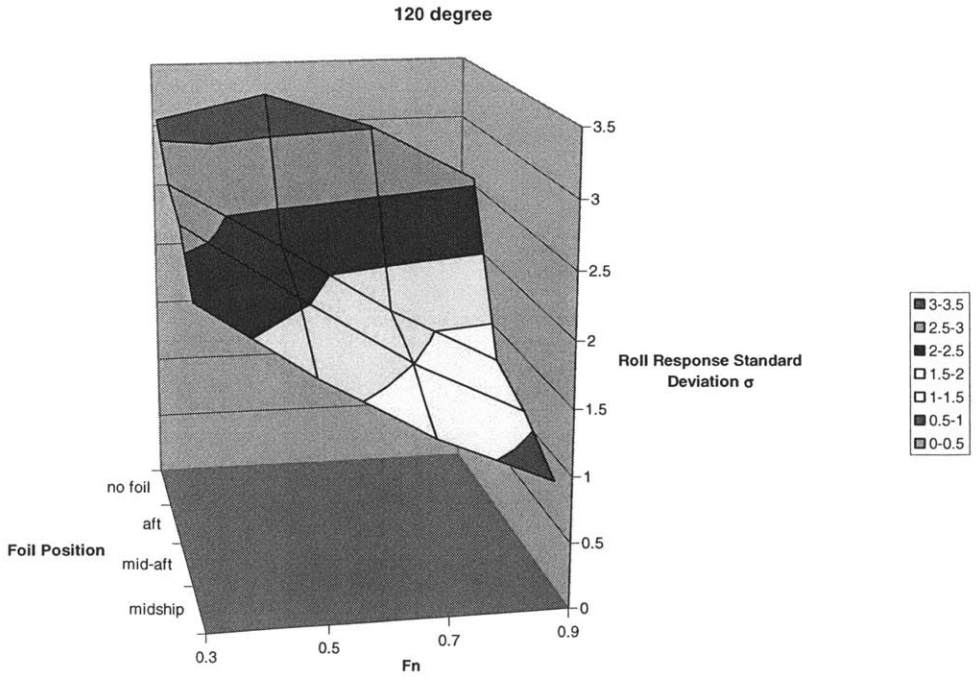

Figure 101: Roll Standard Deviation surface graph for varying vessel speed and hydrofoil longitudinal position, S=8 m^2, β=120°

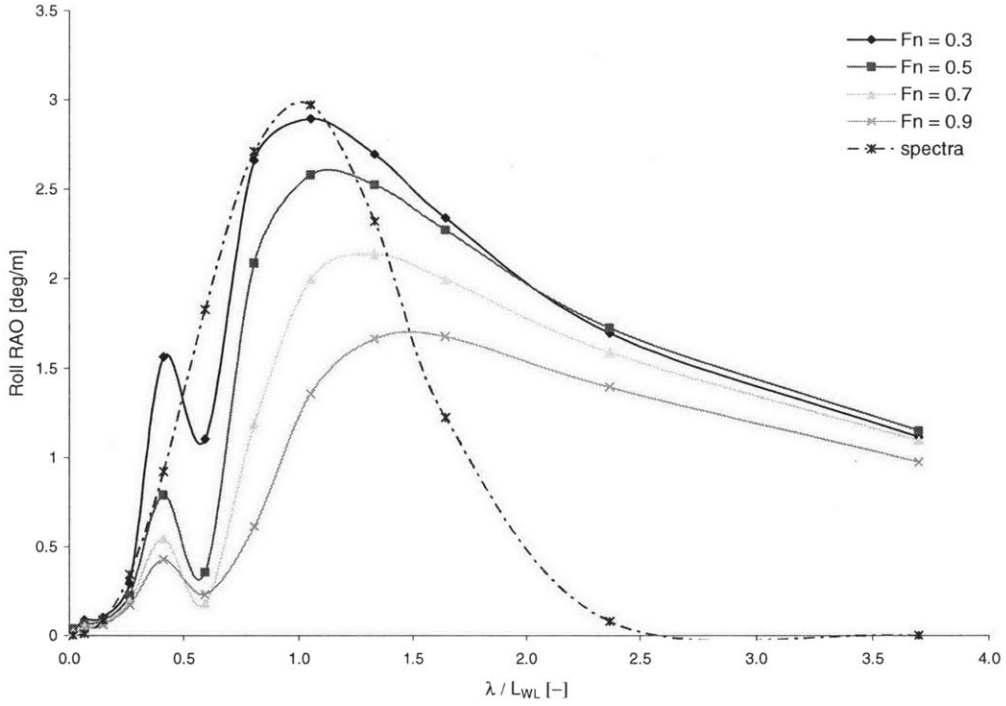

Figure 102: Roll RAOs, varying speed [Fn], β=135° and χ_{foil}=midship, S= 8 m^2

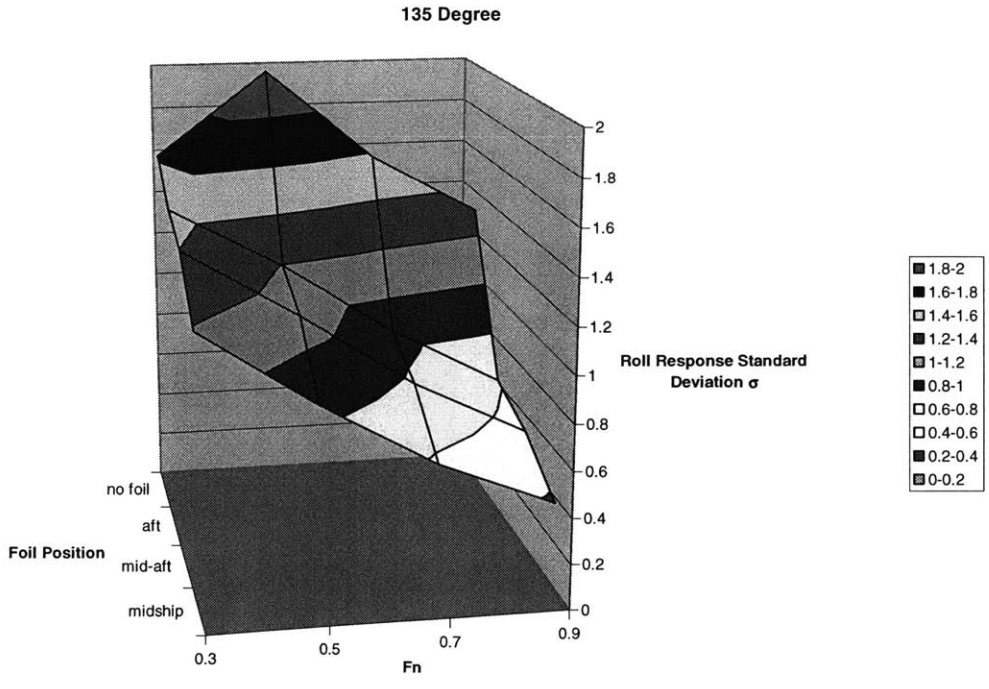

Figure 103: Roll Standard Deviation surface graph for varying vessel speed and hydrofoil longitudinal position, S=8 m^2, β=135°

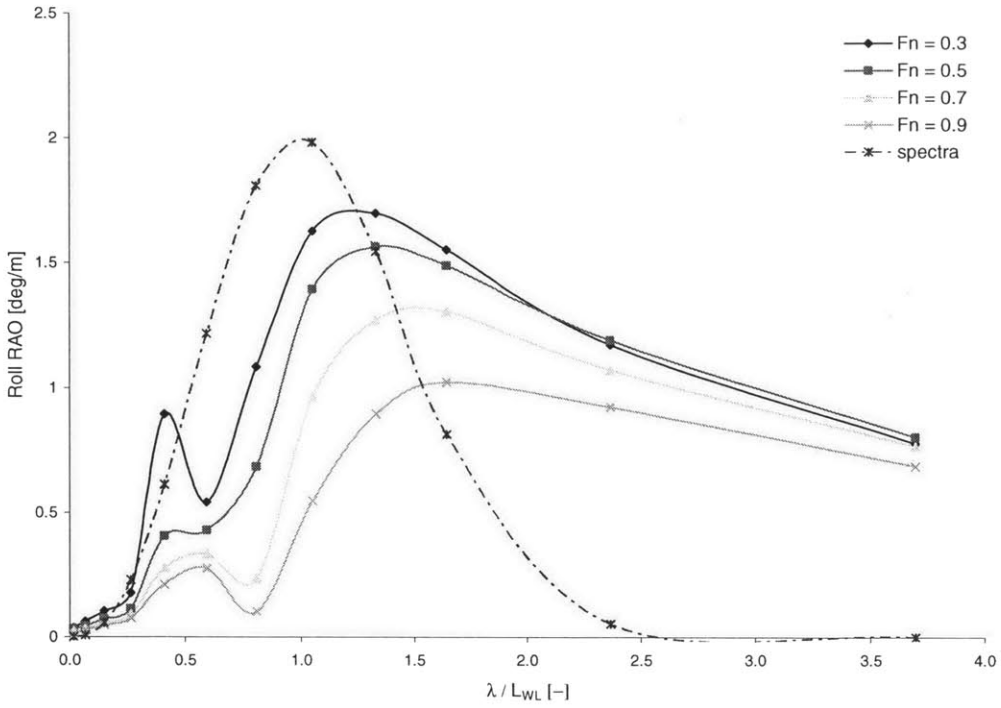

Figure 104: Roll RAOs, varying speed [Fn], β=150° and χ_{foil}=midship, S= 8 m^2

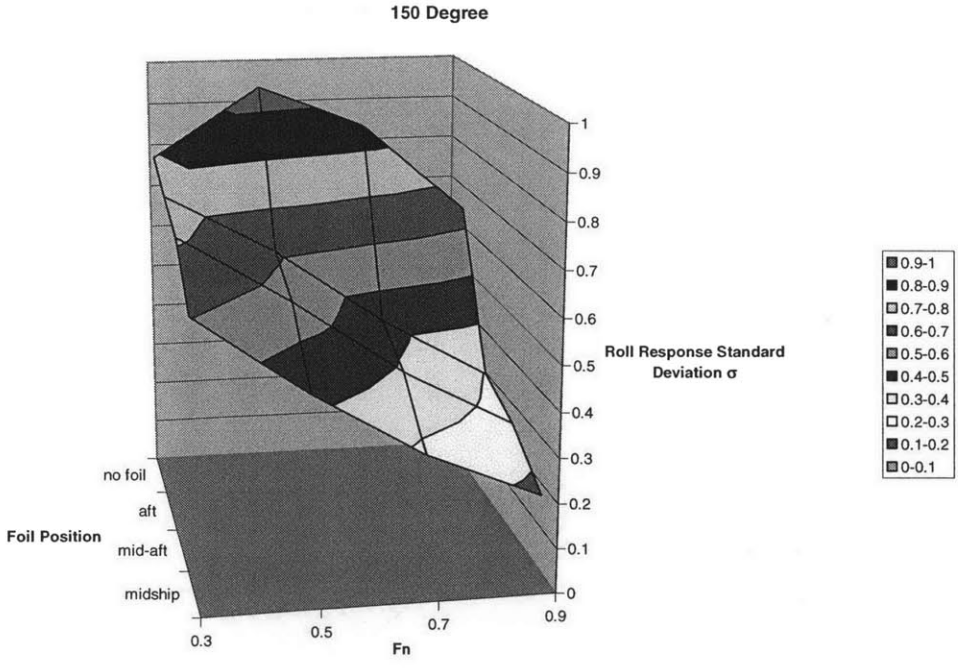

Figure 105: Roll Standard Deviation surface graph for varying vessel speed and hydrofoil longitudinal position, S=8 m^2, β=150°

12. Appendix D: The Influence of Active Roll Control

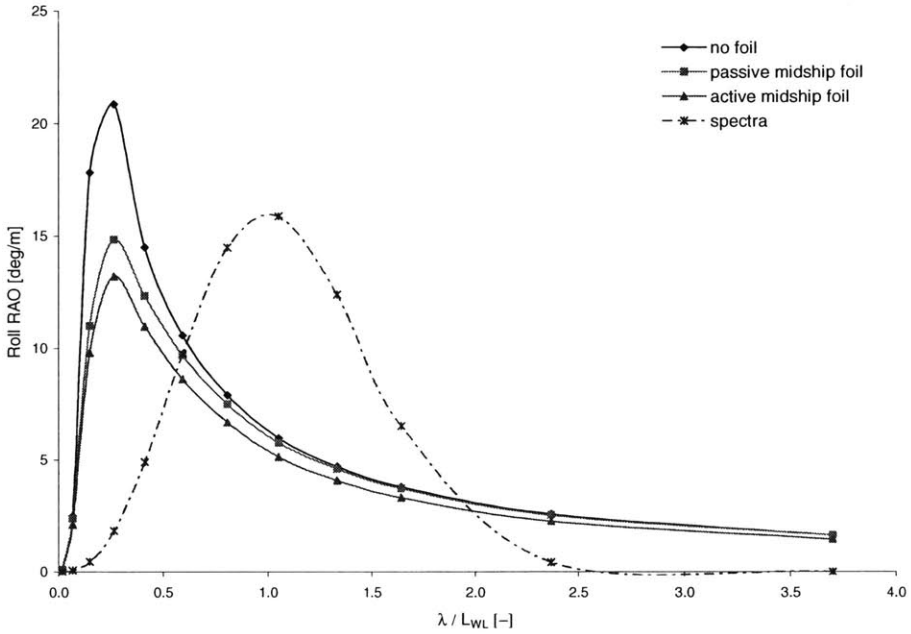

Figure 106: Roll RAOs, Fn=0.3, β=090° and χ_{foil}=midship, S= 8 m^2

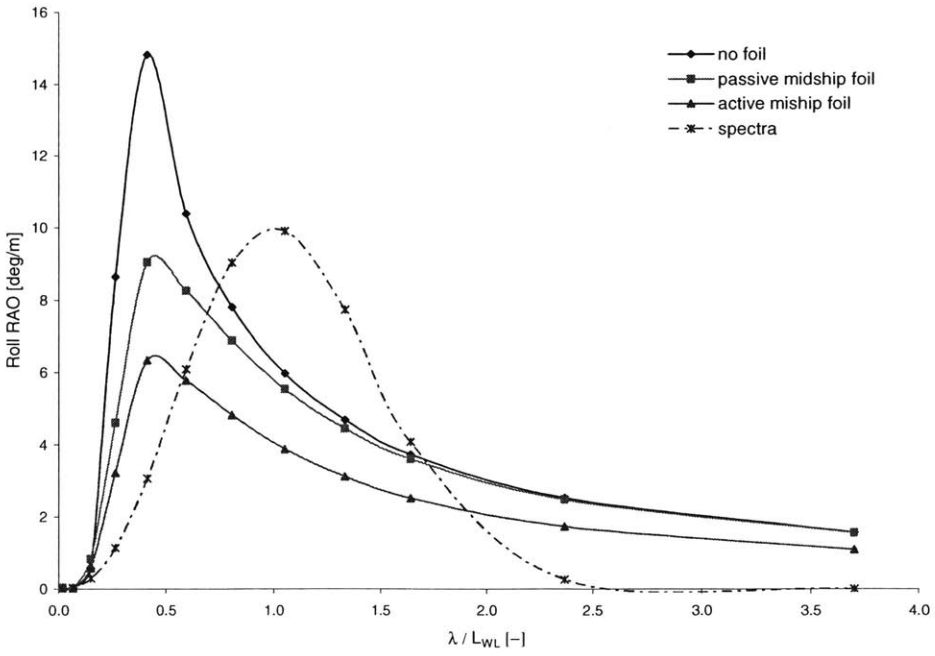

Figure 107: Roll RAOs, Fn=0.3, β=105° and χ_{foil}=midship, S= 8 m^2

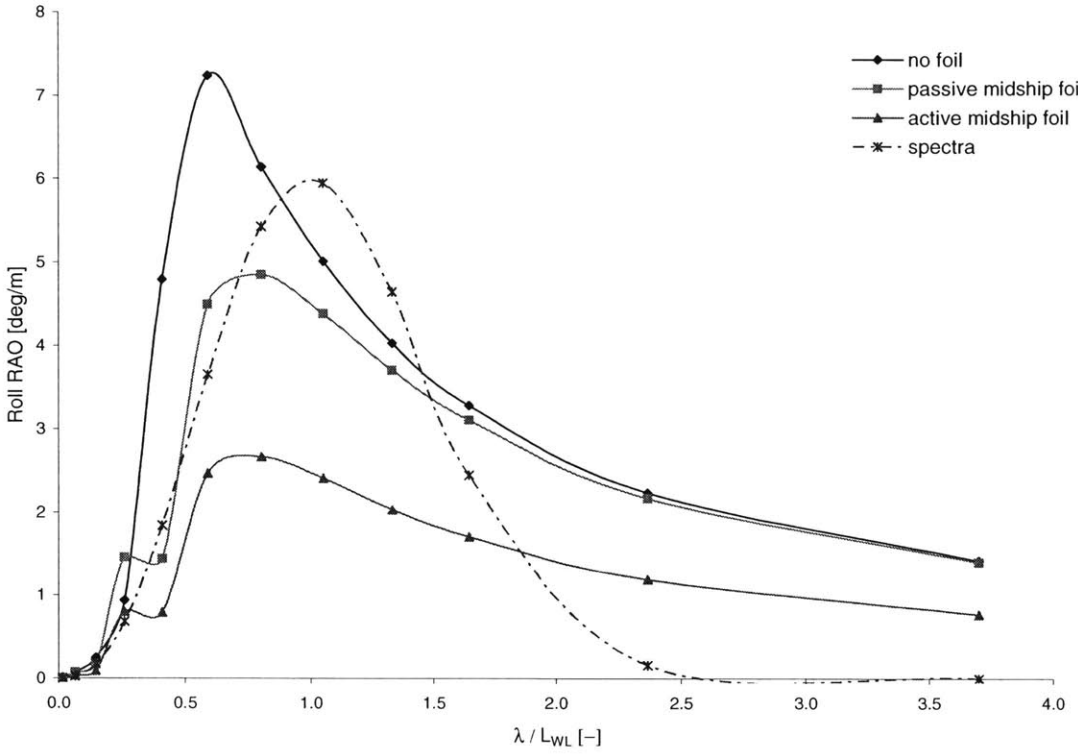

Figure 108: Roll RAOs, Fn=0.3, β=120° and χ_{foil}=midship, S= 8 m²

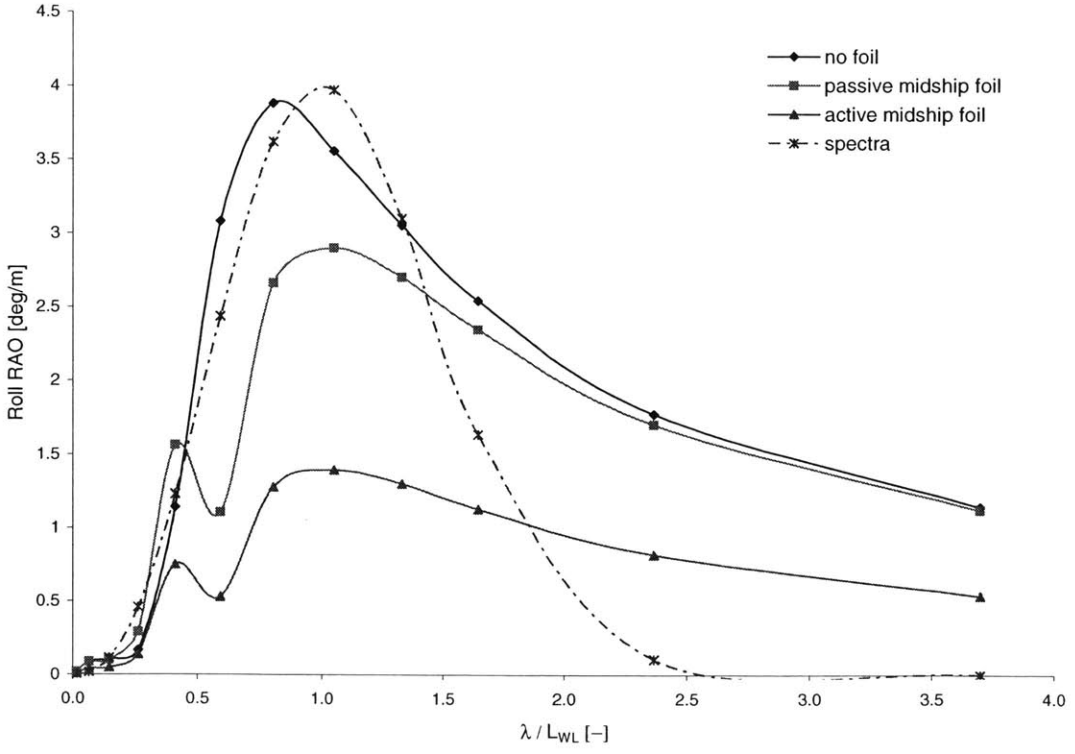

Figure 109: Roll RAOs, Fn=0.3, β=135° and χ_{foil}=midship, S= 8 m²

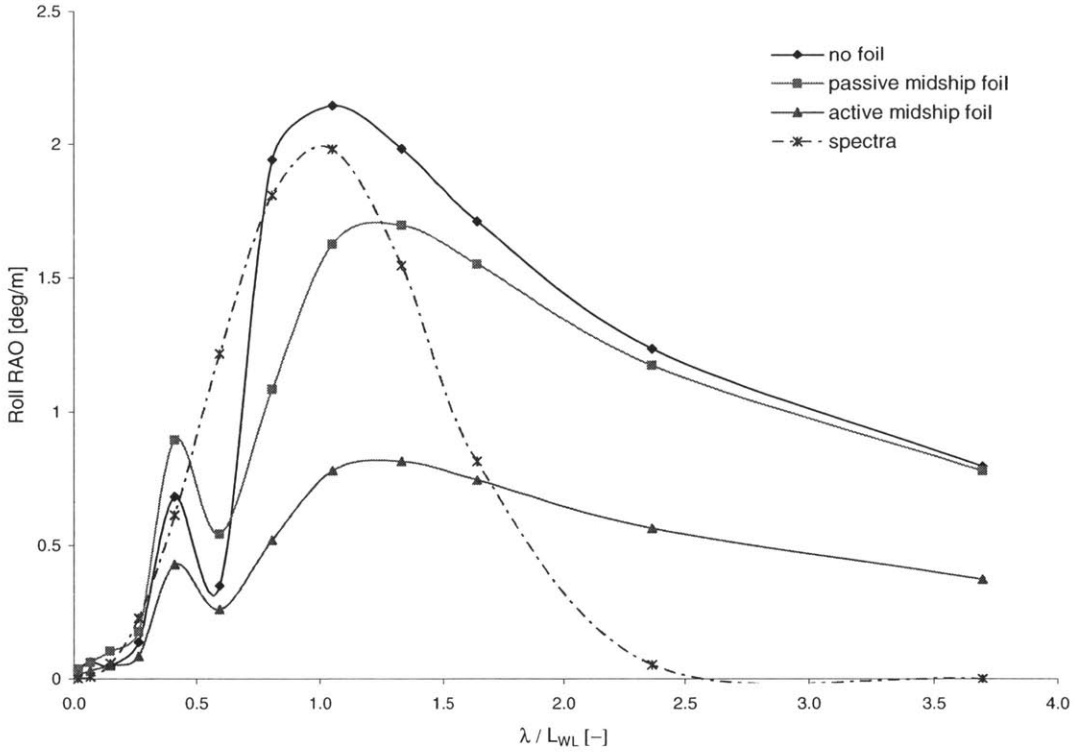

Figure 110: Roll RAOs, Fn=0.3, β=150° and χ_{foil}=midship, S= 8 m^2

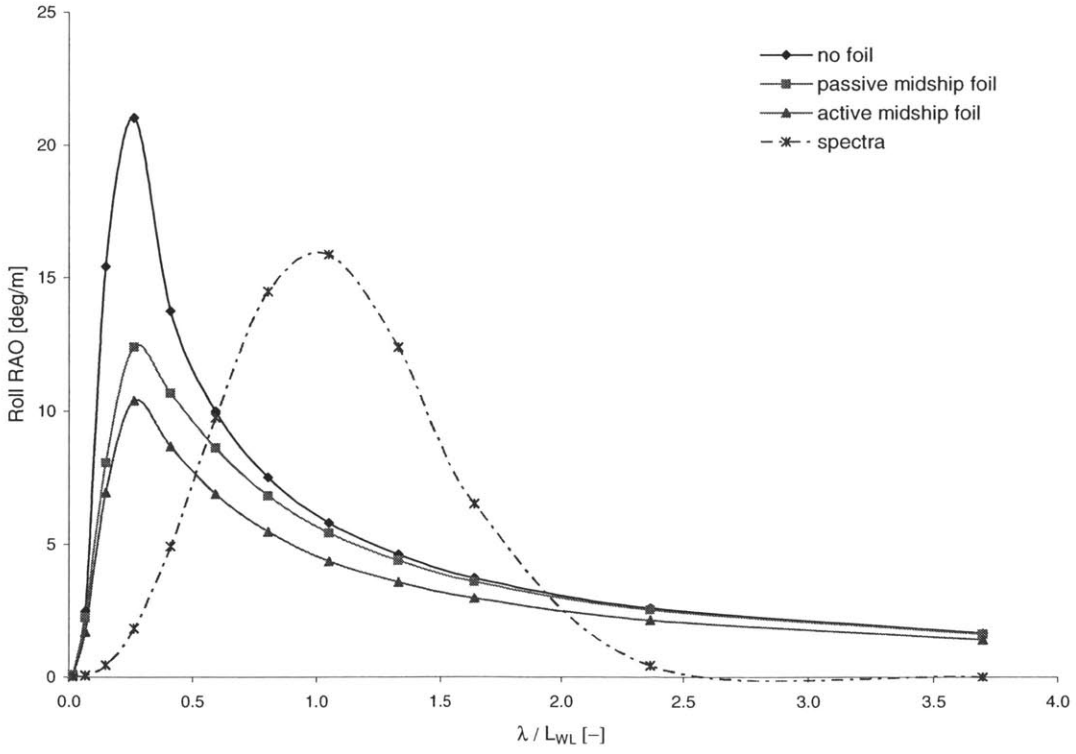

Figure 111: Roll RAOs, Fn=0.5, β=090° and χ_{foil}=midship, S= 8 m^2

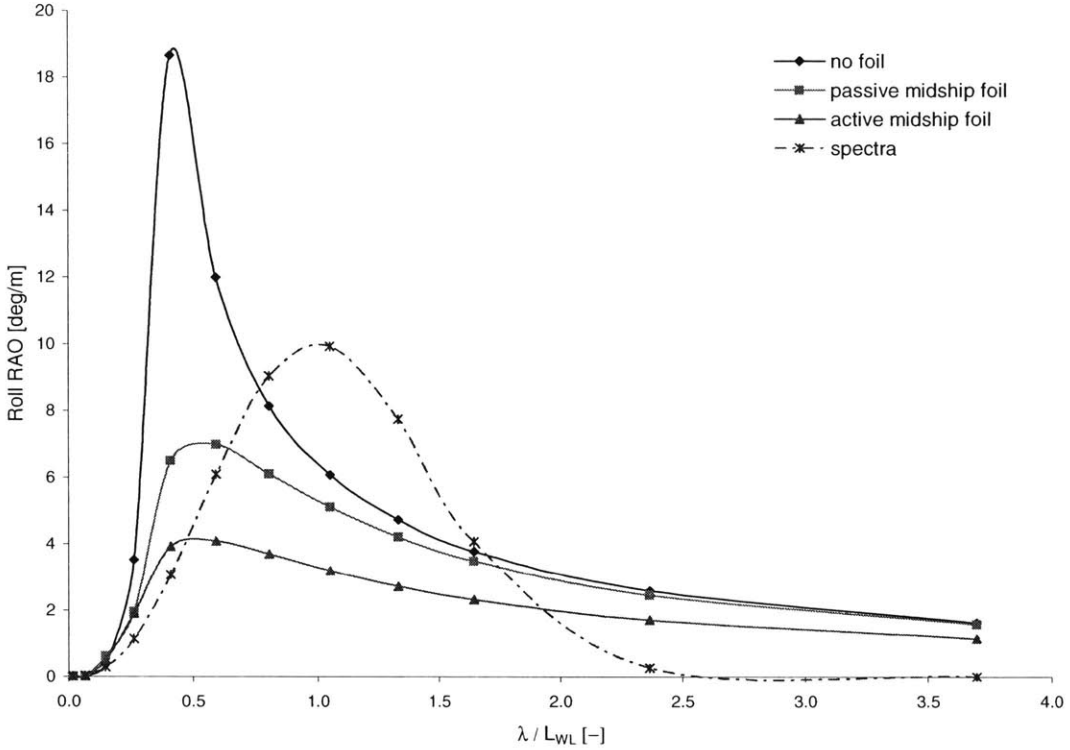

Figure 112: Roll RAOs, Fn=0.5, β=105° and χ_{foil}=midship, S= 8 m^2

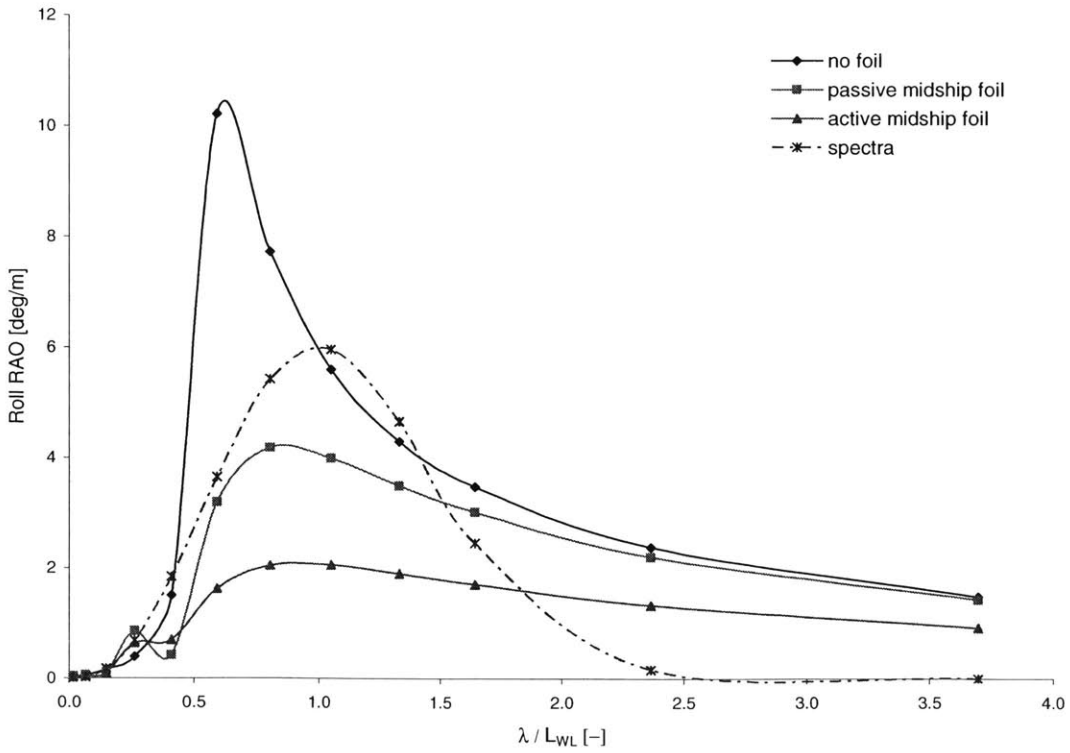

Figure 113: Roll RAOs, Fn=0.5, β=120° and χ_{foil}=midship, S= 8 m^2

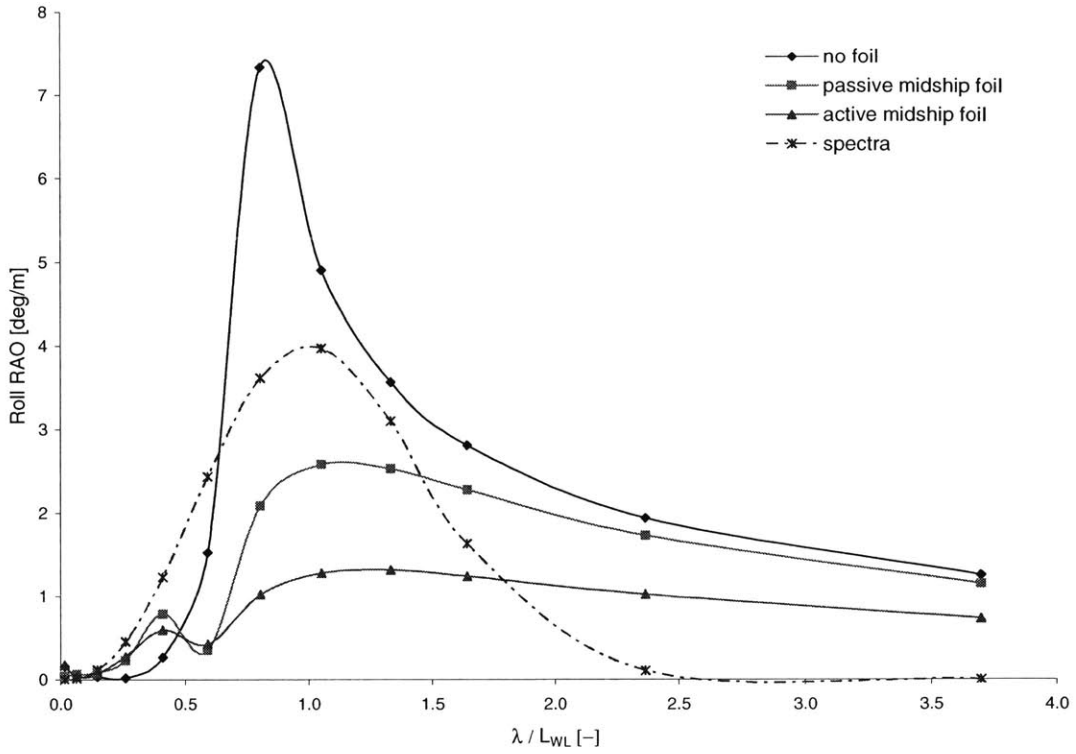

Figure 114: Roll RAOs, Fn=0.5, β=135° and χ_{foil}=midship, S= 8 m²

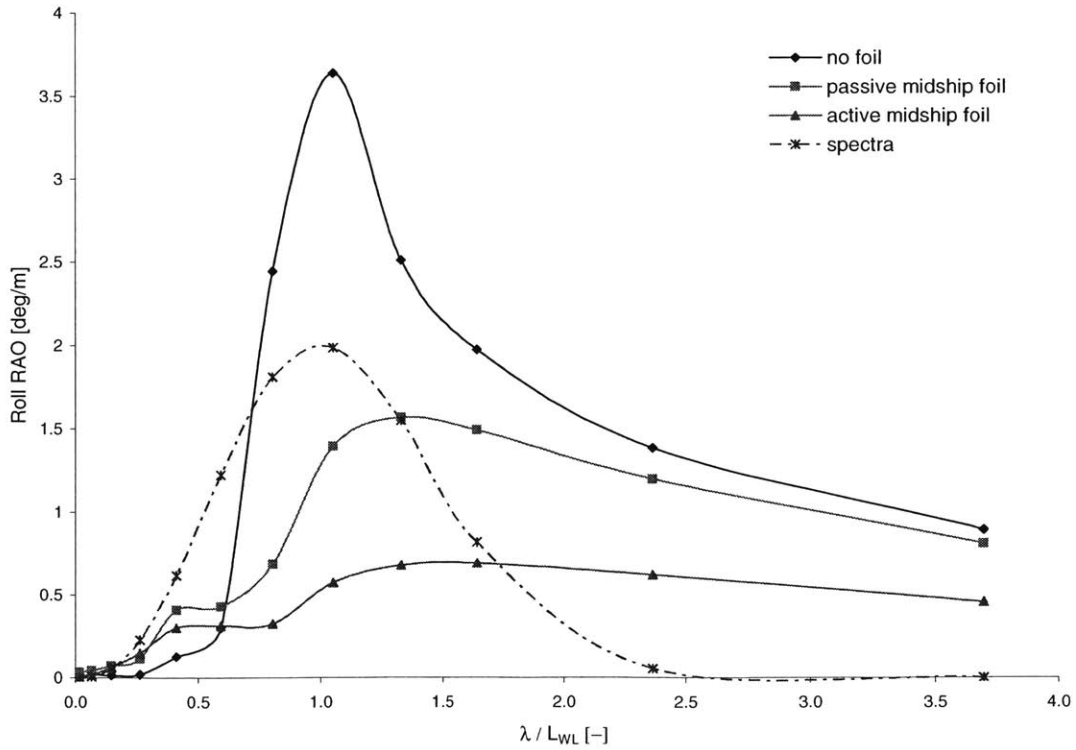

Figure 115: Roll RAOs, Fn=0.5, β=150° and χ_{foil}=midship, S= 8 m²

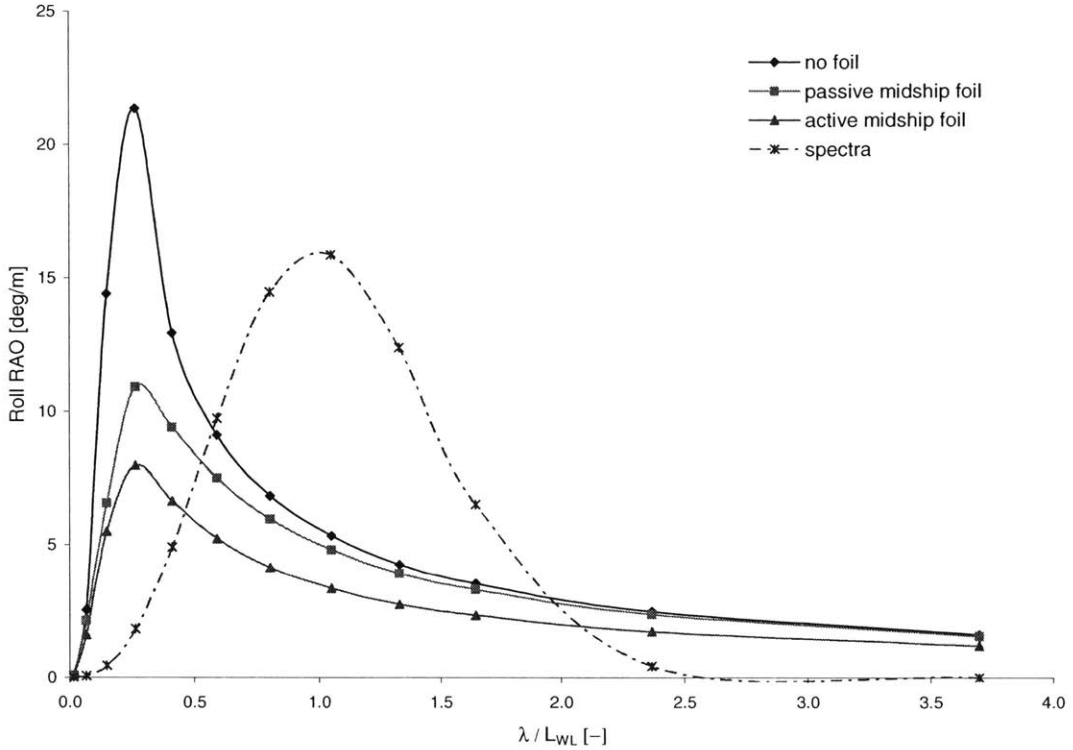

Figure 116: Roll RAOs, Fn=0.7, β=090° and χ_{foil}=midship, S= 8 m^2

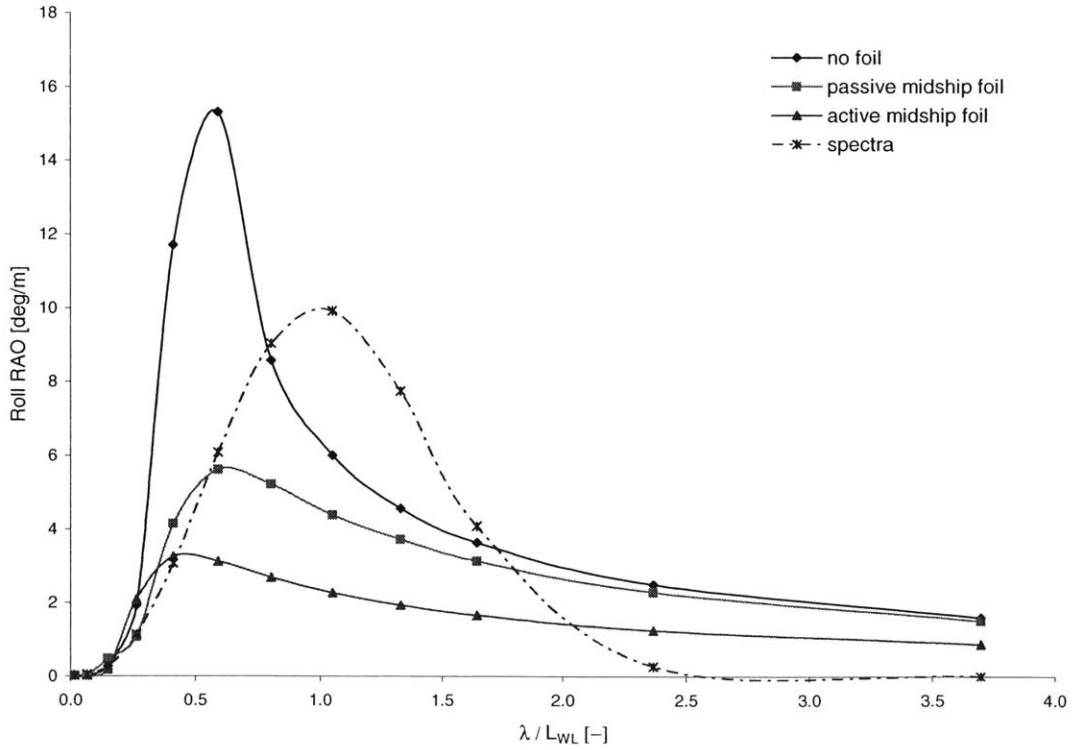

Figure 117: Roll RAOs, Fn=0.7, β=105° and χ_{foil}=midship, S= 8 m^2

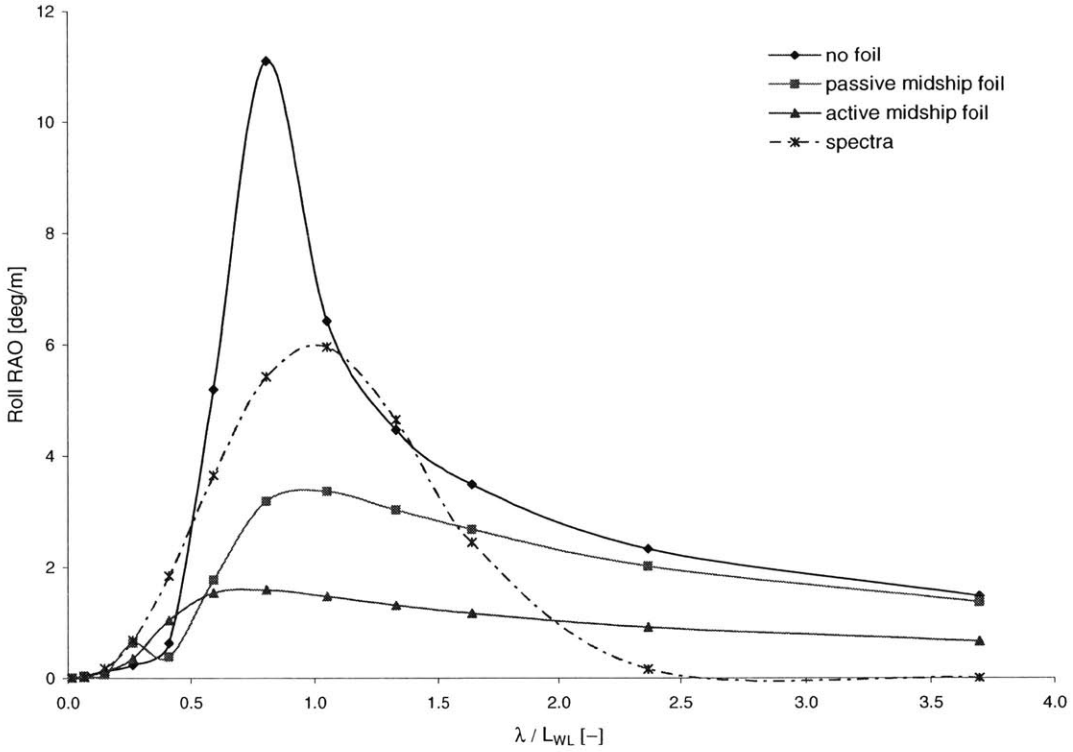

Figure 118: Roll RAOs, Fn=0.7, β=120° and χ_{foil}=midship, S= 8 m²

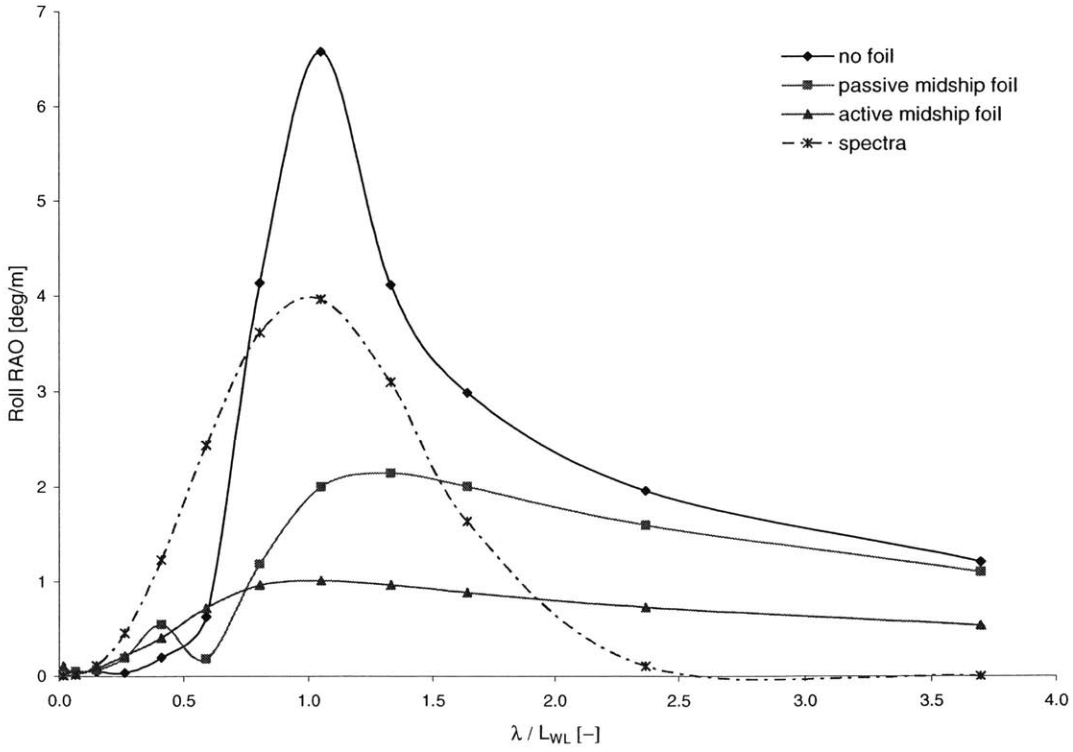

Figure 119: Roll RAOs, Fn=0.7, β=135° and χ_{foil}=midship, S= 8 m²

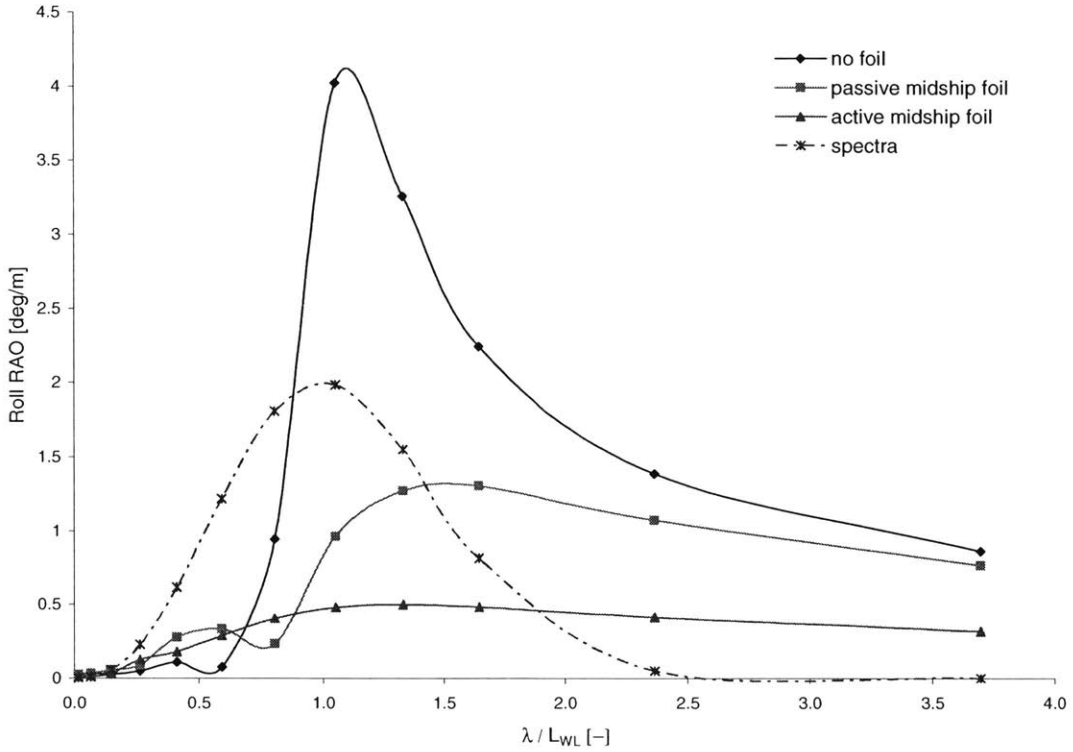

Figure 120: Roll RAOs, Fn=0.7, β=150° and χ_{foil}=midship, S= 8 m^2

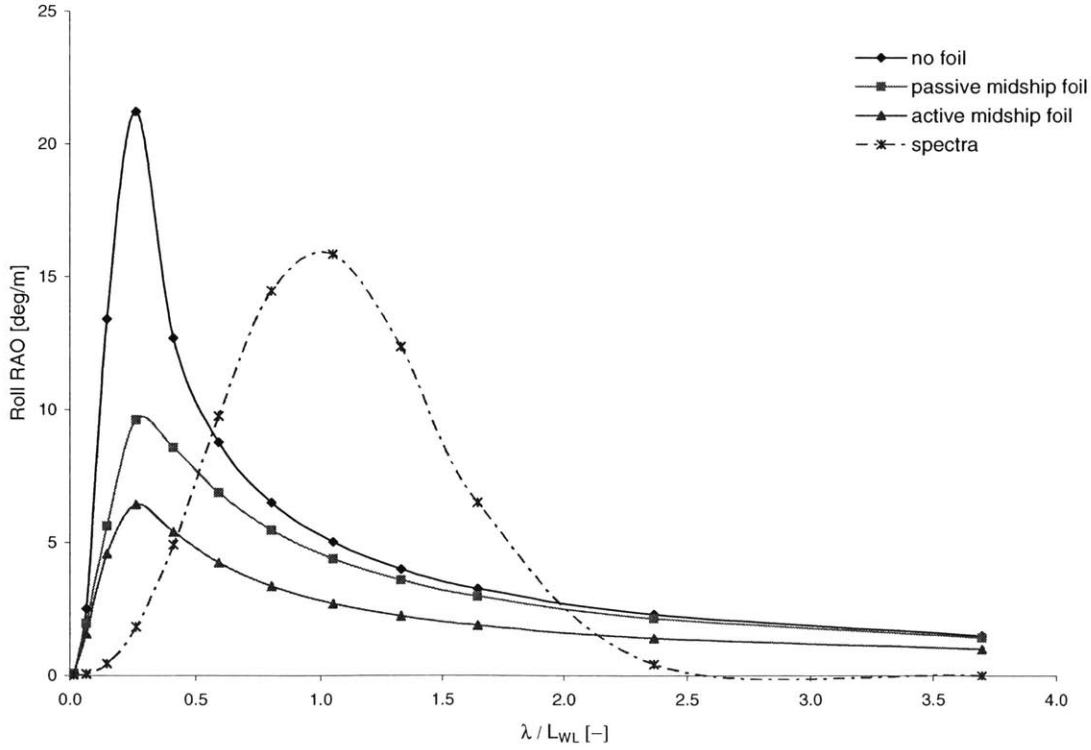

Figure 121: Roll RAOs, Fn=0.9, β=090° and χ_{foil}=midship, S= 8 m^2

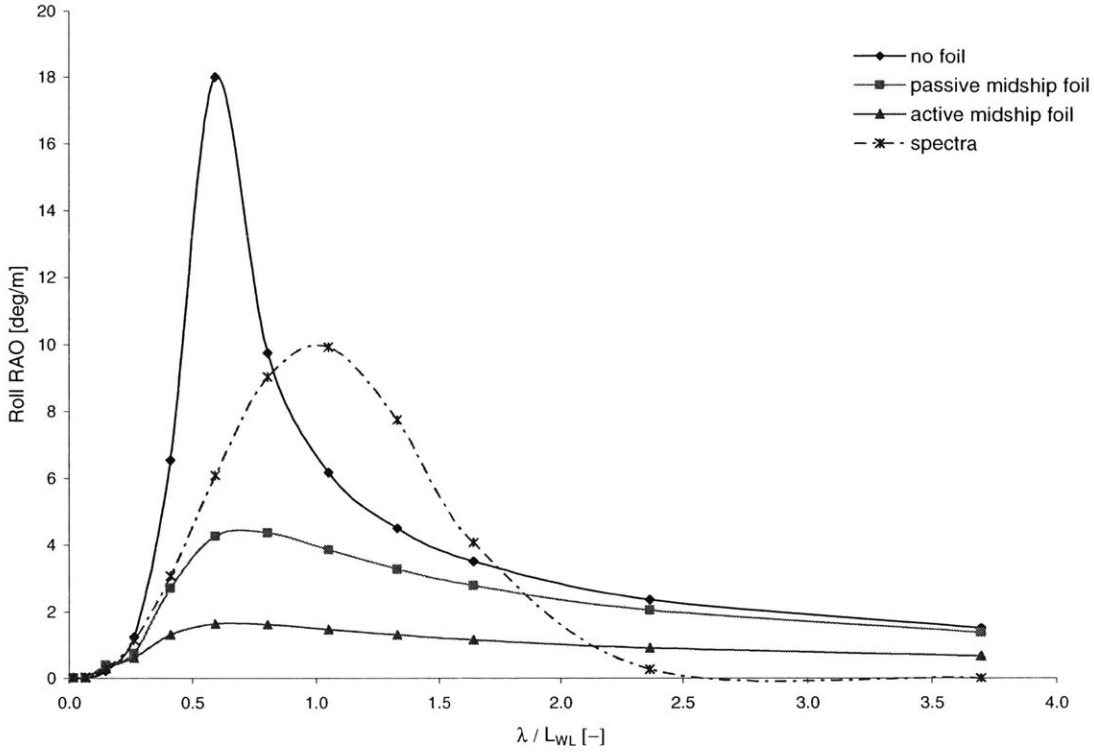

Figure 122: Roll RAOs, Fn=0.9, β=105° and χ_{foil}=midship, S= 8 m^2

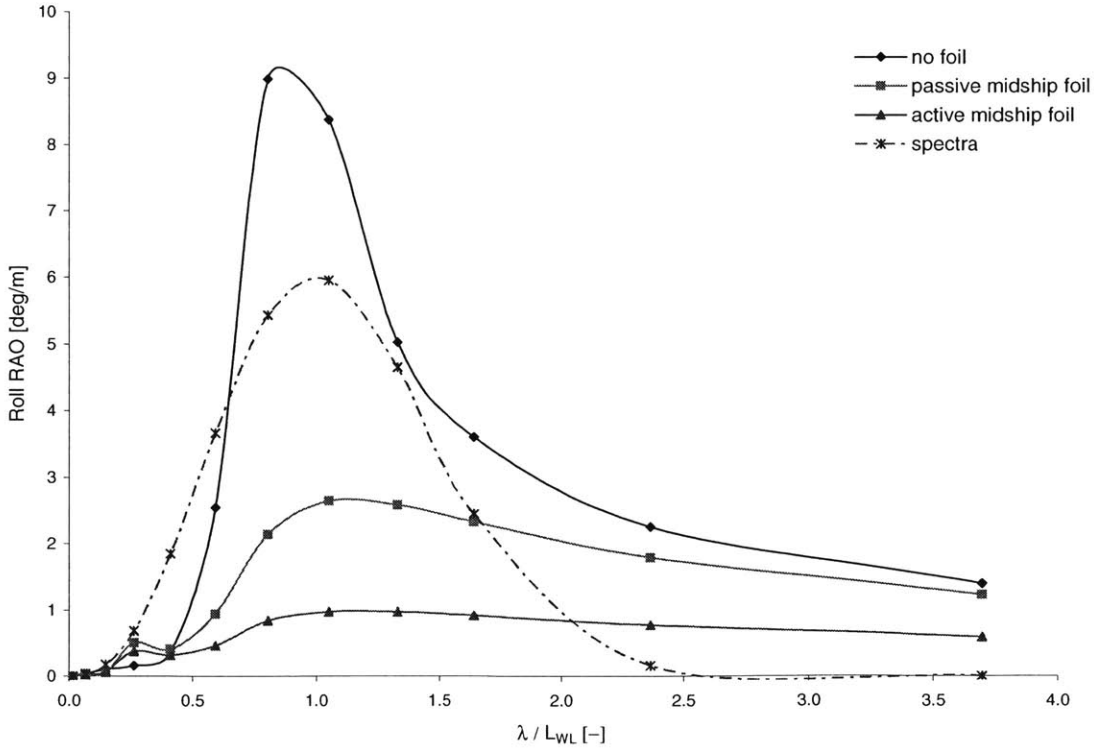

Figure 123: Roll RAOs, Fn=0.9, β=120° and χ_{foil}=midship, S= 8 m^2

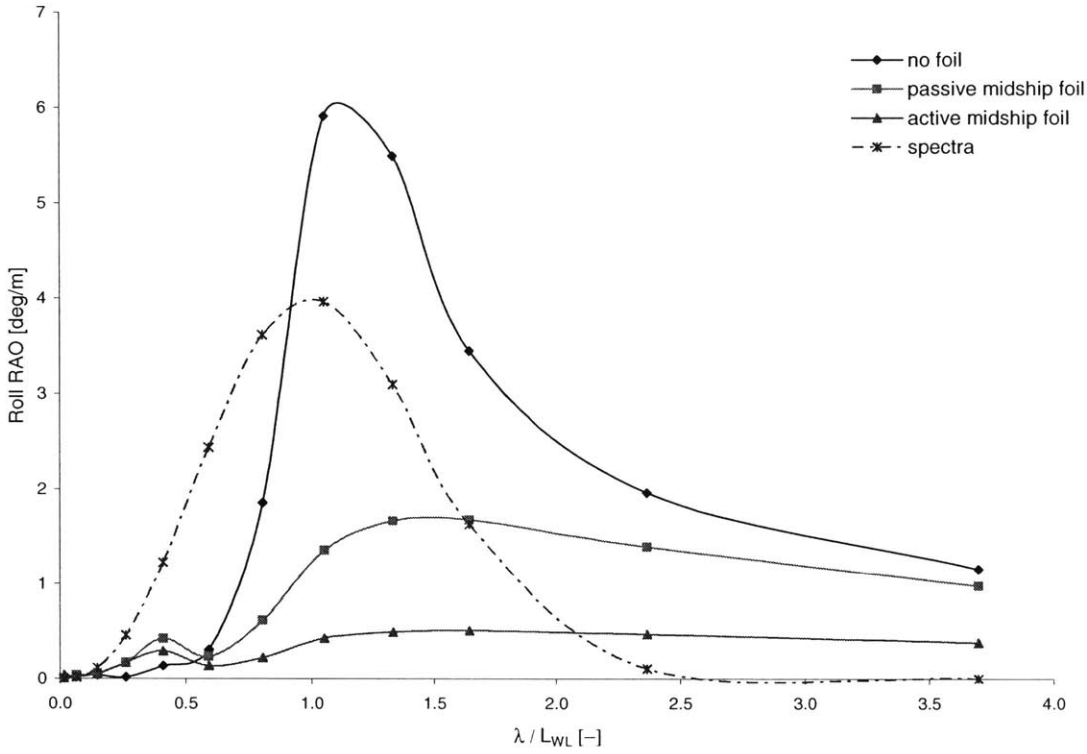

Figure 124: Roll RAOs, Fn=0.9, β=135° and χ_{foil}=midship, S= 8 m²

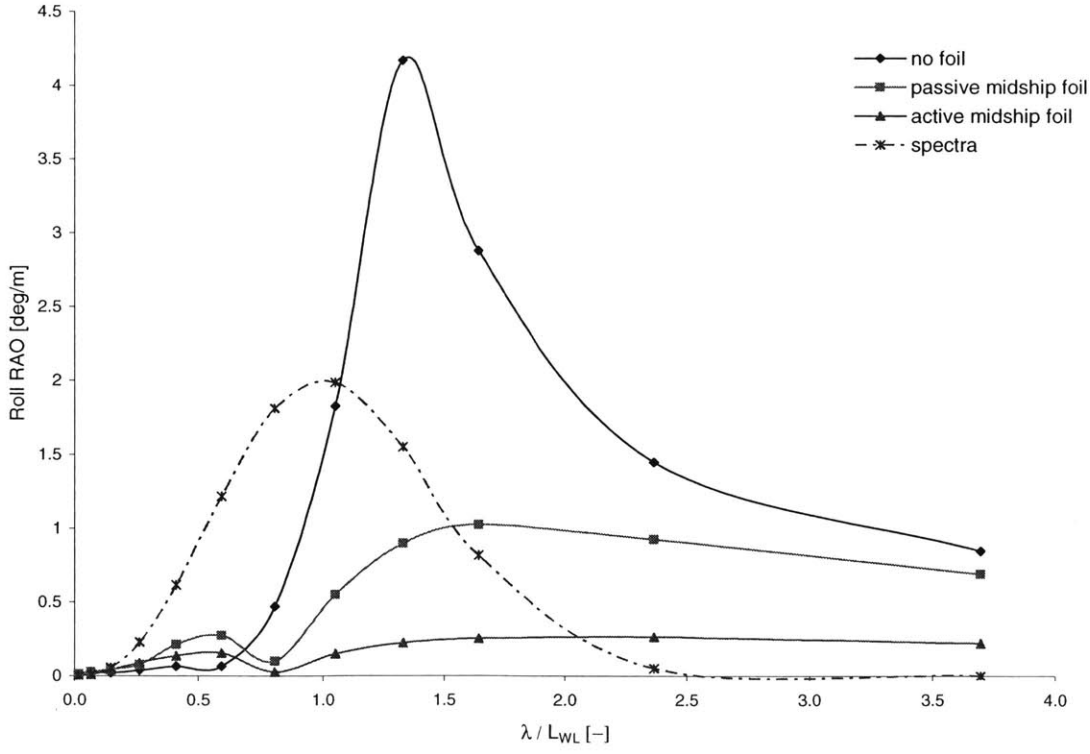

Figure 125: Roll RAOs, Fn=0.9, β=150° and χ_{foil}=midship, S= 8 m²